PROTECTING THE PREGNANT OCCUPANT: DYNAMIC MATERIAL PROPERTIES OF UTERUS AND PLACENTA

Sarah Jeanette Manoogian

Dissertation submitted to the faculty of the
Virginia Polytechnic Institute and State University
in partial fulfillment of the requirements for the degree of

Doctor of Philosophy
In
Mechanical Engineering

Dr. Stefan M. Duma, Ph.D., Chair
Dr. H. Clay Gabler, Ph.D., Co-chair
Dr. Joel D. Stitzel, Ph.D.
Dr. Warren N. Hardy, Ph.D.
Dr. Raffaella De Vita, Ph.D.
Dr. Heather L. Mertz, M.D

May 29, 2008

Blacksburg, Virginia

Keywords: Pregnant, Uterus, Placenta, Chorion, Abruption, Motor Vehicle Crash

PROTECTING THE PREGNANT OCCUPANT: DYNAMIC MATERIAL PROPERTIES OF UTERUS AND PLACENTA

Sarah Jeanette Manoogian

ABSTRACT

Automobile crashes are the largest cause of death for pregnant females and the leading cause of traumatic fetal injury mortality in the United States. The first way to protect the fetus is to protect the mother considering that maternal death has a near 100% fetal loss rate. If the mother survives, protection of the fetus may best be accomplished by preventing placental abruption. Placental abruption, which is the premature separation of the placenta from the uterus, has been shown to account for 50% to 70% of fetal losses in motor vehicle crashes.

Since real world crash data for pregnant occupants is limited to a retrospective analysis and pregnant cadaver studies are not feasible, crash test dummies and computational modeling have been utilized to evaluate the risk of adverse fetal outcome. Although pregnant occupant research has progressed with these tools, they are based on limited tissue data. In order to have more accurate research tools, better pregnant tissue material data are needed. Therefore, the purpose of this dissertation is to provide material properties for the placenta and pregnant uterine tissue in dynamic tension.

ACKNOWLEDGEMENTS

I would like to thank all of the people who had a part in helping me complete my degree. Without the help and encouragement of so many individuals the work would not have been possible. Most importantly they made the experience an enjoyable and educational one.

Certainly I would not have had this opportunity without the encouragement of my parents and grandparents. From a young age they emphasized the importance of an education and hard work. My family has always supported my endeavors and I cannot thank them enough for the endless love and encouragement.

Dr. Stefan Duma has been a key to my successes and achievements in the Center for Injury Biomechanics. I am grateful for the opportunities and instruction he has provided throughout my years at Virginia Tech. Of course my experiences with Dr. Clay Gabler and Dr. Joel Stitzel have also been critical to my understanding of injury biomechanics and I have greatly benefited from their roles in my educational process.

As a student Eric Kennedy took the role as my mentor and I can say with absolute certainty that my research is better quality because of his guidance. I cannot summarize everything he taught me in a few sentences but I can say that I am very thankful for his role as my mentor and friend. I am a better person and a better researcher for the time that I spent learning from Eric.

There have been so many officemates, lab mates, and interns. During my time at Virginia Tech I have worked with so many people it is not possible to list them all. I do appreciate all of the hard work everyone contributed to helping me achieve my research goals. I also want to thank all of my friends I have had while at Virginia Tech for making this experience so enjoyable and reminding me to keep my head up when the work load was overwhelming.

Thank you everyone for helping with all of my accomplishments!

TABLE OF CONTENTS

LIST OF FIGURES

LIST OF TABLES

Chapter 1:
Introduction of Anatomy, Injury Risk, Current Research, and Goals of Proposed Research

Introduction

This document outlines the research completed to evaluate pregnant occupant risk and determine the material properties for pregnant uterus and placenta. Each chapter of this document proposes a research hypothesis and explains the methodology along with the results and discussion which best answer the hypothesis. Each research question builds on the previous knowledge to advance the research for pregnant occupant safety.

Pregnant Anatomy

This research utilized tissue specimens from pregnant humans as well as pregnant sows. The anatomy of a pregnant human abdomen is necessary in understanding the injury mechanism as well as the tissues that were evaluated. At full term the uterus is 500 to 1000 times greater than its size when nonpregnant (Cunningham and Williams 2005). It will have undergone physiological changes to sustain fetal life and prepare for delivery of the fetus and fetal membranes. While there are several obstetrical complications that can lead to preterm distress, the focus of this research is placental abruption in a motor vehicle crash. Therefore, the anatomy discussed in this section will pertain to the uterus, the placenta, and the uteroplacental interface (Figure 1). Moreover, this research targets the end of the gestational period when the average pregnant occupant is at a higher risk. The anatomical structure between 30 and 40 weeks gestation is described.

In the uterus, not at the location of the placenta, there are three layers on the surface of the myometrium. The myometrium is the smooth muscle layer of the uterine wall. Inside of the smooth muscle layer, the uterus transitions to a decidua layer. The decidua layer is a result of hormones activating a transformation in the innermost surface of the endometrium referred to as the decidua vera. The next two layers, the chorion and amnion are important to molecular transfer and metabolic activity. The chorion is a thin membrane, less than 1 mm thick, that is

between the amnion and decidua layers. The innermost fetal membrane is the amnion, which is tough and pliable and defines the amniotic sac. Inside the amniotic sac, the fetus is surrounded by amniotic fluid.

The placenta is normally located at the fundus of the uterus (Cunningham and Williams 2005). The fetal connection to the placenta is through the umbilical cord which contains, two arteries and one vein that spiral together from the fetus to the placenta. The fetal surface of the placenta is covered by the amnion and then contains the chorionic plate where the fetal vessels from the umbilical cord branch out to the edges of the placenta (Figure 2). The blood flow reaches the lobes of the placenta for fetal maternal transfer. The maternal surface of the placenta consists of lobes separated by grooves referred to as placenta septa. These grooves are filled in on the maternal side of the placenta with the decidua layer. At the placental bed site the decidua layer is the decidua basalis. The decidua layer is then attached to the myometrium of the uterine wall. In natural birth, the fetus is delivered and the fetal membranes are delivered in the after birth, separating from the uterine wall at the decidua layer. The contraction of the uterus aids in the delivery of these membranes.

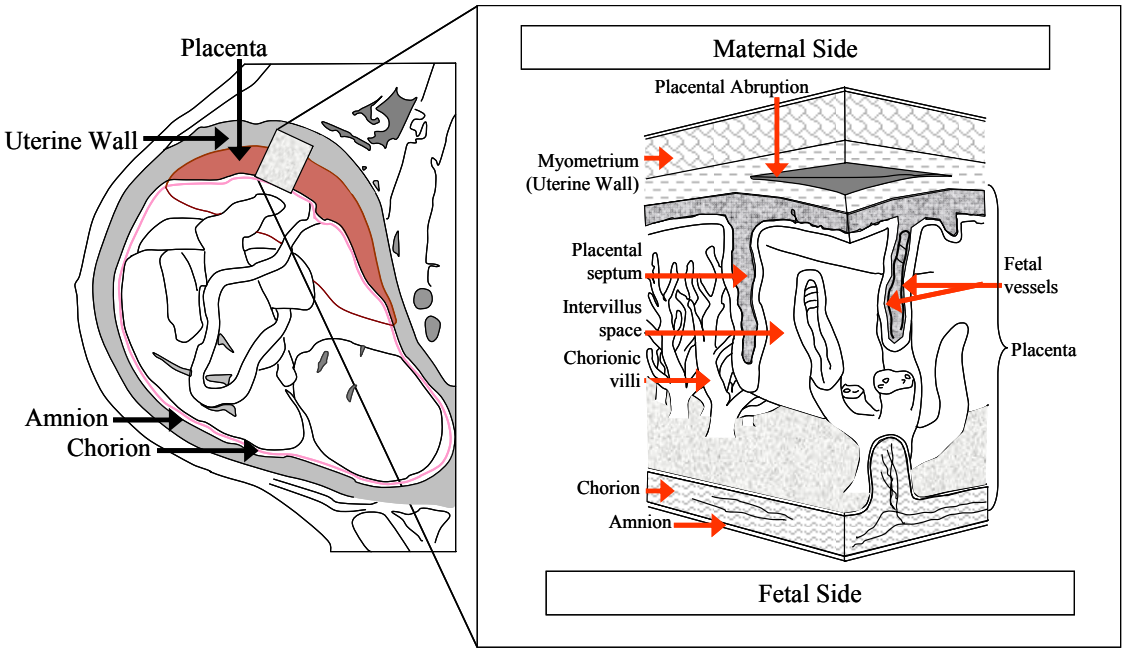

Figure 1: The pregnant abdomen at full term normally has the placenta located at the fundus of the uterus.

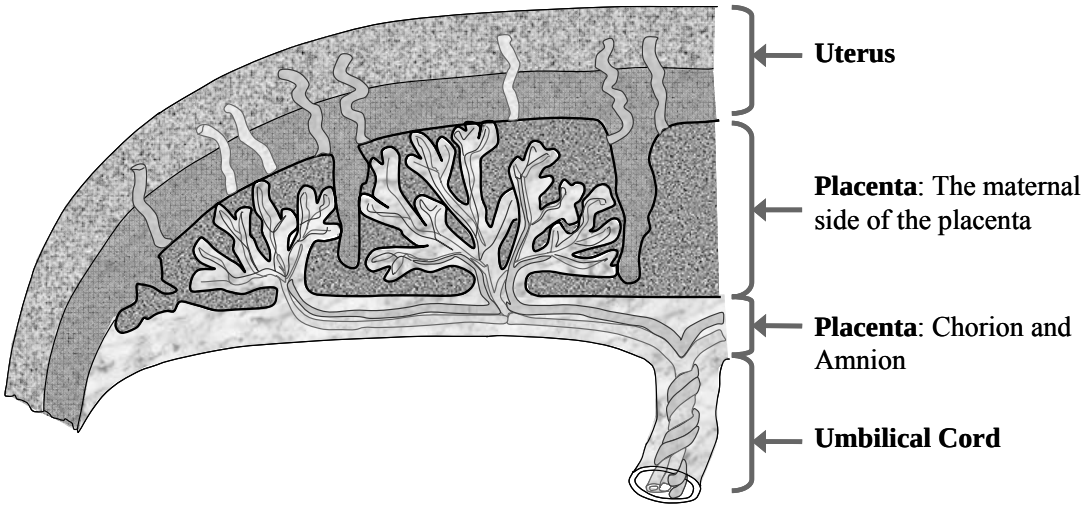

Figure 2: The structure of the placenta varies from the maternal to the fetal side.

Animal Surrogate

This study utilized pregnant porcine uterine tissue as a model of the pregnant human uterus because of its similarity and availability. The similarities between a porcine uterus and a human uterus are in the structure of the uterine layers and their development during gestation. In a porcine uterus, as in a human uterus, the inner lining of the uterine cavity is the endometrial layer. This layer is attached to the myometrium and contains connective tissue and epithelium. During pregnancy, the porcine myometrium grows in size due to hypertrophy and develops elastic tissues as in the human (Marrable 1971). The human uterus has an anisotropic response with two groups of smooth muscle fibers, circular and longitudinal, that originate at the fallopian tubes and fan outward (Marrable 1971, Mizrahi and Karni 1975, Young and Hession 1999, Weiss et al. 2006). The myometrium for a sow is also anisotropic with two groups of muscle fibers, circular and longitudinal, that cross perpendicularly (Marrable 1971). Externally the porcine uterus has two uterine horns supported by the mesometrium, which serves the same function as the supporting ligaments for the human uterus (Figure 3 and Figure 4).

There are differences between the porcine and human uterus. One difference is the shape, the human uterus has a simplex shape, and the porcine uterus is bicornuate, the closest stage to the simplex in evolution (Finn and Porter 1975). The simplex shape means that there is only one part that is the uterus (Figure 3). Bicornuate means the uterus is comprised of two parts referred to as horns (Figure 4). The function of the porcine uterus differs from the human uterus in that

the number of fetuses and gestational period are different. A typical human birth has a single fetus for 40 weeks while a typical porcine birth has more than 6 fetuses for a 16 week gestation (Marrable 1971). Moreover, the placenta for the sow is diffuse and fills the entire uterus while the human placenta is discoid and only connects to part of the human uterus, usually at the fundus of the uterus (Ramsey 1975). In spite of the different shape, size, and placenta, the porcine and human uterine walls have similar myometria with anisotropic composition. In this study, only the material properties of the porcine uterine wall were considered and therefore the differences described above do not eliminate the pregnant porcine uterus as a useful model for the pregnant human uterus.

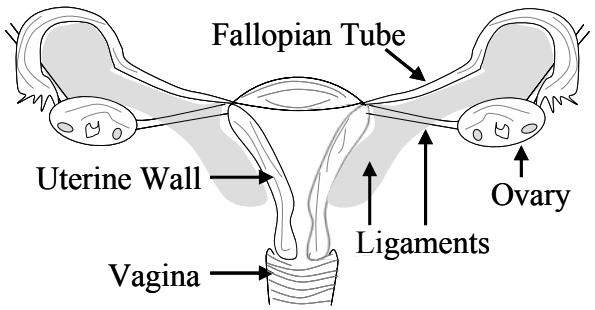

Figure 3: Diagram of a simplex human uterus.

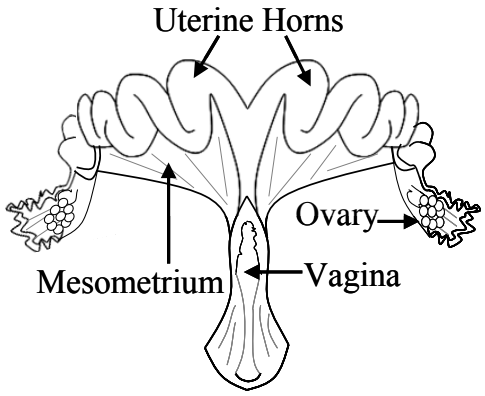

Figure 4: Diagram of a bicornuate porcine uterus.

Annual Fetal Death Rate

According to the Center for Disease Control, 25,600 fetal deaths occurred in the United States in 2002 from all causes. The exact incidence of fetal deaths that occur from trauma during motor vehicle crashes (MVCs) is not well documented. Current literature estimates come from various methods that indicate the number of fetal deaths per year from motor vehicle trauma can be as low as 92 or as high as 4800. This section analyzes all previous estimates of fetal loss rates from motor vehicle trauma and to determine a more accurate range that represents all of the various methods in the literature.

First, a review of the available literature for pregnant occupant data and fetal loss rates was completed. All papers which included estimations of the annual fetal loss data in the United

States from motor vehicle trauma were included in the study. The underlying data used by the individual studies come from individual National Automotive Sampling System (NASS) studies, Center for Disease Control (CDC) live birth and fetal mortality records, Traffic and Safety Facts, and previous literature regarding fetal loss. The minimum and maximum values for estimated fetal deaths from each study were used to calculate a more accurate range. The results include a description of the calculations as well as the resulting maximum and minimum estimates of fetal losses per year in the US from MVCs for the 10 methods found in the literature.

Weiss (2001) used the percentage of fetal deaths that have trauma as calculated from Pennsylvania death certificates (0.0065%) and the percentage of fetal injures that are a result of MVC (80%) to calculate the number of fetal deaths each year equal to 208. Similarly, Weiss (1999) used the same calculation with a percentage of fetal deaths as a result of MVC, 0.0023%, determined from death certificates in 16 states during 1995-1997 to approximate 92 fetal deaths from MVC each year.

Jernigan (2002) used the NASS database (1995-2000) to determine the number of pregnant women who died directly from MVC (509) and the number of severe placental injuries that resulted in fetal loss over a 6 year period (434) to acquire a minimum estimate of fetal losses per year equal to 157.

Klinich et al. (1999b) estimated the number of pregnant women injured in crashes with vehicle damage to be 29923. This value in conjunction with the percentage of pregnancies that have trauma with subsequent fetal loss (1-3%) plus the number of pregnant women killed (163) estimates the average number of fetal deaths each year to be 462 to 1061. This estimate does not include fetal losses from accidents in which there was no vehicle damage or the woman was uninjured and is based on an approximation of pregnant women injured in crashes.

Klinich et al. (1999b) also used the percentage of women with an ISS score greater than or less than 20 and the respective risk of fetal loss based on the severity to approximate the number of fetal deaths from pregnant women injured in vehicle damage crashes. Those approximations, in addition to the number of pregnant women killed, estimates 496 fetal losses each year.

Jernigan et al. (2002) utilized the NASS database to calculate the number of crashes involving pregnant women for three different crash severities. The groups included crash severities with a change in velocity greater than 30 mph, between 15 and 30 mph, and those less than 15 mph. The incidence by crash severity was combined with the risk curve previously developed by Klinich (1999) relating the risk of adverse fetal outcome with crash severity. The associated risk of adverse fetal outcome and the percentage of that number that was fetal death were used to accordingly to determine an average number of fetal losses. Each of these estimates were averaged over the 6 year period and combined to get an average annual fetal death rate from MVC ranging from 743 to 1858.

Pearlman and Phillips (1996) used the national average number of births, the percentage of pregnancies that have trauma (6.5%), the percentage of trauma that is MVC (50%), and the percentage of MVC that result in death (1-3%) to obtain a range of fetal deaths per year of 1300 to 3900. Klinich et al. (1999b) used the same equation assuming the percentage of pregnancies that have trauma as 6% and the percentage of trauma that is MVC as 67% which changed the estimated fetal deaths per year to 1600-4800.

Klinich et al. (1999b) used the total number of pregnant women in crashes with vehicle damage in which the occupant was killed, injured, or uninjured (128255) and multiplied that by the percentage of pregnancies that have trauma and subsequent fetal loss (1-3%). The result was an average number of fetal deaths from MVC trauma equal to 1283 to 3848 each year.

Moreover, Klinich et al. considered the total number of women injured in crashes with vehicle damage and multiplied that number by the percentage of women at childbearing age in the NASS database that experienced crashes with a change in velocity greater than 30 mph, between 15 and 30 mph, and less than 15 mph (Klinich et al. 1999b). The associated risk of adverse fetal outcome from the risk curve relating adverse fetal outcome to crash severity and the percentage of that number that was direct fetal deaths were used to determine an average number of fetal losses. This value plus the number of women killed estimates 1653 to 3887 fetal deaths each year.

A final range of all motor vehicle trauma fetal death rates for fetal ages equal to or greater than 20 weeks gestation is calculated from averaging the minimum and maximum approximations

from each of the 10 methods (Table 1). The range of rates is substantially narrowed to a low of 865 fetal deaths per year and a high of 2795 fetal deaths per year.

Table 1. Estimations of annual fetal death rate from motor vehicle crashes in the United States.

Author	*Brief Description*	*Minimum*	*Maximum*
Weiss	Pennsylvania Death Certificates	n/a	208
Weiss	US Death Certificates	92	n/a
Jernigan	NASS	157	n/a
Klinich	1-3% Fetal Loss of Pregnant Women Injured plus Pregnant Women Killed	462	1061
Klinich	Fetal Loss Adjusted for Crash Severity plus Pregnant Women Killed	496	n/a
Jernigan	Fetal Loss Calculated by DeltaV	743	1858
Pearlman	6.5% Trauma, 50% MVC, 1-3% Fetal Loss	1300	3900
Klinich	6.0% Trauma, 67% MVC, 1-3% Fetal Loss	1600	4800
Klinich	1-3% Fetal Loss of Pregnant Women in MVC with Damage	1283	3848
Klinich	Fetal Loss Calculated by DeltaV plus Pregnant Women Killed	1653	3887
	Average	**865**	**2795**

In conclusion, a summary is provided of fetal death rates as estimated in the literature. These 10 different methods have been incorporated in order to narrow the broad range. As a result, the average number of fetal fatalities per year in the United States from motor vehicle crashes range from 865 to 2795.

Pregnant Occupant Injuries

Automobile crashes are the largest cause of death for pregnant females (Attico et al. 1986) and the leading cause of traumatic fetal injury mortality in the United States (US) (Weiss and Strotmeyer 2002). In a three year study of fetal traumatic injury deaths in select states, 82% were a result of maternal injury in a motor vehicle crash (MVC) (Weiss 1999). Each year in the US, approximately 160 pregnant women are killed in motor vehicle crashes and an additional 700 to 2600 fetuses are killed when the mother survives (Klinich et al. 1999a, Klinich et al. 1999b). For comparison, Fatality Analysis Reporting System (FARS) data on child fatalities in the year 2005 indicate pedestrian, bike, and infant MVC fatality numbers are less than half the number of fetal deaths (Figure 5) (FARS 2005).

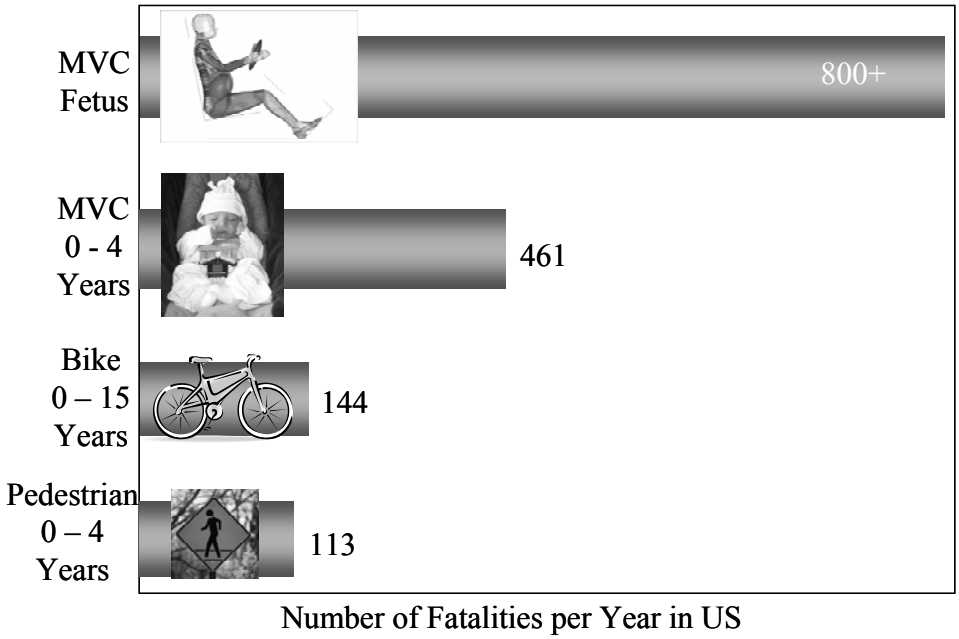

Figure 5: A comparison of fetal deaths to child deaths each year in the US (Klinich et al. 1999a, FARS 2005).

Pregnant occupant crash exposure has also been evaluated. According to a study using the National Automotive Sampling System Crashworthiness Database System (NASS CDS) for the years 1993 to 2003, the pregnant occupant is the driver in 75% of crashes (Duma et al. 2006b). She is the passenger in 22% of crashes and only in the rear seat 3% of the time. The most common impact direction is the front, 53% of the total, with a side impact being the next common impact direction, 26% of the occurrences (Figure 6).

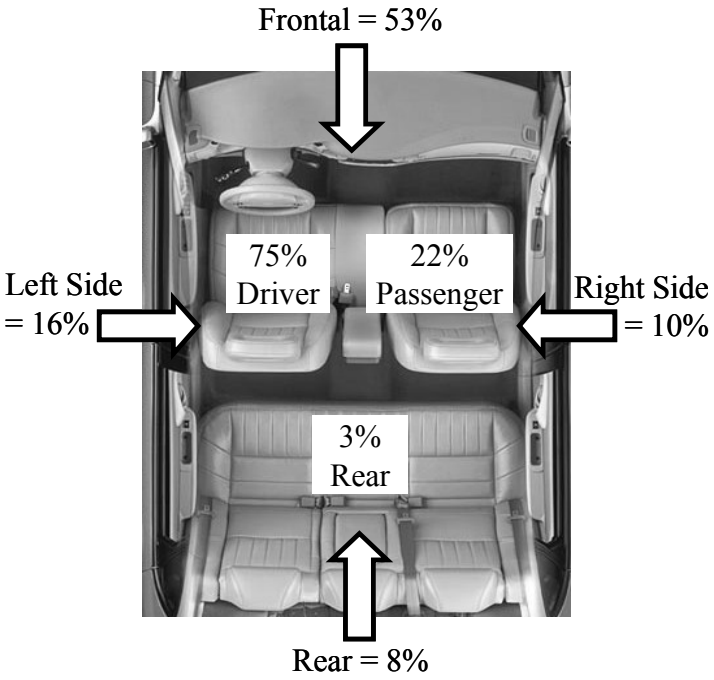

Figure 6: NASS CDS data indicating pregnant occupant position and impact direction during a motor vehicle crash.

The first way to protect the fetus is to protect the mother considering that maternal death has a near 100% fetal loss rate (Pearlman et al. 1990a). If the mother survives, protection of the fetus may best be accomplished by preventing placental abruption. Placental abruption, which is the premature separation of the placenta from the uterus, has been shown to account for 50% to 70% of fetal losses in motor vehicle crashes (Pearlman et al. 1990b). Information gathered from crash investigations shows that placental abruption can occur without other, more severe injuries, such as uterine rupture or direct fetal injury. However, when these more severe injuries do occur they are often accompanied by placental abruption (Rupp et al. 2001a). The different material properties of the uterus and the placenta are one reason they separate naturally after birth when the uterus contracts and the placenta maintains its shape (Pearlman 1997). A similar mechanism can occur prematurely in a motor vehicle crash if there is a large strain in the uterus. The relative motion of the two tissues causes a local failure of the uteroplacental interface (Pearlman 1997).

Current Research Tools

Since real world crash data for pregnant occupants is limited to a retrospective analysis and pregnant cadaver studies are not feasible, crash test dummies and computational modeling have been utilized to evaluate the risk of adverse fetal outcome. The most current version of a

pregnant female crash test dummy is called the Maternal Anthropomorphic Measurement Apparatus version 2B (MAMA-2B) (Rupp et al. 2001a). This pregnant surrogate is a 30-week gestation 5th percentile female crash test dummy. Validation tests have related the peak pressure inside the simulated uterus in the MAMA-2B with real world fetal loss risk data. The pregnant surrogate has been used in further analysis to determine the risk of fetal loss for different restraint conditions in a frontal impact.

A previously validated MADYMO computer model of a 30-week pregnant occupant has been created to investigate pregnant occupant biomechanics in motor vehicle crashes. The details of model development and validation are available in Moorcroft et al. (2003a, 2003b, 2003c) but are briefly summarized here. In order to create the model of the pregnant occupant, the finite element model of a pregnant uterus was inserted into the abdomen of a multibody human model. The finite element model anthropometry was designed to represent an occupant in her 30^{th} week of gestation based on data from Klinich (1999a) for the second-generation pregnant dummy. The abdomen consists of the uterus, placenta, and amniotic fluid. A fetus was not included because the injury mechanism that predominantly contributes to fetal loss is placental abruption, as described by Rupp (2001a). The human model is a 5^{th} percentile female (1.52 m tall, 50 kg) and the weight of the pregnant occupant model is 61.2 kg (135 lbs). This multibody human model provides biofidelic response of an occupant in a motor vehicle crash, while reducing the computational time compared to a more complex full finite element human model.

Four techniques were used to validate the pregnant model. First, a global biofidelity response was evaluated by using a seatbelt to compress dynamically the pregnant abdomen (Moorcroft et al. 2003c). The force versus compression results were within the published corridors from scaled cadaver tests (Hardy et al. 2001). Second, a similar validation procedure was performed with a 2.54 cm diameter rigid bar (48 kg) at an impact speed of 6 m/s and these results were also consistent with previous data (Hardy et al. 2001, Rupp et al. 2001a). The third technique involved validating the model against real-world crashes in order to investigate the model's ability to predict injury. Using crashes involving pregnant occupants, the model showed strong correlation ($R^2 = 0.85$) between peak strain at the utero-placental interface (UPI) as measured in the model compared to risk of fetal demise as reported in the real-world crashes over a range of

impact velocities and restraint conditions (Klinich et al. 1999b). The forth method compared the physiological failure strain from placental tissue tests to the failure strain measured in the model. Rupp presented a summary of pregnant uterine and placental tissue tests which suggest approximately a 60% failure strain for the UPI (Rupp et al. 2001a). This is in agreement with the model's prediction of 80% risk of fetal loss at a 60% strain in the UPI (Moorcroft et al. 2003a). In summary, the global, injury, and tissue level validation techniques all indicate the model is good at predicting injurious events for the pregnant occupant.

Previous studies have utilized a validated Mathematical Dynamic Modeler (MADYMO) computer model of a 30-week pregnant occupant to assess the risk of fetal loss based on occupant position, belt placement, impact direction, advanced restraint systems, and standard frontal barrier impacts (Moorcroft et al. 2003a, Moorcroft et al. 2003b, Moorcroft et al. 2003c, Moorcroft et al. 2004, Duma et al. 2006a, Manoogian et al. 2007a). Although pregnant occupant research has progressed with these tools, they are based on limited tissue data (Rupp et al. 2001a, Moorcroft et al. 2003a). In order to have more accurate research tools, better pregnant tissue material data are needed.

Previous Tissue Research

Placenta

Previous material testing on human placenta is limited. Pearlman (1999) tested full thickness placenta in quasi-static tension. These tests were sub-failure and only consisted of five specimens. The gage lengths of the specimens were 30 mm and they were pulled at a rate of 1.6 mm/s. For all five specimens, the average peak strain was 0.43 ± 0.16 and the average elastic modulus was 32.7 ± 18.6 kPa. The average peak stress was 15.6 ± 7.6 kPa. There are not data available in the literature to quantify the stress relaxation or rate dependent properties of placental tissue.

Uterus

Previous researchers have conducted material tests on nonpregnant, pregnant, human, and animal uterine tissues at quasi-static loading rates (Ohara 1953, Csapo and Goodall 1954, Conrad and Kuhn 1967, Yamada 1970, Pearsall and Roberts 1978, Mizrahi et al. 1980, Pearlman 1999,

Deyer et al. 2000, Rupp et al. 2001b). Research on uterine tissue material properties began in the early 1950's with a basic uniaxial tensile failure test at a quasi-static rate on animal uterus (Yamada 1970). Ohara found the tensile strength of a nonpregnant rabbit uterus in the longitudinal direction to be 177 kPa with a corresponding ultimate elongation of 1.5 (Ohara 1953). In addition to failure properties, Csapo and Goodall used electrical stimulation on rabbit uteri to quantify active muscle tensile strength. The result of their research was normalized force versus normalized length activation curves for myometrium under estrogen and progesterone domination (Csapo and Goodall 1954). Myometrium is the smooth muscle layer of the uterus.

To follow this work, research progressed to study pregnant versus nonpregnant myometrium. Wood pioneered human uterine tissue testing by using strips of human uterus that were extracted during a cesarean section at the incision location (Wood 1964). Uniaxial quasi-static tensile tests of these uterine samples of the lower uterine region had a failure true stress of 483 kPa and the elastic moduli of the samples at 69 kPa stress averaged to 1207 kPa (Pearsall and Roberts 1978). No failure strain was reported.

In 1967, Conrad used pregnant and nonpregnant human uterine samples in uniaxial quasi-static tensile tests with a step increase in load (Conrad and Kuhn 1967). Results of his study indicated the pregnant uterine tissue, from a cesarean section sample, had a lower elastic modulus at 69 kPa than the nonpregnant tissue from a uterus extracted during a hysterectomy. The respective elastic moduli from engineering stress-strain data were 586 kPa and 965 kPa (Pearsall and Roberts 1978).

By the late 1970's, Pearsall tested more than 20 nonpregnant human uterine specimens in uniaxial tension (Pearsall and Roberts 1978). Human uterine specimens were acquired from the fundal region of three nonpregnant uteri which had been removed in hysterectomy operations. The tests were at a quasi-static rate of less than 0.01 strains/s and had failure stresses that ranged from 550-2069 kPa. The maximum failure strain from those tests was in the range 0.30-0.95. Additional tests were completed to evaluate the tissue response to compressive loads. Results of these tests showed that the tissue has a stiffer response in tension than in compression.

Mizrahi's research goal was to measure strains during labor by placing strain rosettes on the skin and the uterus (Mizrahi et al. 1980). He recorded strains on 36 women while in their 36th to 42nd weeks of pregnancy. The peak strain recorded during labor was less than 0.03, which is inconsistent with other *in vivo* studies that report a much higher strain. Although Mizrahi's study has several limitations, the main result was that the uterus has an anisotropic response.

More recently, four sub-failure uniaxial tensile tests were completed on human uterine samples taken from the location of a cesarean incision and frozen before testing. At a quasi-static rate, the uterine tissue had an average peak stress of 45 kPa with a maximum strain equal to 0.65 (Pearlman 1999). Deyer and Ashton-Miller researched the uterine tissue response during labor by quantifying the uterine wall thickness from ultrasound measurements (Deyer et al. 2000). From this study, it was determined the uterus reaches maximum contractile strain before the placenta separates. The results reported contractile strains consistent with smooth muscle data. At the time of placental separation, the peak contractile uterine strains were 4.5 radial and 0.75 circumferential. A single failure test by Ashton-Miller performed on a uterus sample that included the uteroplacental interface (UPI) indicated 0.60 strain in the uterus when the UPI failed (Rupp et al. 2001b).

There are limitations with nonpregnant, cesarean, and hysterectomy uterus samples as material models for the fundal region of a pregnant uterus. A pregnant uterus undergoes several changes necessary to the care and delivery of the fetus. Hypertrophy, increase in elastic tissue, accumulation of fibrous tissue, and uterine stretching are all physiological changes to strengthen the uterus for care and delivery of the fetus (Cunningham and Williams 2005). A nonpregnant uterus will not have the same shape or structure as a pregnant one and therefore has different material properties. Moreover, whole uteri available from a hysterectomy are not accurate models because there is additional deterioration of the myometrial and endometrial layers if the uterus is from a postmenopausal donor (Cunningham and Williams 2005).

Additional considerations make these previous data sets unsuitable for use in modeling high rate impact events for pregnant occupants in motor vehicle crashes. All of the previous tests are at quasi-static rates but loading in a motor vehicle crash is at a dynamic rate. Soft tissue such as the

uterus is viscoelastic; therefore, it should be loaded at the rate in which the material properties are needed (Weiss et al. 1996, Sacks and Sun 2003). Moreover, several of the previous research studies did not include failure stress and strain information.

Research Objectives

This dissertation provides new and significant research to the field of injury biomechanics. Specifically, the research objectives focus on providing data for modeling of pregnant tissue. First, current research tools were used to evaluate the risk to a pregnant occupant in a severe frontal motor vehicle crash as well as during everyday activities. Next, uniaxial tensile tests were used to characterize the various layers of placental tissue from quasi-static to dynamic loading rates. The response of pregnant porcine uterine tissue in dynamic biaxial tension was quantified. Additionally, pregnant porcine uterine tissue and pregnant human uterine tissue material properties were determined in uniaxial dynamic tensile tests. As a whole, these objectives provide data that can advance pregnant occupant modeling and ultimately advance pregnant occupant protection in motor vehicle crashes. In order to achieve the ultimate goal of characterizing the uterine and placental tissues for pregnant occupant modeling, there are multiple research objectives that are addressed.

1. Determine the risk to a pregnant occupant from inertial loading only in a standard NCAP frontal barrier impact.
2. Determine the risk to a pregnant female from inertial loading only in everyday activities and exercises.
3. Determine the effect of the chorion layer on the stress versus strain curve, the ultimate stress, and ultimate strain for human placental tissue when tested in dynamic tension.
4. Determine the stress versus strain curve, the ultimate stress, and ultimate strain for the villous section of the placenta at quasi-static to dynamic strain rates.
5. Determine the stress versus strain curve, the peak stress, and peak strain for pregnant porcine uterine tissue when tested in biaxial dynamic tension.

6. Determine the stress versus strain curve, the peak stress, and peak strain for pregnant human uterine tissue and pregnant porcine uterine tissue when tested in uniaxial dynamic tension.

The result of this research will be material properties of the uterus and placenta to advance computational modeling of the pregnant occupant.

Chapter 2:
Pregnant Occupant Risk in a Standard Frontal NCAP Motor Vehicle Crash

Introduction

Previous studies have completed a retrospective analysis of pregnant occupant risk using data from real world motor vehicle crashes (Klinich et al. 2000). These data include mild to severe impacts with a range of vehicle type and restraint conditions. Because of the high incidence of fetal loss, a better understanding of the fetal risk associated with a MVC is needed. According to previous research, the pregnant occupant with a proper restraint in a severe motor vehicle crash has a 93% risk of fetal loss (Klinich et al. 2000). This study evaluates the risk of adverse fetal outcome with an ideal loading scenario. An ideal loading scenario is one where there is no abdominal compression or contact loading from the vehicle interior or restraints. Additionally there is no thoracic rotation causing an increase in abdominal pressure. Only the inertial loading to the uterus from the pelvic acceleartion pulse will be considered to evaluate the risk of adverse fetal loss.

A previously validated Mathematical Dynamic Modeler (MADYMO) computer model of a 30-week pregnant occupant has been a useful tool in researching risk of adverse fetal outcome for motor vehicle crashes involving a pregnant occupant (Moorcroft et al. 2003a). Adverse fetal outcome is defined as placental abruption, uterine laceration, direct fetal injury, premature delivery due to the crash, and fetal loss (Klinich et al. 1999b). Previous studies have utilized the pregnant occupant computational model to assess the risk of fetal loss based on occupant position, belt placement, impact direction, and advanced restraint systems (Moorcroft et al. 2003b, Duma et al. 2006b). The model calculates the risk of adverse fetal outcome, or fetal loss, on the basis of statistical analyses of case report data performed by Klinich, et al. (1999b). A two variable linear regression of the entire data shows that the uterine strain from the computational model is a good predictive measure of the risk of fetal injury due to placental abruption ($R^2 = 0.85$). The regression shows that uterine strain increases linearly to tissue failure

as the risk approaches 100%. This model was used in combination with data from the New Car Assessment Program.

The National Highway Traffic and Safety Administration (NHTSA) uses the New Car Assessment Program (NCAP) to rate vehicles based on their safety performance. The NCAP frontal test is a standardized test to crash a vehicle with an initial velocity of 56.3 kph (35 mph) into a fixed barrier with the full width of the front of the vehicle. This yields an equivalent change in velocity of 59.5-64.4 kph (37-40 mph) when the vehicle rebounds. During this test, the driver and front seat passenger of the vehicle are 50th percentile Hybrid III male crash test dummies. Although there are several instrumentation devices on board the vehicle and the dummies, only head and chest acceleration measurements are used for the injury criteria which determine the NCAP star rating. The highest NCAP rating is five stars and indicates a 10% or less chance of a serious injury. The lowest NCAP star rating, one star, is associated with 46% or greater chance of serious injury. The NHTSA definition of a serious injury is one requiring immediate hospitalization and may be life threatening. The purpose of simulating the pregnant occupant in a standard NCAP frontal barrier test for several different vehicles is to have a better understanding of the effect of pelvic acceleration pulse on pregnant occupant risk.

Methods

In order to use the data from the NCAP test in the pregnant occupant model, a few methodological assumptions were made. First, since the data collected is for the 50th percentile male, it was assumed that the 50th percentile male response was similar to what the 5th percentile female would experience in the motor vehicle crash. Second, it was assumed that the effect of the vehicle structure and restraints on the passenger kinematics is incorporated in the pelvic acceleration response. Moreover, only the linear acceleration of the pelvis was known, so the simulation assumes there was negligible pelvic rotation. Because there is no method to validate the interaction with the restraints and vehicle interior, the only cause of uterine strain in the simulations was due to inertial loading from pelvic acceleration.

The MADYMO simulations in this study modeled a total of twenty-six NCAP tests from the years 1996 to 2006. Three vehicle models were selected from each of the three vehicle classes:

passenger car compact (PC/C), passenger car medium (PC/Me), and sport utility vehicle (SUV). All of the tests chosen had a three point seatbelt and at least a front airbag for the passenger. Previous research shows the pregnant occupant is the driver in 75% of pregnant occupant related motor vehicle crashes (Duma et al. 2006a). However, the pregnant occupant in the driver seat also has more interaction with the vehicle interior in a motor vehicle crash (Moorcroft et al. 2004). Because the goal of this study is only modeling the inertial loading and not the contact loading to the abdomen, the simplified case of the pregnant occupant passenger was chosen. Data were collected from the front seat passenger pelvis accelerometer in each of the NCAP tests evaluated.

The MADYMO pregnant occupant model was locked in a standard sitting position as measured by Klinich et al. for the small female group at 30-weeks gestation (Klinich et al. 1999a) (Figure 7). By locking the occupant's joints, she moved as a rigid body in inertial space. Internally the uterus, placenta, and amniotic fluid were allowed to translate and rotate in the abdomen (Figure 8). Since no vehicle interior or restraints were added to the model, only the inertial response of the uterus is measured without external contact forces or compression due to thoracic movement. The pelvic linear acceleration data extracted from the NCAP tests was filtered to CFC600 per SAE J211. Applying the x, y, and z components of the pelvic acceleration pulse to the model for 0.125 seconds provided a simulation of the inertial effect pelvic acceleration would have on a pregnant abdomen. As a result, the uterus strained and rotated from the inertial loading. Since the assumed injury mechanism is placental abruption, the simulations output uterine strain at the fundus of the uterus for the duration of the impact. The peak von mises uterine strain corresponds to a risk of fetal demise using the linear relationship from the previous validation of this model. It is anticipated that this loading presents a best case scenario for the pregnant occupant in an NCAP style crash given no abdominal intrusion from the steering wheel or belt.

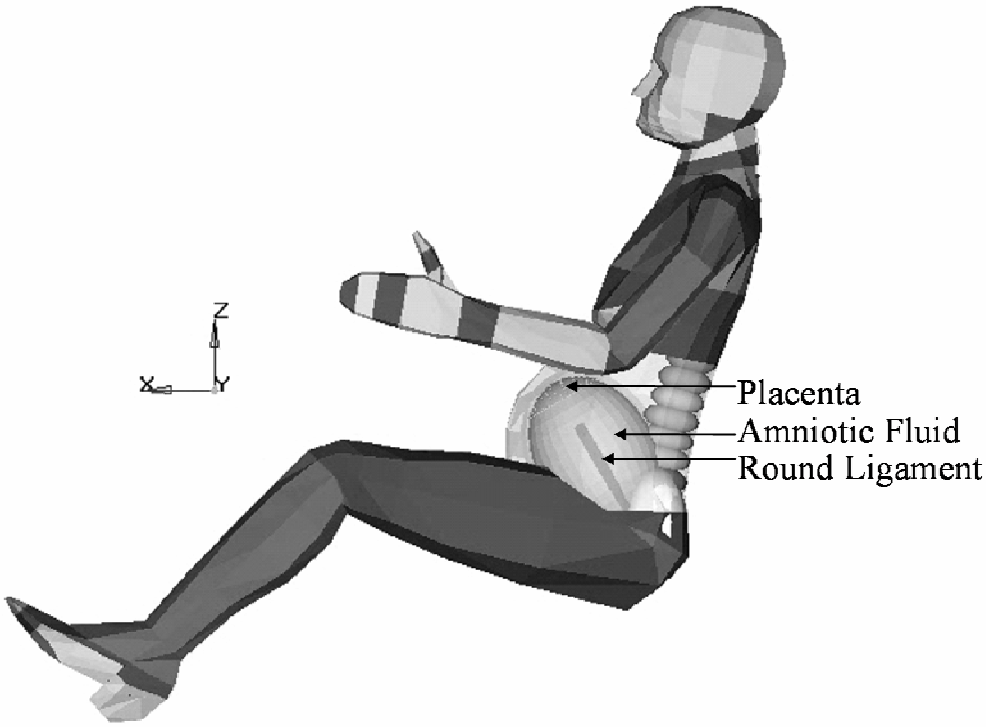

Figure 7: Pregnant occupant in standard sitting position.

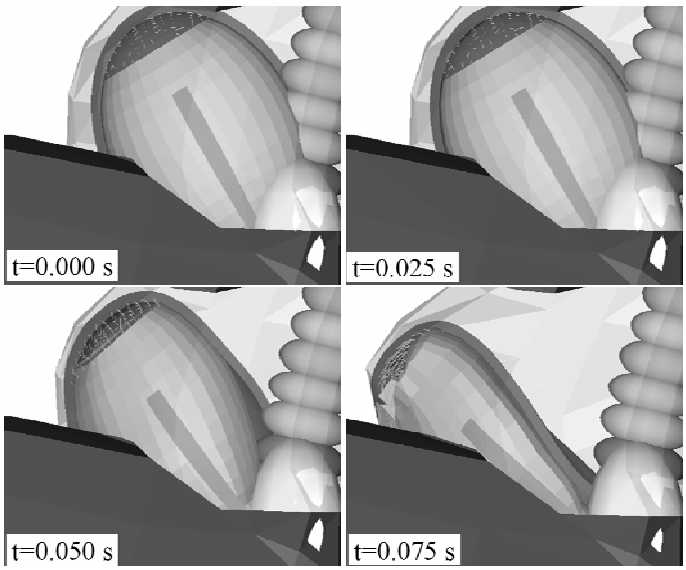

Figure 8: The simulation will emulate the response of the uterus from pelvic acceleration due to a motor vehicle crash.

Results

The results for this study include the risk of fetal loss for 26 different NCAP frontal barrier tests (Table 2). The average risk associated with these tests is 85 ± 13% with a minimum risk of 55% and a maximum risk of 100%. This information provides insight into how the vehicle type and pelvis acceleration correlate to the inertial loading of a 30-week pregnant uterus in a motor vehicle crash.

Table 2: A total of 26 simulations included nine vehicles in three vehicle size groups.

Vehicle Type	Model Year	NCAP Star Rating	Peak Pelvis X Acceleration (g)	Risk of Adverse Fetal Outcome (%)
PC/C 1	1996	5	49.4	87
	1999	4	48.5	74
	2006	5	44.0	55
PC/C 2	1998	4	55.6	82
	2003	5	42.4	77
	2005	5	46.3	97
PC/C 3	2000	4	73.0	100
	2002	4	92.8	100
PC/Me 1	1998	4	53.1	77
	2000	4	51.5	72
	2003	5	46.5	65
PC/Me 2	1996	4	42.2	88
	2000	5	59.6	75
	2004	5	39.3	72
PC/Me 3	1997	4	53.1	93
	2000	5	51.9	67
	2004	4	79.7	78
SUV 1	1998	3	74.2	100
	2001	4	84.3	100
	2004	5	59.7	80
SUV 2	1998	4	66.8	99
	2002	3	80.1	100
	2005	4	69.6	100
SUV 3	1996	3	66.4	95
	2001	4	67.5	100
	2004	4	58.1	83

Vehicle Type

When the risk of adverse fetal outcome is considered for each vehicle type, the medium size passenger car group had the lowest risk associated to it with an average of 76 ± 9%. The sport utility vehicle group had the highest average risk of 95±8%. The passenger compact car group was in between these two with an average risk of 84 ± 16%. The former group had the largest standard deviation with the minimum risk being 55% and the maximum risk being 100%. The only statistically significant difference ($p<0.001$) was between the medium passenger car and the sport utility vehicle groups (Figure 9). Within each vehicle group, the risk was evaluated for a vehicle model as the model year progressed. In the 17 comparisons made between the same model car and an increase in model year, the risk of injury did not always decrease over time (Figure 10). The peak uterine strain increased in five of these cases with the associated risk either increasing or remaining the same at 100% (Figure 11). The remaining 12 cases showed a decrease in uterine strain and risk with an increase in model year. Because some vehicles had poor performance in recent years, there is not a significant trend associated with an increase in model year.

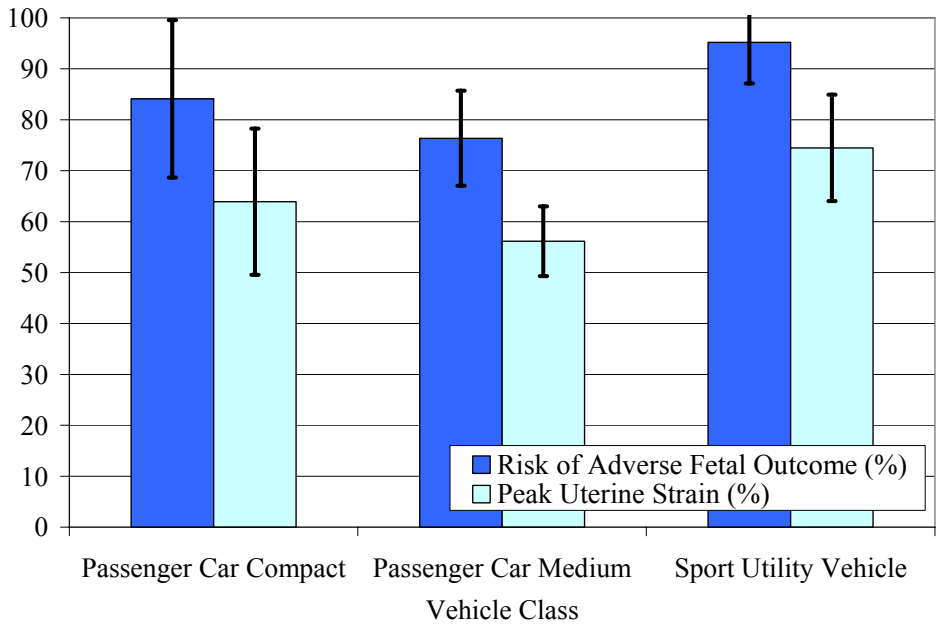

Figure 9: The risk of adverse fetal outcome and the peak uterine strain for each vehicle class.

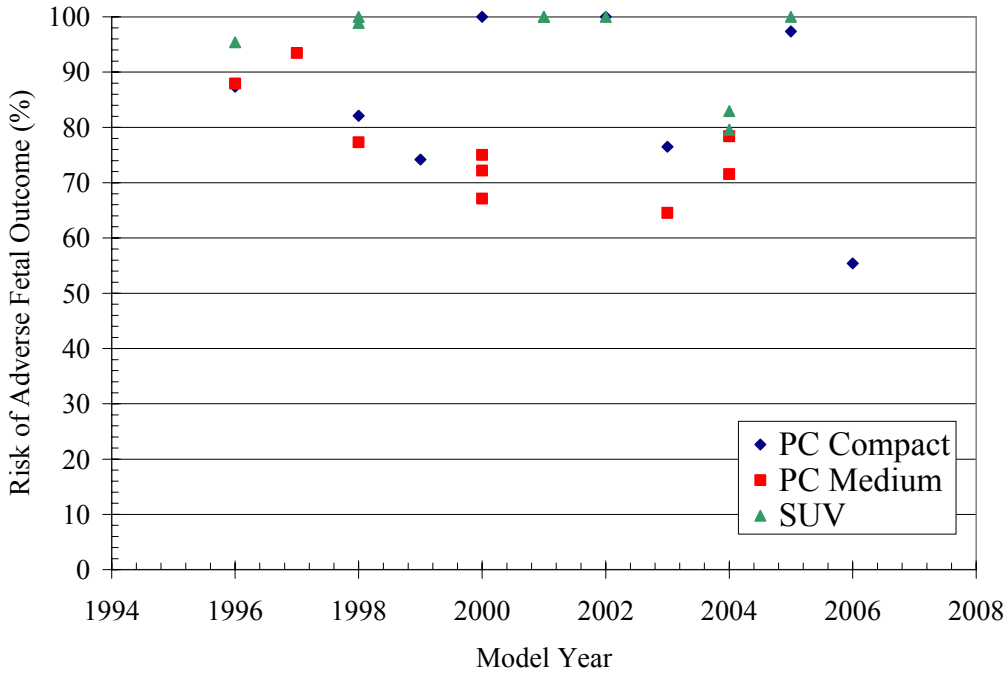

Figure 10: The risk of fetal loss versus vehicle model year.

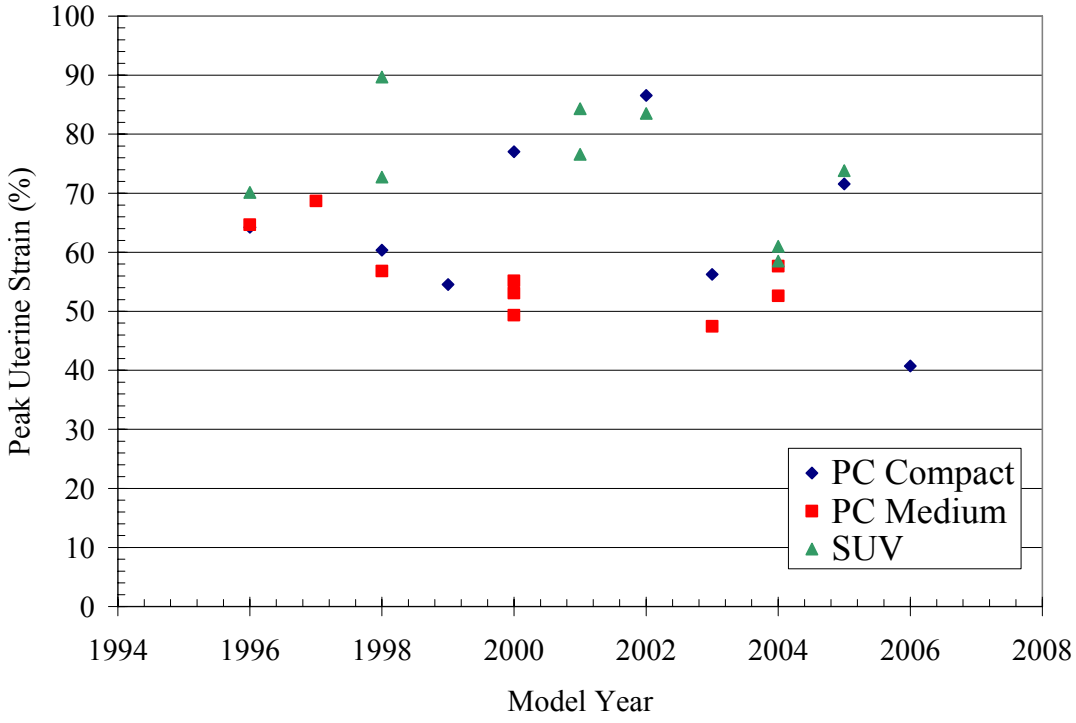

Figure 11: Peak uterine strain decreases in 12 of the 15 vehicle model year comparisons in this study.

Peak Pelvic Acceleration

The risk of placental abruption and peak pelvic acceleration in the x direction had a statistically significant relationship ($p<0.001$). The peak pelvic x acceleration is used rather than the resultant pelvic acceleration because in the frontal crash this value is dominant. Due to inertial loading only, 7 out of 8 vehicles with a peak pelvic acceleration above 67 g had a 100% risk of fetal loss (Figure 12). The relationship between peak pelvic acceleration and peak uterine strain is also shown, although a strain of above 74% corresponds to a 100% risk of fetal demise (Figure 13). Since all of these vehicles experience approximately the same change in velocity, the acceleration curves differ mainly in their peak acceleration and duration. This difference is seen best between the acceleration pulses that resulted in the least and greatest uterine strain (Figure 14). The acceleration curve with a peak pelvis x acceleration of 74.2 g maintains above a 5 g load for 0.0493 seconds and corresponds to the highest value of peak uterine strain, 90%. However, the acceleration curve with the lowest resulting peak uterine strain of 41% holds an acceleration above 5 g for 0.0889 seconds with a peak of 44.0 g. The longer duration, lower peak g acceleration curve results in a lower peak uterine strain and an analogous reduction in risk of fetal loss for the pregnant occupant.

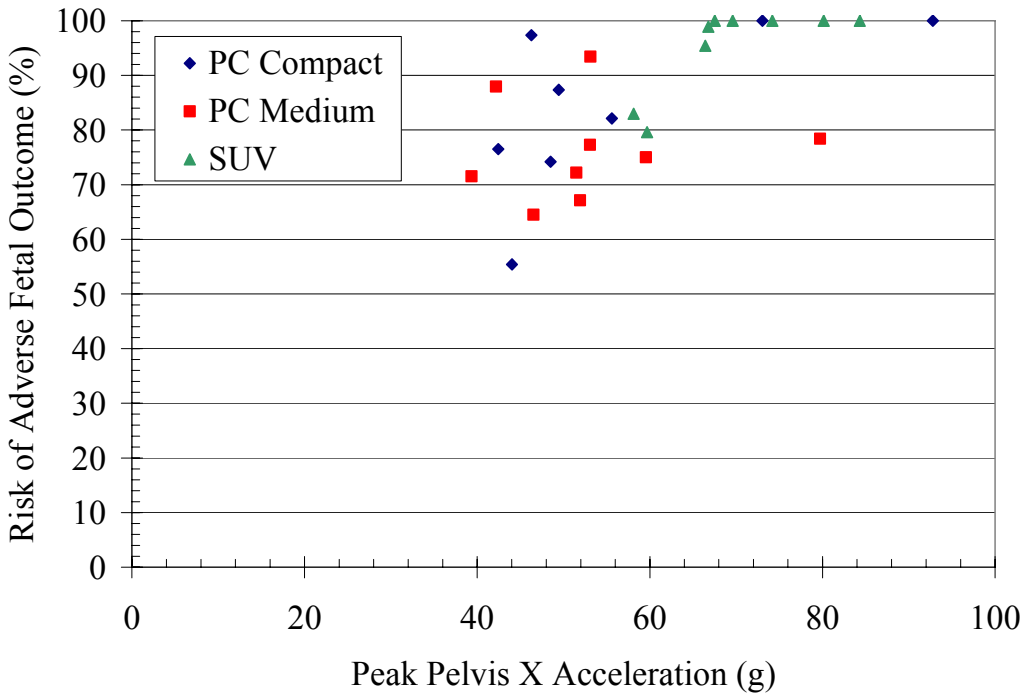

Figure 12: Overall, the SUV class had higher peak accelerations which correspond to higher risks of fetal demise.

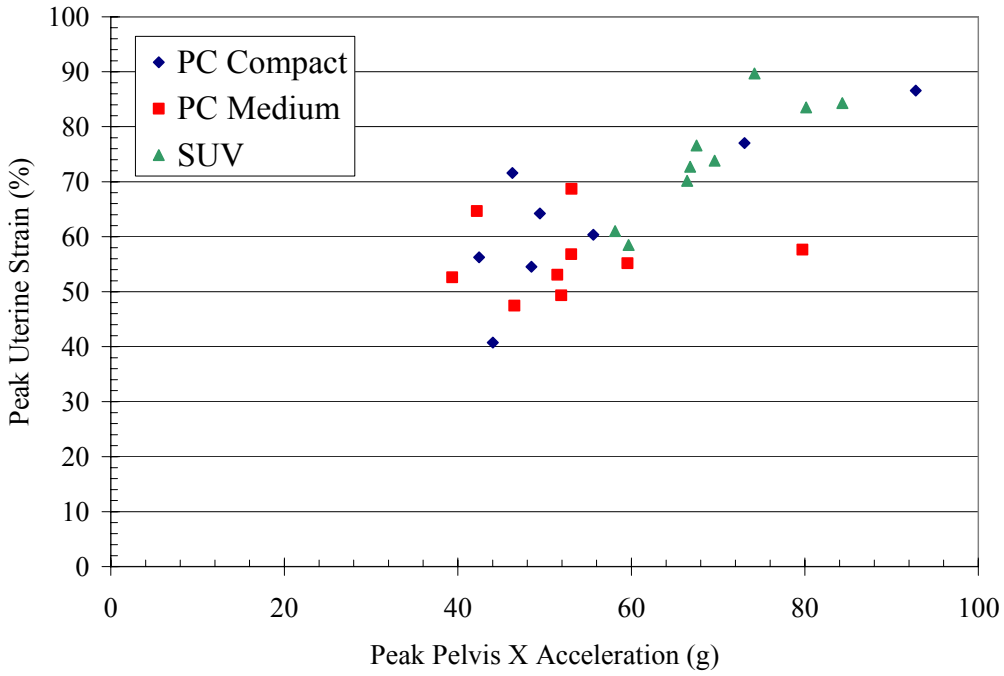

Figure 13: The linear relationship between peak pelvis x acceleration and peak uterine strain is significant but not strongly correlated due to differences in the acceleration profiles.

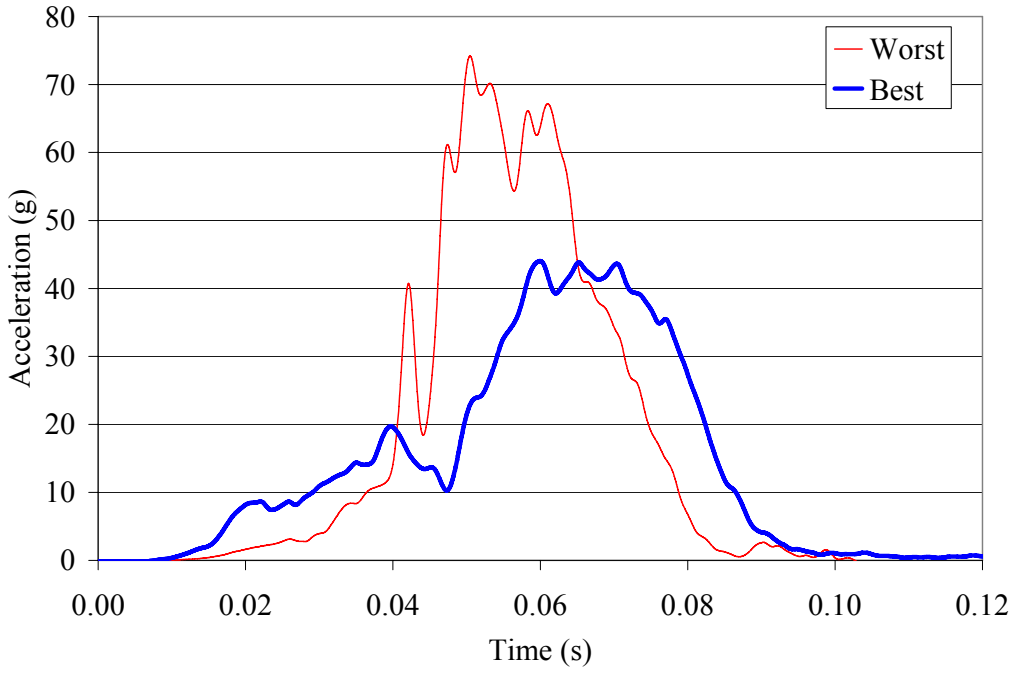

Figure 14: The acceleration pulses that resulted in the least and greatest uterine strain are plotted for comparison.

Although there was an increase in risk with an increase in pelvic acceleration, it was not strongly correlated. Some vehicles had similar peak pelvis x acceleration values and very different associated peak uterine strains. A closer evaluation of the acceleration profiles and their matching strain outputs addresses the weak correlation. When the pelvic acceleration and uterine strain profiles are plotted together, a time delay between the input and the response is present for the inertial loading. Due to the delay, a rapid change in pelvic acceleration does not have time to load the uterus. For example, an acceleration curve which has a peak duration of less than 5 milliseconds does not have a parallel large peak in the uterine strain (Figure 15). On the other hand, a curve with a steady increasing acceleration causes a similar steady increase in uterine strain (Figure 16). Therefore, two acceleration profiles with similar peak values can have different fetal injury risks associated with them.

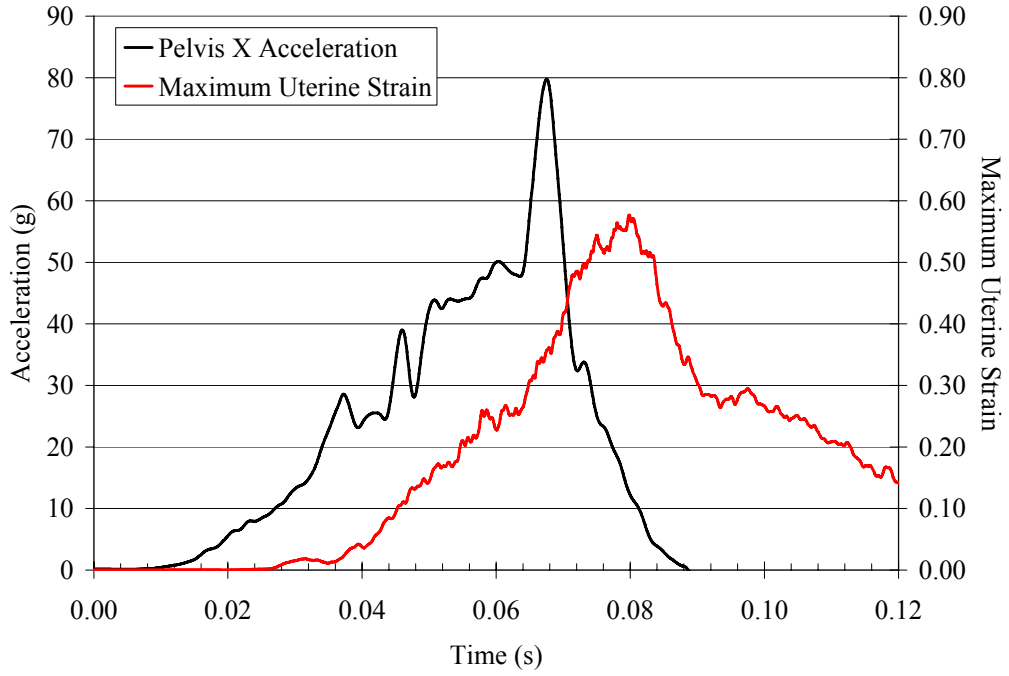

Figure 15: The large peak in the pelvis x acceleration does not have an equivalent large peak in the uterine strain measure.

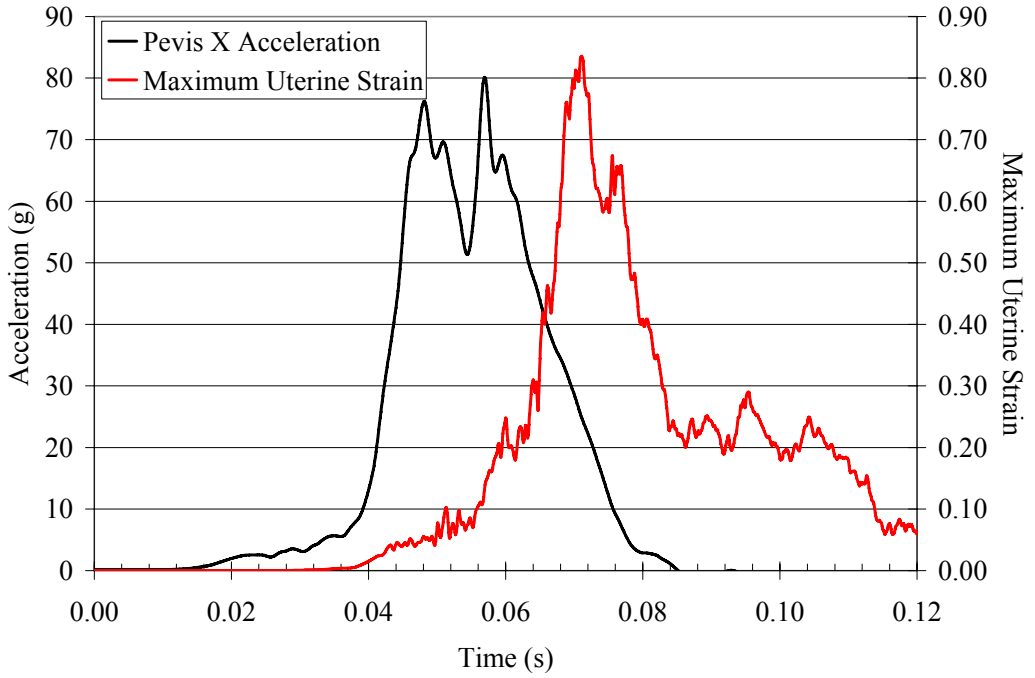

Figure 16: The steady increase in pelvis x acceleration has a corresponding increase in the peak uterine strain.

NCAP Score

The NCAP star rating for each vehicle indicates the risk of injury for the occupant based on head and chest criteria. The NCAP data used in this study was the pelvic acceleration. It was found that with an increase in the frontal NCAP star rating there was a decrease in peak pelvic acceleration for the x direction. The five star rating corresponds to a 48.8±7.2 g peak pelvic acceleration for the tests evaluated in this study. This value increased to 73.6±6.9 g for a low rating of three stars. Additionally, it was found that the star rating had a statistically significant relationship to the risk of fetal loss ($p=0.001$). The NCAP tests with 3 stars have an average risk of 99 ± 3% (n=3), 4 stars have an average risk of 89 ± 11% (n=14), and 5 stars have an average risk of 75 ± 13% (n=9) (Figure 17). These three groups are statistically different from each other and show that risk of adverse fetal outcome from placental abruption increases to almost 100% in a vehicle that passes the NCAP frontal barrier test with 3 stars. While the best NCAP rating of 5 stars indicates less than 10% risk of injury to the front passenger, it corresponds to a 75% risk of injury to the fetus.

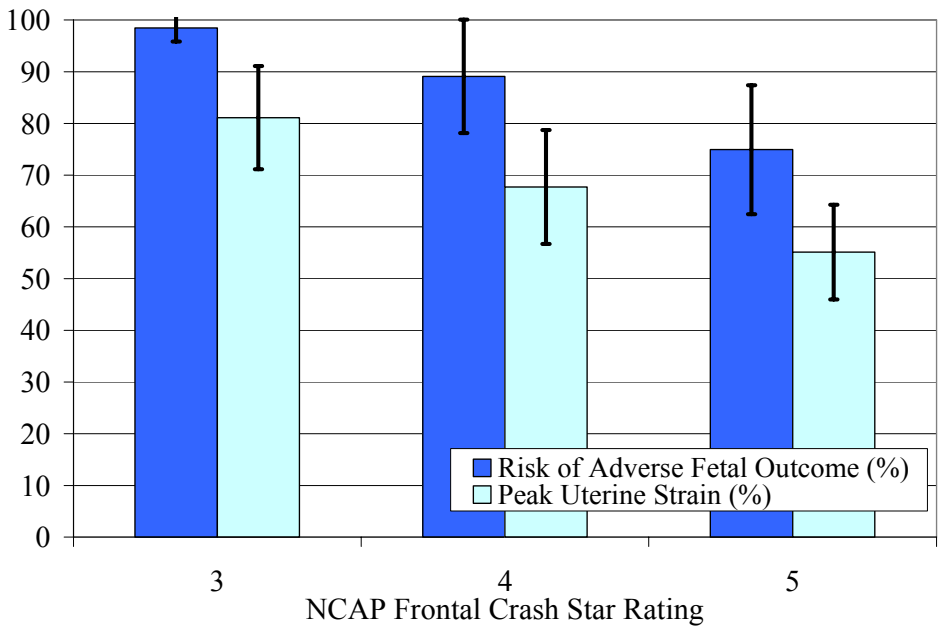

Figure 17: The best NCAP rating of 5 stars is indicative of a 75% risk of fetal loss in a 56.3 kph frontal barrier crash.

Discussion

Real world pregnant occupant motor vehicle crash data and pregnant crash dummy data confirms the results from this study. In an analysis of case data for pregnant occupants, the estimated risk of fetal loss for a crash severity of 56.3 kph (35 mph) is 93% when the occupant has the proper restraint (Klinich et al. 1999b) (Figure 18). This risk is the minimum value associated with an NCAP test since the actual change in velocity with the rebound is generally 59.5-64.4 kph (37-40 mph). A crash severity of 64.4 kph (40 mph) is associated with 97% risk of fetal loss. Previous research using the pregnant crash test dummy MAMA-2B evaluated the uterine pressure during a sled impact with a 52.6 kph (32.7 mph) change in velocity. The result of this impact with the dummy as the passenger and wearing a 3 point belt was a risk of adverse fetal outcome equal to 87.5%. The average risk calculated in the current study for the inertial loading condition during a front impact is 85 ± 13%. All three of these methods of evaluating the pregnant occupant with the proper restraint indicate a high risk of fetal loss for a crash severity equivalent to that of an NCAP test.

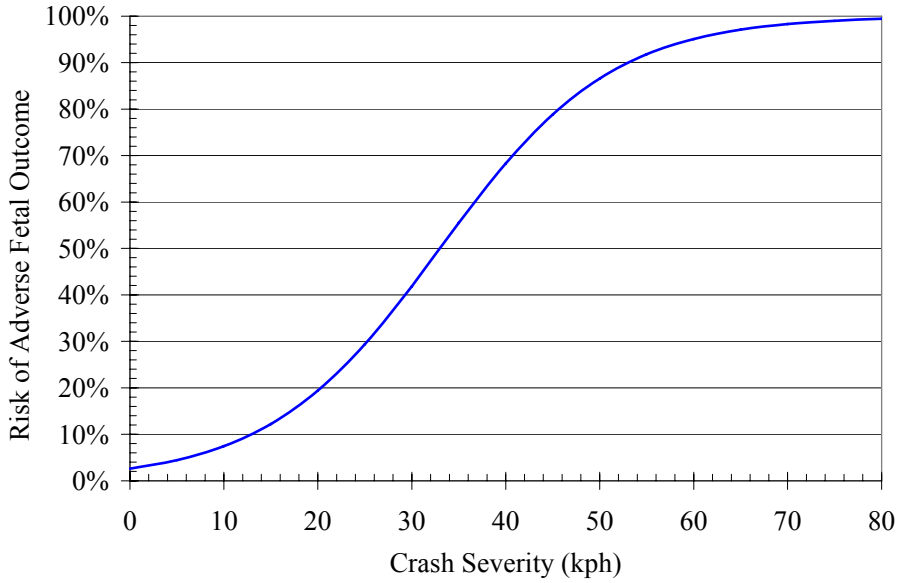

Figure 18: Risk of adverse fetal outcome as a function of crash severity for the properly restrained pregnant occupant indicates a 92% risk with a 56.3 kph impact (Klinich, 1999b).

Limitations of this study arise from the information available from a frontal NCAP barrier test. A pregnant surrogate is not used in the NCAP frontal barrier test so it is assumed that the kinematic response of the 50th percentile male is similar to that of a 30-week gestation 5th percentile female. Anthropometric differences would cause variations in the loading by the restraint system and ultimately the kinematics of the dummy. Since this cannot be accounted for, it is assumed that the pelvis of the small female has the same acceleration profile as that of the large male. As a result of a smaller mass and equivalent acceleration, a lesser force would be required by the restraints to stop the pelvis.

The data is not adequate to recreate the full body kinematics such as torso rotation and contact loading from the restraints or vehicle interior that contribute to uterine strain. Therefore, the model predicts the fetal outcome for an ideal loading scenario of a pregnant occupant in a 56.3 kph (35 mph) frontal impact. The assumption of a 3-point seatbelt positioned correctly minimizes the risk because placing the seatbelt too high on the abdomen can increase the risk of fetal loss by contributing unfavorably to uterine compression (Moorcroft et al. 2004). Additionally, using the shoulder belt and airbag decreases the risk of injury (Klinich et al. 1999b). These simulations do not consider contact loads from the seatbelt and vehicle interior to

the abdomen since they could not be validated. Contact loads can increase the risk of fetal complications because of abdominal compression. Early research on the pregnant occupant indicated that bending of the torso also increased uterine pressure (King et al. 1971). These effects are not modeled since the body is locked in a seated position.

Moreover, this model does not predict the additional complications for the fetus due to maternal injury. A 3 star NCAP rating for the front passenger indicates a 21% to 35% risk of serious injury to the mother. Serious injury to the mother further increases risk of adverse outcome to the fetus. Because the model simulations are evaluating an ideal scenario, the associated risk is expected to be greater in a real world crash for a 56.3 kph (35 mph) impact. Overall, the attachment of the placenta is very delicate, and the data from this study and previous studies indicate that prevention of placental abruption with such a severe impact may not be plausible.

Conclusion

Using a validated pregnant occupant computer model, this study assessed the risk of fetal loss for the pregnant front seat passenger in 26 different NCAP frontal barrier tests. Nine vehicles were selected that ranged 10 model years and three vehicle weight classes. The results from this study show that in an ideal loading condition the average risk of adverse fetal outcome is 85% due to inertial loading only. Moreover, all vehicle models for all years showed a greater than 50% risk of fetal loss. When compared to previous research, the results from this study are confirmed. Although this study is limited to computational modeling, it suggests even with the best case restraint system scenario the risk of fetal death is highly probable in severe crashes like those that the NCAP standard emulates.

Chapter 3:
Evaluation of Pregnant Female Injury Risk During Everyday Activities

Introduction

For severe maternal trauma that is life threatening such as head trauma or maternal shock, there is a corresponding 50% fetal loss rate (Pearlman and Tintinalli 1991). Conversely, non life threatening injuries are associated with less than a 5% fetal loss rate (1999). Current research efforts on the risk of adverse fetal outcome have focused primarily on trauma from motor vehicle crashes (Klinich et al. 1999b, Duma et al. 2006a). While there have been case studies on other trauma such as falls and abuse, more information is needed about the more common everyday activities that pregnant females experience. The American College of Obstetricians and Gynecologists recommends exercise during pregnancy to maintain a healthy gestation (2003). However, it is unclear the level of exercise that is safe for the pregnant female. The purpose of this study is to use acceleration traces from exercises performed by non-pregnant small females and assess risk of fetal loss by simulating these exercises using the pregnant computational model.

Methods

A previously validated Mathematical Dynamic Modeler (MADYMO) computer model of a 30-week pregnant female has been created to investigate pregnant occupant biomechanics in motor vehicle crashes. This model has been a useful tool in researching risk of adverse fetal outcome for motor vehicle crashes involving a pregnant occupant (Moorcroft et al. 2003a). Adverse fetal outcome is defined as placental abruption, uterine laceration, direct fetal injury, premature delivery due to the crash, and fetal loss (Klinich et al. 1999b). Previous studies have utilized the pregnant computational model to assess the risk of fetal loss based on occupant position, belt placement, impact direction, and advanced restraint systems (Rupp et al. 2001a, Duma et al. 2006a). This study used the model to consider the risk of fetal loss from everyday accelerations.

In a previous study to evaluate the magnitude of thoracic and lumbar accelerations in everyday activities, healthy volunteer subjects were asked to perform six daily activities (Ng et al. 2006). Four of these subjects were categorized as small female because their average height and weight corresponded to the anthropometric target size for a Hybrid III 5th percentile female. The subjects had an average height of 1.58 ± 0.04 m and an average weight of 53.64 ± 2.45 kg. The activities performed included sitting in a chair normally, walking at 1.3 m/s, running at 2.7 m/s, performing jumping jacks, achieving maximum vertical leap in place, and jumping off of a step 20 cm high. All subjects read and signed an informed consent form and had the opportunity to withdraw from any or all parts of the testing at any time. All test procedures were reviewed and approved by the Virginia Tech Institutional Review Board.

Each subject was instrumented with three linear accelerometers (Endevco 7596A, 30G, San Juan Capistrano, CA) mounted posterior to the L5 vertebrae and data were recorded at a sampling frequency of 2 kHz. The accelerometers were secured directly onto the skin using adhesive tape. Additionally, foam covered the accelerometer package and an elastic bandage was wrapped around the body to hold the accelerometers in the proper position for the duration of the testing. For each activity, the acceleration curves chosen for computational modeling were for the individual with the highest peak acceleration and the individual with the lowest peak acceleration. This established a range of expected acceleration profiles for one activity.

Although the subjects in the previous study were not pregnant, they provided an approximation for the acceleration profile of a small female performing the everyday activities. Therefore, to approximate the risk for a pregnant female, the acceleration profiles recorded were applied to the pregnant computational model. Each acceleration profile, the maximum and minimum for an activity, had a corresponding pregnant female computer simulation. For the simulations in this study, the MADYMO pregnant model was locked in an upright position. By locking the joints in the model, she moved as a rigid body in inertial space so that the uterus, placenta, and amniotic fluid were allowed to translate and rotate in the abdomen in response to the acceleration input. The three accelerations in the X, Y, and Z directions for each acceleration profile were applied to the MADYMO pregnant model. Applying these accelerations to a locked model calculated a risk for only the inertial response of the uterus. All other body motion was excluded from the simulation. The peak fundal uterine strain in the model corresponds to a risk of fetal demise

using the linear relationship from the previous validation of this model. Additionally, linear regression analyses were used to determine if a strong correlation existed between peak acceleration data and corresponding risk of injury.

Results

The results for this study are 12 simulations with an average risk of fetal loss equal to 10.0 ± 4.1%. The minimum risk from the simulations is 3.1% for walking and the maximum risk is 18.8% for running. Each of the six activities has a minimum and maximum risk associated with it based on two participant acceleration responses (Figure 19). An increase in peak acceleration is significantly related with an increase in risk of injury for the X, Y, Z, and resultant acceleration profiles ($p<0.01$). However, when the peak accelerations for the X, Y, and Z directions are related to the risk of injury using linear regression, the correlations are weak ($R^2<0.5$). The peak resultant accelerations for the low impact activities such as walking and sitting are less than 2 g. This is lower than the peak resultant acceleration values for the high impact events like running and jumping jacks which can range from approximately 2 to 10 g (Table 3).

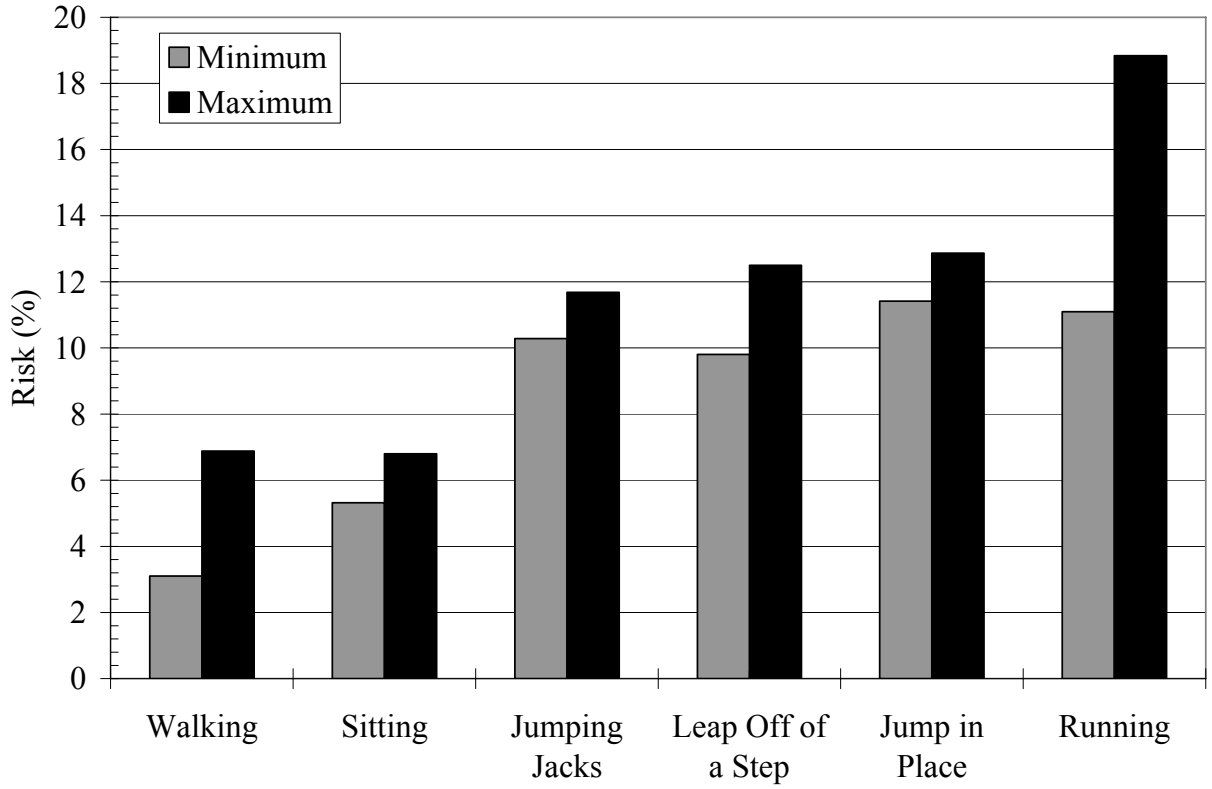

Figure 19: Each activity is presented with a corresponding maximum and minimum risk of fetal injury from the acceleration profiles recorded during everyday activities.

In addition to the peak of the acceleration trace, the profile of the curve can be related to the uterine strain in the model and therefore the risk of adverse fetal outcome. For an activity that has a cyclic loading such as repetitive jumping jacks, there are corresponding peak events in the uterine strain from the computational model (Figure 20). These peak events have a short duration of 0.15 seconds and a sharp increase in the uterine strain. Conversely, for a lower level activity such as sitting in a chair, there is one rise in the uterine strain as a response to the acceleration pulse that has a longer duration of greater than one second (Figure 21). The risk presented for each activity is the total probability of an adverse fetal outcome given the corresponding uterine strain for the duration of the event.

Table 3. The activities are tabulated with their risk of adverse fetal outcome and peak acceleration in all directions.

Activity	Risk of Injury (%)	Peak Acceleration (g)			
		Absolute X	Absolute Y	Absolute Z	Resultant
Walking	3.1	0.74	0.58	0.53	0.92
	6.9	0.43	0.38	0.63	0.67
Sitting	5.3	0.43	0.16	0.40	0.45
	6.8	0.80	0.50	1.51	1.70
Jumping Jacks	10.3	2.19	1.60	5.45	5.67
	11.7	4.09	1.54	10.52	10.56
Leap Off of a Step	9.8	2.47	1.75	2.21	2.92
	12.5	6.54	1.28	9.01	9.75
Jump in Place	11.4	1.47	0.95	7.10	7.15
	12.9	3.27	1.44	1.95	3.49
Running	11.1	1.19	1.34	2.03	2.13
	18.8	1.78	1.34	2.55	2.59

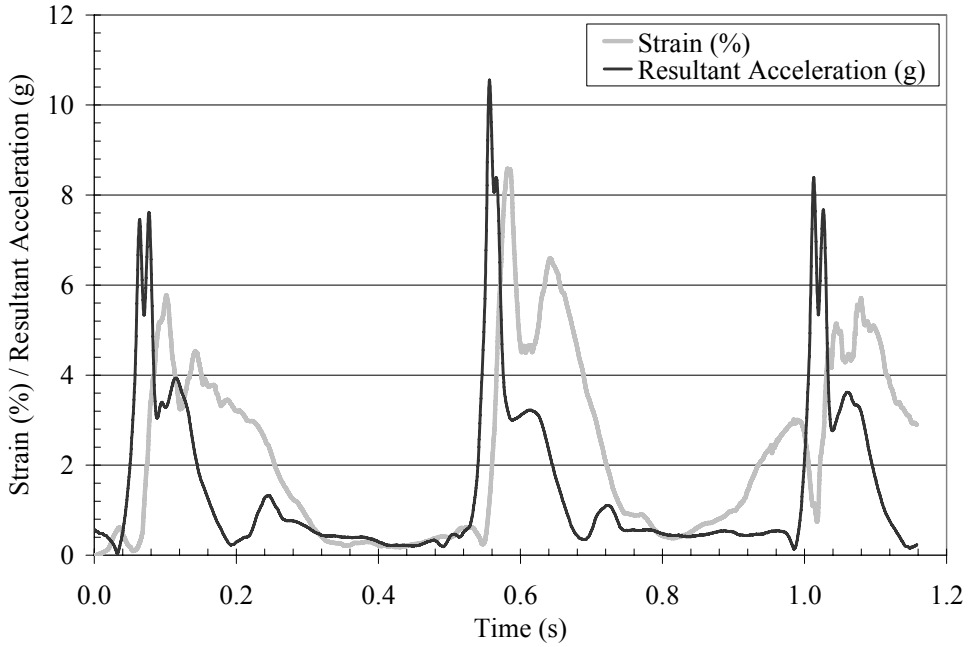

Figure 20: The resultant acceleration peaks during cyclic loading from jumping jacks and the corresponding short duration peaks in the uterine strain.

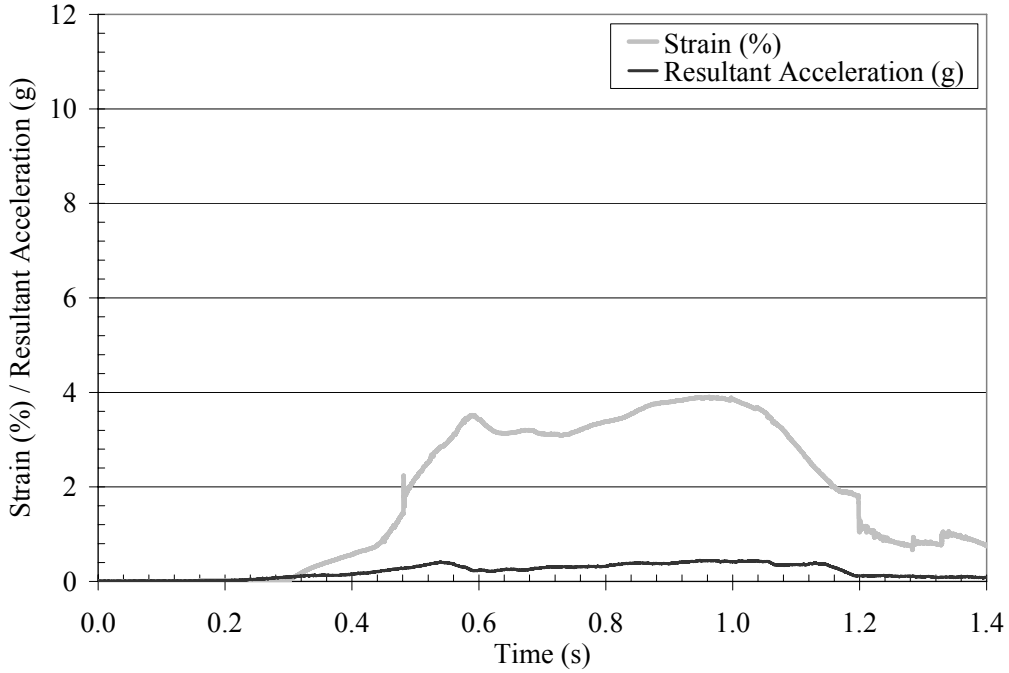

Figure 21: Sitting in a chair is one event with a long duration and low peak acceleration with a low peak uterine strain.

Discussion

This study presents the risk of adverse fetal outcome in a pregnant female for six daily activities based on the accelerations of four small females that are not pregnant. The low impact exercises had an average risk of 5.5 ± 1.8%. The high impact exercises had an average risk of 12.3 ± 2.8%. The low impact exercises have effectively no risk when taken in context with the validation of the computational model from motor vehicle crash data. The range of validation for the model was an impact with a risk of fetal loss equal to 10% to 90% (Moorcroft et al. 2003a). However, the pregnant female can have an appreciable risk of adverse fetal outcome for the higher impact activities. The American College of Obstetricians and Gynecologists promotes regular exercise during pregnancy for its health benefits (Artal and O'Toole 2003). Furthermore, the risk of adverse fetal outcome from daily activities is dependent on the health of the mother; poor health habits can increase the risk of placental abruption (2003).

The computational model's validation for the calculation of risk based on uterine strain was for a dynamic loading condition in a motor vehicle crash at 30 weeks gestation. As a result of validating this model to a very severe level of impact, the model is only an approximation to the risk of fetal loss during events such as daily activities. However, the results show that the model is a reasonable approximation for these activities and distinguishes between a low-level activity such as sitting versus a high impact activity like running. The peak acceleration values could not be used solely to predict risk of fetal loss in this study. The rate of acceleration as well as the duration of the pulse contributed to the resulting strain in the uterine wall. Although the entire kinematic response of the uterus is necessary to predict injury risk, there was a trend of increasing risk associated with an increase in peak resultant acceleration.

A limitation of this study is that it used non-pregnant female volunteers. If a study were performed on pregnant females completing daily activities, it is possible that the acceleration profiles for those individuals would be different from those reported in this paper. The pregnant female would have weight and stature changes that would affect her kinematics when carrying out activities such as sitting, walking, jogging, etc. However, for the purpose of this study, the small female is a reasonable approximation.

Conclusion

In summary, this study uses a computational model to asses the risk of adverse fetal outcome from six exercises: sitting, walking, jumping jacks, leaping off of a step, jumping in place, and running. Each exercise has a corresponding maximum and minimum risk of adverse fetal outcome for a pregnant female based on acceleration traces from non-pregnant small females performing the exercises. The results for the four low impact exercise acceleration profiles have an average risk of 5.5 ± 1.8%. This is a very low risk of adverse fetal outcome. The 8 high impact exercises simulations had a more appreciable risk average of 12.3 ± 2.8%. In conclusion, this study confirms a low risk of adverse fetal outcome for a healthy pregnant female during low impact exercise events. However, it is important for pregnant females to consult their physician regarding their level of physical activity during pregnancy.

Chapter 4:
Effect of Chorion on Dynamic Tensile Material Properties of Human Placenta

Introduction

The microstructure of the human placenta is important in modeling the material response to dynamic loading in tension. The human placenta connects to the uterine wall, usually in the fundus of the uterus, and provides a means for the maternal-fetal exchange of gases and nutrients (Ramsey 1975). However, because of the different roles it serves for the mother and fetus, there are microstructure differences on the maternal and fetal sides of the placenta (Cunningham and Williams 2005). The fetal side of the placenta includes the chorionic plate. This layer of the placenta is filled with fetal blood vessels that originate at the umbilical cord and radiate outward to the edge of the placenta in a dense network. The maternal side of the placenta is a network of villi and intervillus spaces. Between the maternal side of the placenta and the uterus is the uteroplacental interface. This decidua basalis layer is where the placenta separates from the uterus during placental abruption. The purpose of this study is to quantify the loading and the failure properties of chorion layer and the placenta without the chorion attached in uniaxial tension at dynamic loading rates. While this does not address the strength of the uteroplacental interface, it does provide material data for computational models to accurately represent the response of the placenta to dynamic loading conditions.

Methods

A total of 30 uniaxial tensile tests were performed on 6 whole placentas. Donor tissue followed the Wake Forest University Baptist Medical Center Institutional Review Board informed consent procedures. Following delivery, the tissue was stored in a saline solution and tested within 36 hours. From each placenta there were 3 to 4 tests of the maternal side of the placenta at a dynamic strain rate of 7.00 strains/s. This strain rate represents loading expected in a motor vehicle crash as determined from previous computational modeling (Moorcroft et al. 2003c). For two of the placentas, additional tests were performed on the chorion layer to obtain material

properties at the same strain rate. There were a total of 10 tests on the chorion layer and 20 tests on the non-chorion structure of the placenta.

All of the uniaxial tensile tests were performed on coupon specimens from either the maternal surface of the placenta or the chorion layer from the fetal side of the placenta. Thin slices of placenta were acquired from the whole placenta using a tissue slicer with a wet rotating blade. This allowed the maternal surface of the placenta to be sectioned into 5 mm slices and separated from the chorion layer of the placenta (Figure 22). Because the placenta function requires it to have a lobe structure, the slices of the placenta had discontinuities. Sections with a continuous structure were chosen for acquiring a smaller coupon section. Each piece of tissue was aligned before stamping to ensure uniformity as much as possible with each sample. Guide rods provided a means for aligning both a stencil and ultimately the stamp. A coupon was then stamped out of the tissue using a steel bent stamp. A sharpened edge to the steel stamp minimized sheer stress in the tissue during the stamping procedure. The result of the tissue stamping procedure was several coupons from the same donor tissue with a uniform shape (Figure 23). Each coupon was kept hydrated throughout the preparation and prior to testing. Due to the process of obtaining the chorion layer of the placenta, the chorion slice had a larger thickness than 5mm. Therefore, those specimens had an average cross sectional area that was larger than the maternal side specimens. The average cross sectional area of the chorion specimens is 42.2 ± 13.2 mm. The maternal side specimens have an average cross sectional area of 27.1 ± 7.9 mm.

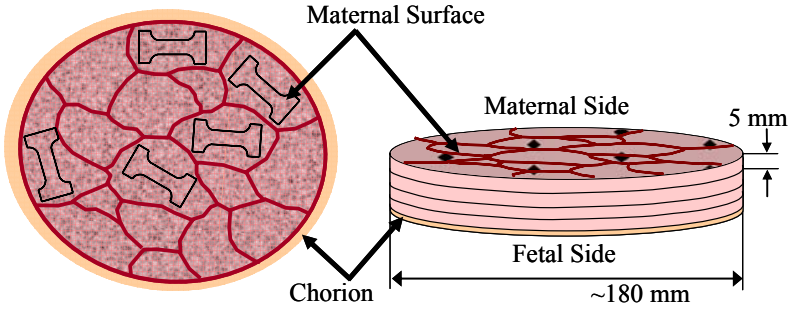

Figure 22: Each placenta is sectioned into 5 mm slices.

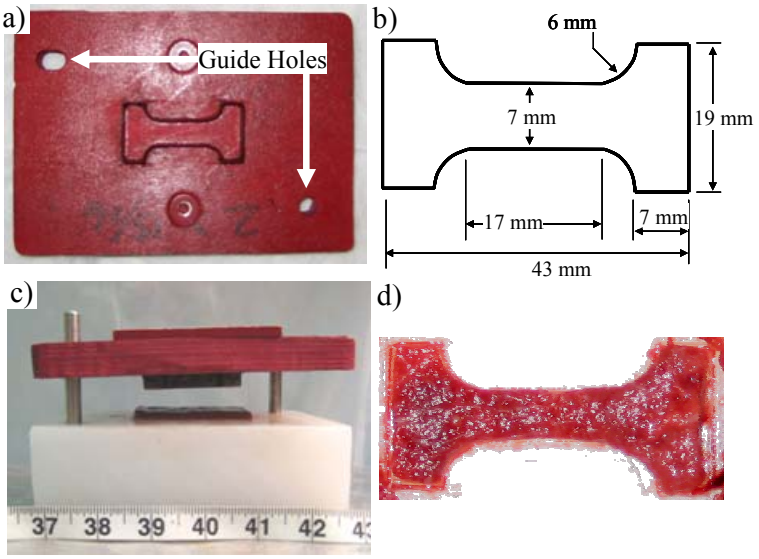

Figure 23: a) A steel bent stamp is used to cut the tissue into a dog bone shape. b) The stamp provides uniform tissue samples. c) Guide rods are used to align the stamp with the specimen. d) The coupon shape is cut where the tissue has a uniform consistency.

A custom designed system of linear motors was used for uniaxial dynamic tensile tests of placental tissue coupons (Figure 24). The system included one multi axis controller (Parker ACR9000, Irwin, PA) that served as a power supply for a motor driver (Parker ViX, Irwin, PA) which controlled the two linear motors with stages (Parker Daedal MX80S, Irwin, PA). The two individual stages were each instrumented with a load cell (OMEGA LC10, 10 lbf, Stamford, CT), potentiometer (Space Age Control, 160-1705, 540 mm, Palmdale, CA), and accelerometer (Endevco 7264B, 2000 G, San Juan Capistrano, CA. On each side of the test specimen, the direct path from the tissue clamp went through the load cell and was rigidly connected to the linear motor stage. The inertial load of the mass in front of the load cell was multiplied by the acceleration to compensate the measured reaction load. Synchronous motion of the motors allowed both of the stages to pull the tissue in tension at the same time for an overall velocity which corresponded to the desired strain rate.

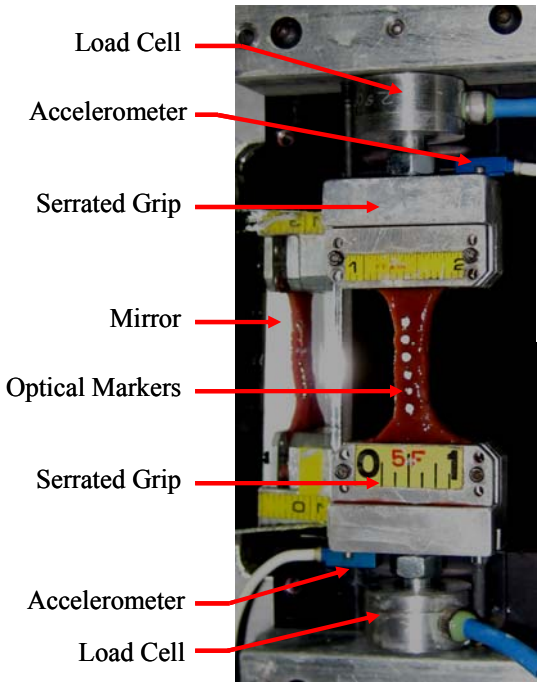

Figure 24: The specimen is mounted between two serrated grips which are instrumented with both a load cell and an accelerometer while high speed video records the test event.

Each specimen was mounted in the testing setup with the same initial conditions. The top grip assembly was removed and laid flat to align the specimen in the grip along the centerline of the loading axis. After the grip was secured, the top grip assembly was then reattached to allow the specimen to rest hanging in 1 g tension. By supporting only its own weight, the tissue had a standard but minimal preload condition. With the tissue hanging, the specimen was clamped in the bottom grip with no additional preload. Optical markers were applied to the tissue after the specimen was mounted.

Local stress and strain were calculated for each specimen. Local deformation was recorded using high-speed video (Phantom V4, Wayne, NJ) at 500 frames per second with 512 by 512 resolution. Optical marker tracking was performed with TEMA® Advanced Motion Analysis Software (Linköping, Sweden). Using the configuration for these tests, the error in the motion analysis is ± 0.030 mm. The optical markers on either side of the location where the specimen tore were used to calculate the local strain. In addition, a mirror aligned at a 45 degree angle was mounted next to the specimen so that the side of the specimen could be viewed in the high speed video. The measured displacement data were fit with a 5^{th} order polynomial. The average R^2

value for the displacement curve fit is 0.999 ± 0.001. Similarly, the measured force data were fit with a 5th order polynomial. The average R^2 value for the force curve fit is 0.994 ± 0.009. Local stress was acquired by determining the location on the specimen where failure occurred and then taking the width and thickness of the specimen in that location from the pretest pictures as the initial cross sectional area. The error in the pretest pictures is ±0.12 mm. The cross sectional area at the time of failure is calculated using the local strain and a Poisson's ratio value of 0.49. This value has been determined in previous placental tissue testing (Manoogian et al. 2007c). The stress and strain data are reported for each specimen until failure was evident in the video. Although, the tissue could have been still supporting the load, the optical markers were not accurately representing the strain in the tissue once there was sub-failure.

A two sample t-test procedure was used to determine statistically significant differences between the chorion and non-chorion test series for both failure strain and failure stress. The peak stresses and strains at failure were also compared between donor groups to tests for any significant differences. Additionally, a standard method of determining the characteristic average was used for each group of tests at one strain rate (Lessley et al. 2004). This process began with normalizing each strain curve to its respective maximum. Interpolation routines determined the stress for each test at set increments of strain. Stress values for all tests at that rate were averaged to determine one value at each strain. The strain data that corresponds to these stress values were obtained by multiplying the normalized strain by the average maximum strain of all tests. The result of this process was an average stress versus strain curve for all of the chorion tests and one for all of the non-chorion tests. Standard deviations of the stress and strain values were also calculated for each group of tests. Elastic modulus values were obtained from the characteristic average curves in the linear region before failure.

Results

Stress versus strain curves for the chorion layer and the maternal side of the placenta are presented for dynamic tensile tests. The data are reported in Green Lagrangian strain and true stress values. Frames from the high-speed video of a maternal side test show the tissue specimen fails in the gage length of the dog bone shape coupon (Figure 25). This is also true of the chorion tests.

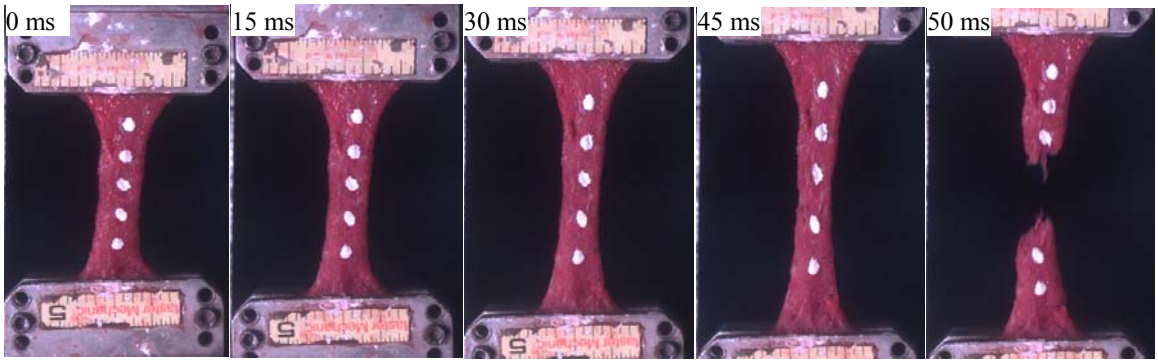

Figure 25: Video captures of one test show a typical failure of a placental specimen pulled in uniaxial tension at 7.0 strains/s.

All of the stress versus strain data are plotted together for the maternal side of the placenta with the characteristic average and the standard deviations for the failure stress and strain (Figure 26). The average failure stress for the maternal side of the placenta was 18.6 ± 5.4 kPa. The corresponding failure strain was 0.56 ± 0.14. The elastic modulus in the linear region of the characteristic average for this group of tests was 45.0 kPa. For the test series that included the chorion layer of the placenta, the material data are plotted together with the average and standard deviations for the failure stress and strain (Figure 27). The failure strain, 0.61 ± 0.09, was similar to the maternal side only tests. However, the failure stress for the chorion layer was 167.8 ± 51.3 kPa. This value is higher than the failure stress for the placental tissue that did not include the chorion layer. As a result, the elastic modulus for this group of tests was much higher with a value of 445.8 kPa.

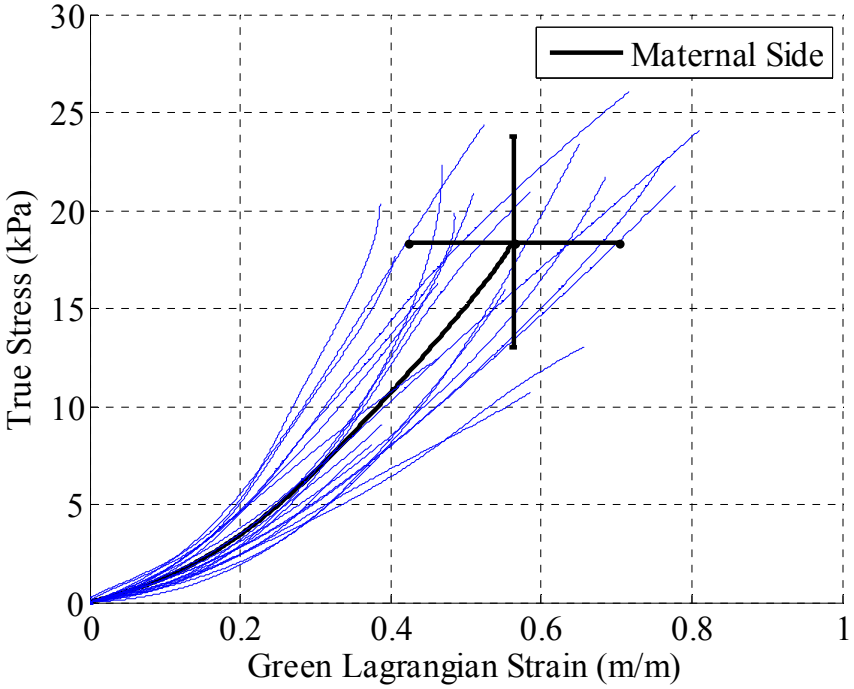

Figure 26: All of the tests for the maternal side of the placenta have similar stress versus strain curves.

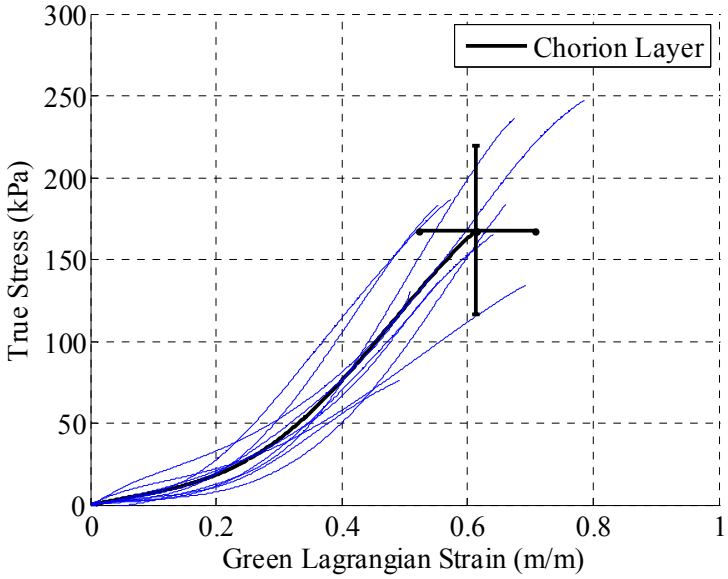

Figure 27: All of the tests for the chorion layer of the placenta have similar stress versus strain curves.

For the two donors of chorion tissue, there were no significant differences in failures stress or strain ($p=0.50$, $p=0.85$). None of the six donors for the maternal side of the placenta had a statistically significant different failure stress or strain than the others ($p>0.2$). When comparing

all of the chorion tests to the all of the tests on the maternal side of the placenta, the failure stresses are significantly different ($p<0.001$) and the failure strains are not significantly different ($p=0.24$). The characteristic averages show the chorion layer of the placenta provides a stiffer response than the maternal portion alone (Figure 28).

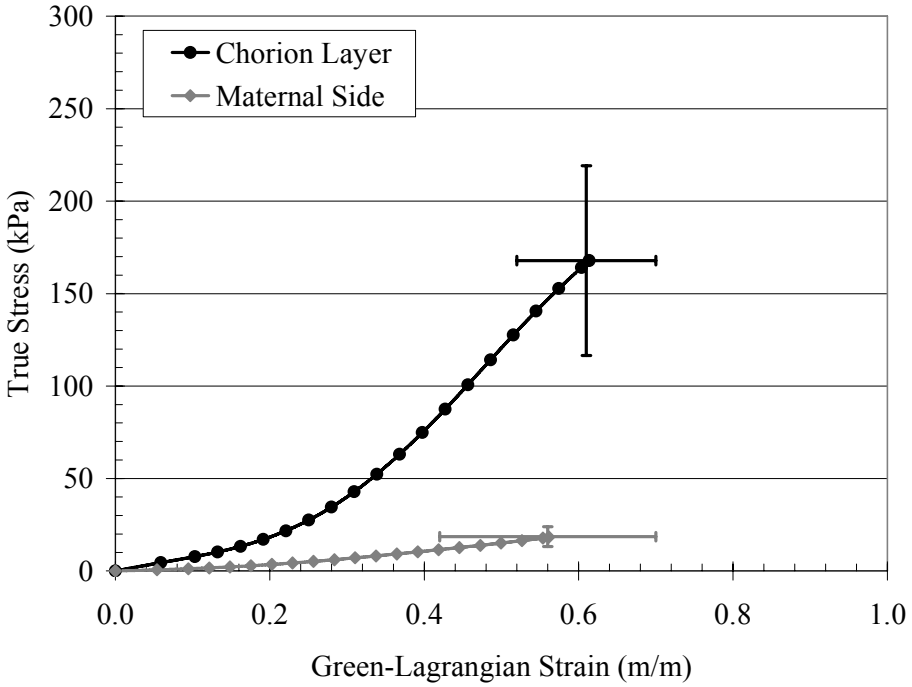

Figure 28: Characteristic averages are shown with bars indicating the standard deviations of the failure values.

Discussion

The results from this study give loading and failure information for the maternal side of the placenta and the chorion layer of the placenta. The maternal portion of the placenta, including only the villus structure, has a compliant stress versus strain response and therefore has a lower failure stress and elastic modulus than the chorion specimens. Due to the presence of the dense layer of blood vessels, the failure stresses are much higher for the chorion tissue. Both layers of placental tissue have similar failure strains.

The standard deviations in the failure values are assumed to be dependent on specimen variability since the testing procedure was the same for each specimen. The microstructure of the placental villi on the maternal side do not have a directional bias of their structure in the plane of the tissue specimens (Cunningham and Williams 2005). It is assumed because of the

transversely isotropic structure, the material properties would not be directionally dependent. While there are discontinuities, careful consideration was used when stamping the specimens to obtain a uniform gage length. However, the porous structure of the placenta could still contribute to specimen variability. Because of the fetal vessels that originate at the umbilical cord and disperse to the edge of the placenta, the chorion layer is not transversely isotropic in its structure (Cunningham and Williams 2005). Although an effort was made to obtain samples in a consistent area of structure, the full complexity of the chorion layer is not addressed with these material tests. However, the average material response is represented. Moreover, the values are not significantly different between the two donors and the standard deviations are low.

These dynamic testing data from the maternal side of the placenta are compared to previous quasi-static placenta tension research (Pearlman 1999). While the quasi-static tests are sub-failure and the tests in this study are failure, this is the most suitable previous research for comparison. The gage lengths of the specimens were 30 mm and they were pulled at a rate of 1.6 mm/s. For all five specimens, the average peak strain was 0.43 ± 0.16 and the average peak stress was 15.6 ± 7.6 kPa. However, it is not clearly stated in the literature if the reported strain values are Green Lagrangian. The data from Pearlman's tests compare favorably to the maternal side tension tests but have significantly lower peak stresses than the chorion layer tension tests ($p<0.001$).

For dynamic testing of placental tissue, sectioning the tissue in thin coupon specimens provided necessary advantages. One advantage of this method was the ability to grip the tissue throughout the tissue thickness. Gripping the placenta without sectioning would be difficult because the internal layers need to strain the same amount as the external layers. Another advantage of the test configuration was the ability to measure local stress and strain of the tissue. In addition to these advantages, there are limitations with this study. It is assumed that since the placenta tissue maintains its size and shape after delivery, the tests postpartum provide a close model to the performance of the tissue *in vivo*. Further, the body temperature and blood flow of the tissue *in vivo* were not modeled in the experiments. In order to model the blood filled organ, the tissue was kept hydrated and saturated prior to testing. The blood flow *in vivo* would likely increase both the viscoelasticity and incompressibility of the placental tissue. Because the tissue is tested hydrated and the failure mode is tension in the fibers, it is expected that the failure properties *in*

vivo would be similar those measured in this study. Previous researchers have evaluated the effect of temperature on material properties of ligaments (Hasberry and Pearcy 1986, Lam et al. 1990). From those studies they have found that there is not a significant difference in tensile failure properties at room temperature versus body temperature. Because the viscosity of blood increases with a decrease in temperature, it is likely the placenta would have a less viscous response at body temperature than was measured in the experiments. However, it is assumed the strength of the fibers that compose the placental tissues would not be greatly affected by the change in temperature. Overall, the effect of blood flow and temperature are expected to have a minimal effect on the material properties of the placenta.

Conclusion

This study presents a total of 20 dynamic uniaxial tensile tests on the maternal side of the placenta and 10 dynamic uniaxial tensile tests on the chorion layer of the placenta. These tests were completed from 6 human placentas to determine material properties at a strain rate of 7.0 strains/s. The results show that the average peak strain at failure for both the maternal portion and the chorion layer of the placenta are similar with a value of 0.56 and 0.61 respectively. However, the average failure stress for the chorion layer, 167.8 kPa, is much higher than the average failure stress for the placenta with the chorionic plate removed, 18.6 kPa. This is due to differences in the structure and function of these layers in the placenta. In summary, dynamic loading data for the placenta have been determined for use in computational modeling of pregnant occupant kinematics in motor vehicle crashes. Moreover the computational model for the maternal side of the placenta should reflect the material properties for the villus structure of the placenta, which is more compliant than the placenta with the chorion attached.

Chapter 5:
Effect of Strain Rate on Material Properties of Human Placenta in Tension

Introduction

Recent research has analyzed the dynamic response of placenta tissue. From this study it was determined that the maternal and fetal side of the placenta have different tensile material properties at a dynamic loading rate (Chapter 4). However, placental abruption occurs between the maternal side of the placenta and the uterine wall at the uteroplacental interface. Therefore, this study will focus on the material properties of the maternal side of the placenta. Although previous research has addressed the material response of placental tissue at dynamic and quasi static loading rates, a larger sample size of material tests which addresses the rate dependence of the tissue is necessary. The purpose of this study is to obtain material properties for the maternal side of the placenta at three physiologic strain rates. This information will advance the ability of pregnant occupant models to accurately model the response of the placenta in a variety of impact conditions.

Methods

A total of 64 uniaxial tensile tests were performed on 6 whole placentas. Donor tissue followed the Wake Forest University Baptist Medical Center Institutional Review Board informed consent procedures. Following delivery, the tissue was stored in a saline solution and tested within 36 hours. Each placenta had 3 to 5 tests at each of the 3 strain rates. The three strain rates chosen for this study were 0.07 strains/s, 0.70 strains/s, and 7.00 strains/s. These rates represent loading from a low level impact up to the level of strain rate expected in a motor vehicle crash as determined from previous computational modeling (Moorcroft et al. 2003c).

All of the uniaxial tensile tests were performed on coupon specimens from the maternal surface of the placenta. Thin slices of placenta were acquired from the whole placenta using a tissue slicer with a wet rotating blade. This allowed the maternal surface of the placenta to be

sectioned into 5 mm slices and separated from the chorion layer of the placenta (Figure 29). Because the placenta function requires it to have a lobe structure, the slices of the placenta had discontinuities. Sections with a continuous structure were chosen for acquiring a smaller coupon section. Each piece of tissue was aligned before stamping to ensure uniformity as much as possible with each sample. Guide rods provided a means for aligning both a stencil and ultimately the stamp. A coupon was then stamped out of the tissue using a steel bent stamp. A sharpened edge to the steel stamp minimized sheer stress in the tissue during the stamping procedure. The result of the tissue stamping procedure was several coupons from the same donor tissue with a uniform shape (Figure 30). Each coupon was kept hydrated throughout the preparation and prior to testing. The coupon specimens have an average cross sectional area of 28.4 ± 7.1 mm.

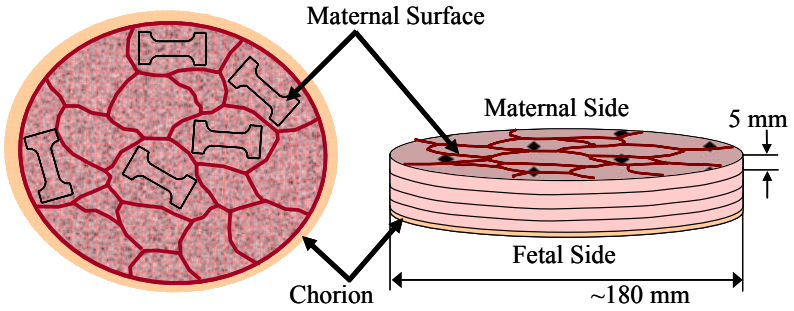

Figure 29: Each placenta is sectioned into 5 mm slices.

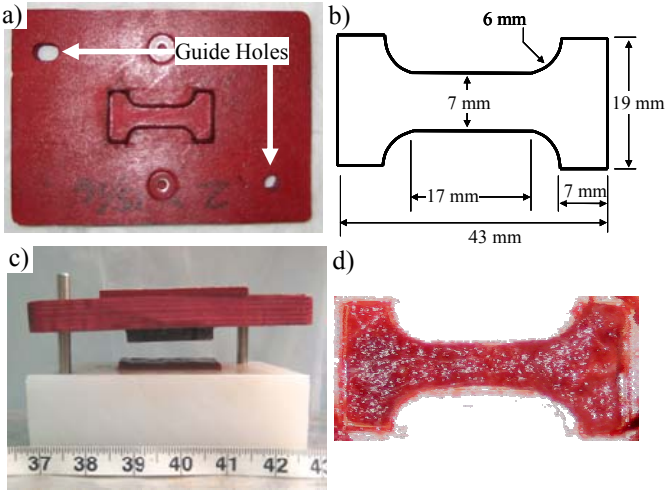

Figure 30: a) A steel bent stamp is used to cut the tissue into a dog bone shape. b) The stamp provides uniform tissue samples. c) Guide rods are used to align the stamp with the specimen. d) The coupon shape is cut where the tissue has a uniform consistency.

A custom designed system of linear motors was used for uniaxial dynamic tensile tests of placental tissue coupons (Figure 31). The system included one multi axis controller (Parker ACR9000, Irwin, PA) that served as a power supply for a motor driver (Parker ViX, Irwin, PA) which controlled the two linear motors with stages (Parker Daedal MX80S, Irwin, PA). The two individual stages were each instrumented with a load cell (OMEGA LC10, 10 lbf, Stamford, CT), potentiometer (Space Age Control, 160-1705, 540 mm, Palmdale, CA), and accelerometer (Endevco 7264B, 2000 G, San Juan Capistrano, CA. On each side of the test specimen, the direct path from the tissue clamp went through the load cell and was rigidly connected to the linear motor stage. The inertial load of the mass in front of the load cell was multiplied by the acceleration to compensate the measured reaction load. Synchronous motion of the motors allowed both of the stages to pull the tissue in tension at the same time for an overall velocity which corresponded to the desired strain rate.

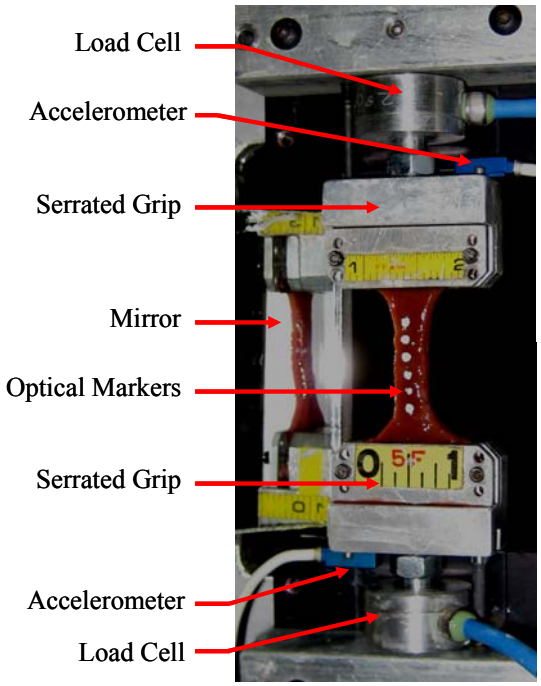

Figure 31: The specimen is mounted between two serrated grips which are instrumented with both a load cell and an accelerometer while high speed video records the test event.

Each specimen was mounted in the testing setup with the same initial conditions. The top grip assembly was removed and laid flat to align the specimen in the grip along the centerline of the loading axis. After the grip was secured, the top grip assembly was then reattached to allow the specimen to rest hanging in 1 g tension. By supporting only its own weight, the tissue had a

standard but minimal preload condition. With the tissue hanging, the specimen was clamped in the bottom grip with no additional preload. Optical markers were applied to the tissue after the specimen was mounted.

Local stress and strain were calculated for each specimen. Local deformation was recorded using high-speed video (Phantom V4, Wayne, NJ) at 500 frames per second with 512 by 512 resolution for the 0.7 strains/s and 7.0 strains/s tests and 70 frames per second with 512 by 512 resolution for the 0.07 strains/s tests. Optical marker tracking was performed with TEMA® Advanced Motion Analysis Software (Linköping, Sweden). Using the configuration for these tests, the error in the motion analysis is ± 0.030 mm. The optical markers on either side of the location where the specimen tore were used to calculate the local strain. In addition, a mirror aligned at a 45 degree angle was mounted next to the specimen so that the side of the specimen could be viewed in the high speed video. The measured displacement data were fit with a 5^{th} order polynomial. The average R^2 value for the displacement curve fit is 0.999 ± 0.001. Similarly, the measured force data were fit with a 5^{th} order polynomial. The average R^2 value for the force curve fit is 0.991 ± 0.013. Local stress was acquired by determining the location on the specimen where failure occurred and then taking the width and thickness of the specimen in that location from the pretest pictures as the initial cross sectional area. The error in the pretest pictures is ±0.12 mm. The cross sectional area at the time of failure is calculated using the local strain and a Poisson's ratio value of 0.49. This value has been determined in previous placental tissue testing (Manoogian et al. 2007c). The stress and strain data are reported for each specimen until failure was evident in the video. Although, the tissue could have been still supporting the load, the optical markers were not accurately representing the strain in the tissue once there was sub-failure.

Statistical tests were completed for the failure stress and failure strain data. A two sample t-test procedure was used to determine statistically significant differences between the failure values among the three strain rates for both failure strain and failure stress. A standard method of determining the characteristic average was used for each group of tests at one strain rate (Lessley et al. 2004). This process began with normalizing each strain curve to its respective maximum. Interpolation routines determined the stress for each test at set increments of strain. Stress values for all tests at that rate were averaged to determine one value at each strain. The strain data that

corresponds to these stress values were obtained by multiplying the normalized strain by the average maximum strain of all tests. The result of this process was an average stress versus strain curve for all tests at 0.07 strains/s, 0.70 strains/s, and 7.0 strains/s. Standard deviations of the stress and strain values were also calculated for each group of tests.

Results

Data for dynamic tensile tests at three different strain rates are reported in Green Lagrangian strain and true stress values. Frames from the high-speed video of a 7.0 strains/s test show the tissue specimen fails in the gage length of the dog bone shape coupon (Figure 32). The stress versus strain data for all tests at 0.07 strains/s have an average failure strain of 0.49 ± 0.15 and a corresponding failure stress of 10.8 ± 5.9 kPa (Figure 33). Similarly, the stress versus strain data for all of the tests at 0.7 strains/s have an average failure strain of 0.53 ± 0.12 and a corresponding failure stress of 11.4 ± 3.7 kPa (Figure 34). The most dynamic strain rate, 7.0 strains/s, has a corresponding average failure stress of 18.6 ± 5.4 kPa and 0.56 ± 0.14 strain (Figure 35).

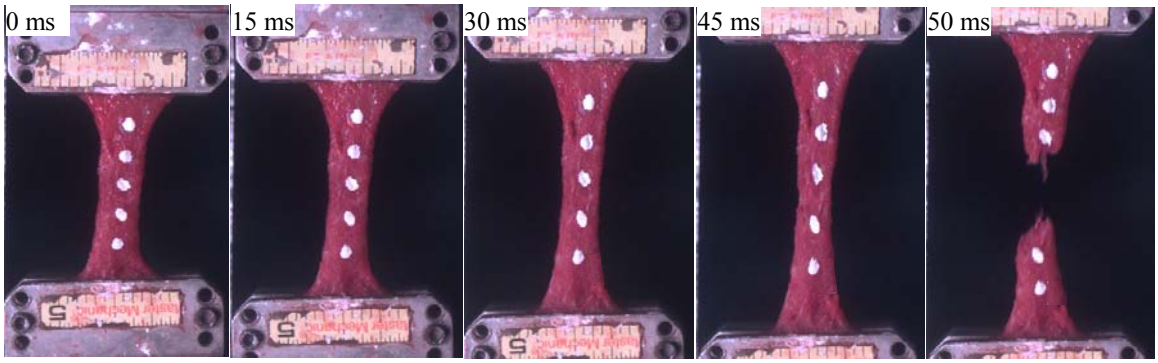

Figure 32: Video captures of one test show a typical failure of a placental specimen pulled in uniaxial tension at 7.0 strains/s.

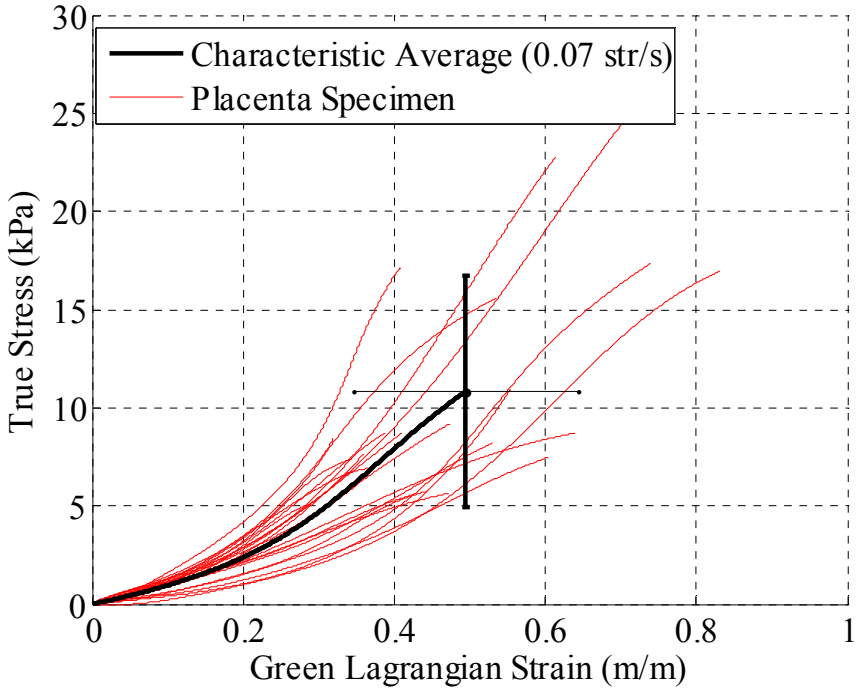

Figure 33: Stress versus strain data for the tests at 0.07 strains/s have an average failure stress of 10.8 ± 5.9 kPa and failure strain equal to 0.49 ± 0.15.

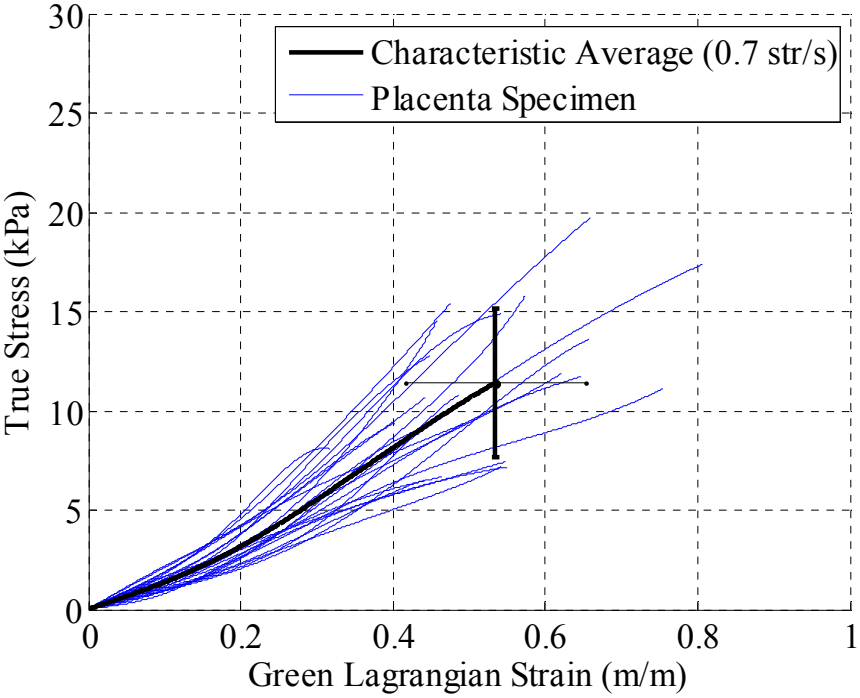

Figure 34: Stress versus strain data for the tests at 0.70 strains/s have an average failure stress of 11.4 ± 3.7 kPa and failure strain equal to 0.53 ± 0.12.

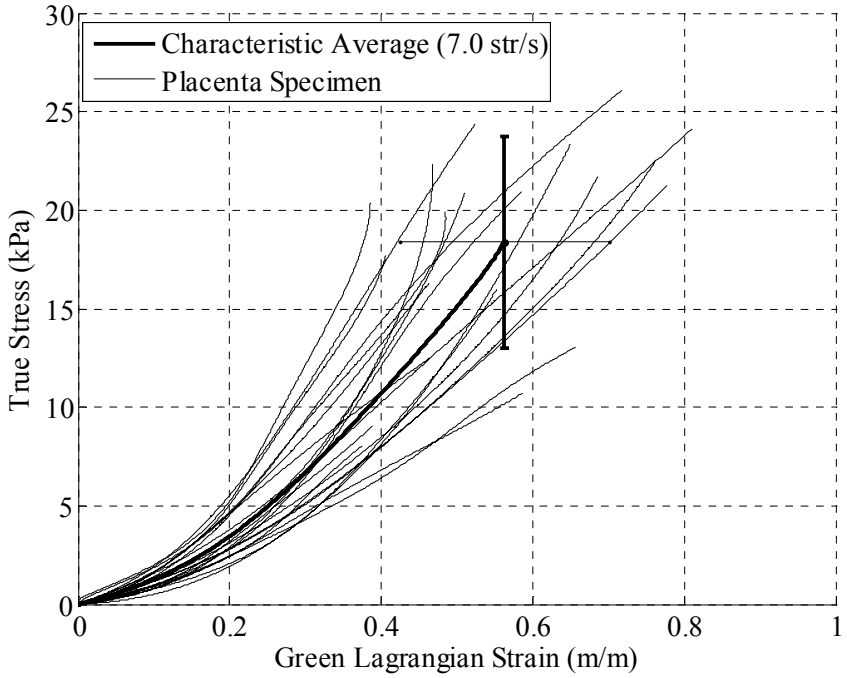

Figure 35: Stress versus strain data for the tests at 7.00 strains/s have an average failure stress of 18.6 ± 5.4 kPa and failure strain equal to 0.56 ± 0.14.

Standard t-tests were used to evaluate the failure stresses and strains among the three strain rate groups. There was no significant difference between the failure stress at 0.07 strains/s and 0.70 strains/s ($p=0.69$). However, the tests at 7.0 strains/s had a significantly higher failure stress than the other two test series at lower strain rates ($p<0.001$). The average failure stresses for each strain rate group are plotted on a log scale to show the relationship between strain rate and failure stress (Figure 36). There were no statistically significant differences among the failure strains for the three groups ($p>0.1$). When plotted together on a log scale, the small change in failure strain over the three rates is evident (Figure 37). The relationship between strain rate and corresponding stress versus strain data is also shown by comparing the characteristic averages for all of the strain rates tested (Figure 38).

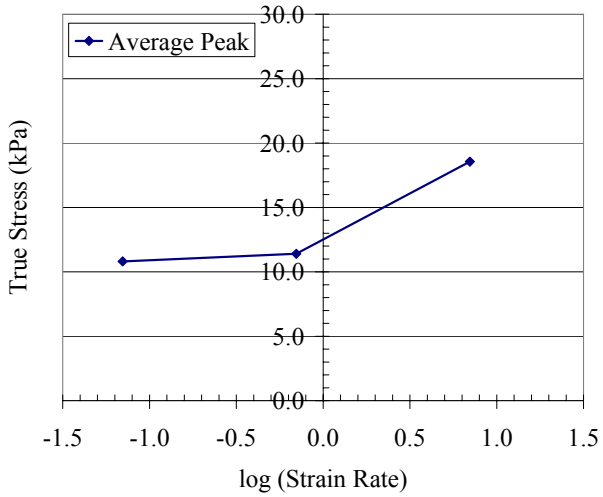

Figure 36: The rate dependence of placenta failure stress.

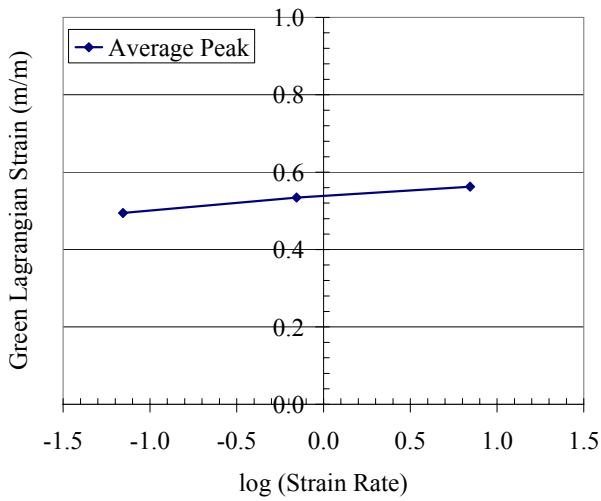

Figure 37: The rate dependence of placenta failure strain.

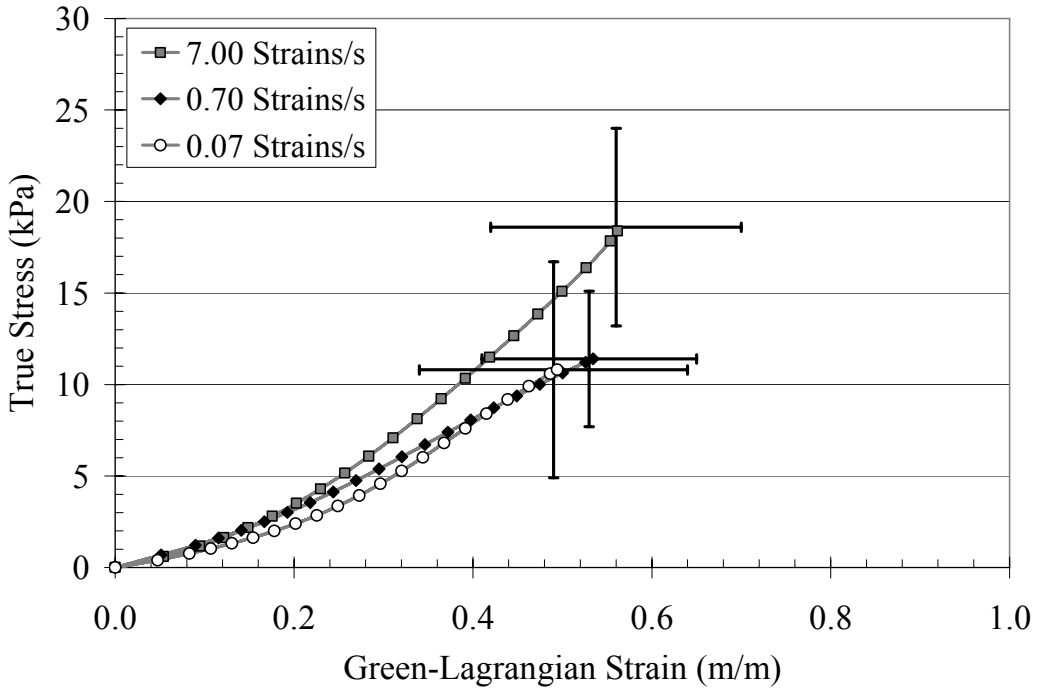

Figure 38: The characteristic averages for each group of tests are shown together with the standard deviations of the failure values.

These results can also be categorized by donor. The average failure strains with the corresponding standard deviations are plotted for each donor group separated by strain rate (Figure 39). For the failure strain values there are no statistically significant differences between

any of the rates for any of the donors ($p>0.2$). The average failure stresses with the corresponding standard deviations are also plotted for each donor group separated by strain rate (Figure 40). This data indicated significant differences between the lowest and highest strain rate for donors 4 and 6 ($p<0.05$). Additionally, there are significant differences between the failure stresses for the intermediate and highest strain rate groups for donors 5 and 6 ($p<0.02$). None of the other relationships had statistical significance ($p>0.05$).

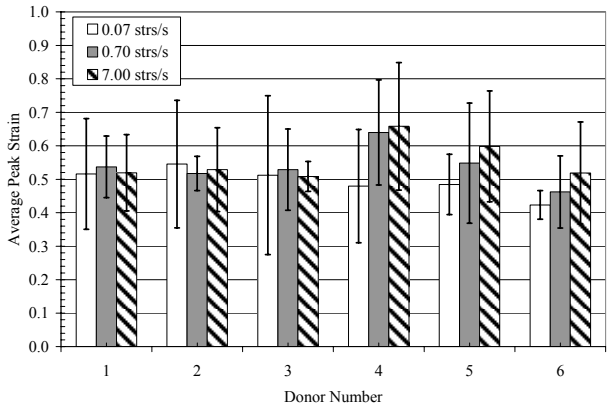

Figure 39: The average failure strain at each rate is shown for each donor.

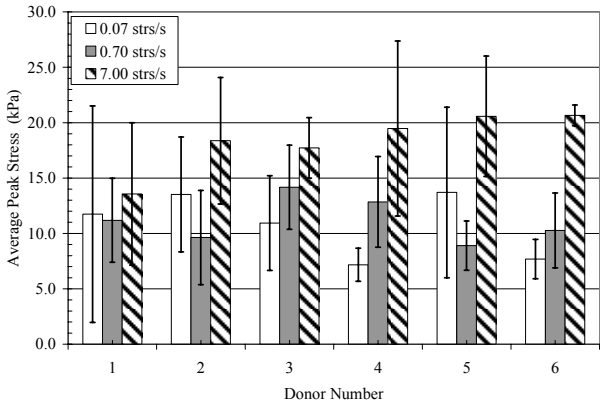

Figure 40: The average failure stress at each rate is shown for each donor.

Discussion

The results from this study give stress versus strain loading and failure information for the villous portion of the maternal side of the placenta for three different loading rates. The standard deviations in the failure values are assumed to be dependent on specimen variability since the testing procedure was the same for each specimen. The microstructure of the placental villi on the maternal side do not have a directional bias of their structure in the plane of the tissue specimens (Cunningham and Williams 2005). It is assumed because of the transversely isotropic structure, the material properties would not be directionally dependent. While there are discontinuities, careful consideration was used when stamping the specimens to obtain a uniform gage length. However, the fibrous structure of the placenta could still contribute to specimen variability.

Although previous material testing on human placenta is limited, Pearlman (1999) tested full thickness placenta in quasi-static tension. These tests were sub-failure and only consisted of five

specimens. The gage lengths of the specimens were 30 mm and they were pulled at a rate of 1.6 mm/s. For all five specimens, the average peak strain was 0.43 ± 0.16 and the average peak stress was 15.6 ± 7.6 kPa. However, it is not clearly stated in the literature if the reported strain values are Green Lagrangian. The peak stresses from Pearlman's tests are similar to the failure stresses measured in the current study.

Additionally, Manoogian (Chapter 4) performed failure testing on 10 placental tissue specimens in dynamic uniaxial tension. These tests determined material properties of placental tissue with the chorion layer attached at a strain rate of 7.0 strains/s. Both the maternal portion and the placenta with the chorion attached have a similar failure strain of 0.56 and 0.61 respectively. However, the failure stress for the placenta with chorion, 167.8 kPa, was much higher than the failure stress for the placenta with the chorion layer removed, 18.6 kPa. There are not data available in the literature to quantify the stress relaxation or rate dependent properties of placental tissue.

For dynamic testing of the same viscoelastic tissue it is expected that the failure strain is reduced and the failure stress and elastic modulus are both increased (Yamada 1970). Although the placenta is a viscoelastic tissue, there was not a large amount of rate dependence over the range tested. This is similar to published results for other tissues. Jin *et al.* (2006) evaluated the bovine pia-arachnoid complex at 0.05, 0.50, and 5.0 strains/s. Similar to the results in this study, the ultimate stress was significantly different ($p<0.05$) at 5.0 strains/s than the two slower rates, but over that range there was no significant difference in the ultimate strain recorded ($p>0.05$). Likewise, previous quasi-linear viscoelastic studies on ligaments have shown a minimal change in the stress-strain response from 0.01 strain/s to 1.0 strains/s (Woo et al. 1981, Funk et al. 2000). A significant rate-dependent response has been reported for tissues when the range of strain rates tested is increased to 100 or 1000 strains/s (van Dommelen et al. 2005, Jin et al. 2006). Strain rates of this magnitude were not predicted in the computational model and therefore were not considered in characterizing the response of the placental tissue to a dynamic impact.

There are limitations with this study. It is assumed that since the placenta tissue maintains its size and shape after delivery, the tests postpartum provide a close model to the performance of the tissue *in vivo*. Further, the body temperature and blood flow of the tissue *in vivo* were not

modeled in the experiments. In order to model the blood filled organ, the tissue was kept hydrated and saturated prior to testing. The blood flow *in vivo* would likely increase both the viscoelasticity and incompressibility of the placental tissue. Because the tissue is tested hydrated and the failure mode is tension in the fibers, it is expected that the failure properties *in vivo* would be similar those measured in this study. Previous researchers have evaluated the effect of temperature on material properties of ligaments (Hasberry and Pearcy 1986, Lam et al. 1990). From those studies they have found that there is not a significant difference in tensile failure properties at room temperature versus body temperature. Because the viscosity of blood increases with a decrease in temperature, it is likely the placenta would have a less viscous response at body temperature than was measured in the experiments. However, it is assumed the strength of the fibers that compose the placental tissues would not be greatly affected by the change in temperature. Overall, the effect of blood flow and temperature are expected to have a minimal effect on the material properties of the placenta.

Conclusion

This study presents a total of 64 uniaxial tensile tests on the villous structure of the placenta. Six human placentas were used to acquire coupon specimens for tensile testing at three physiologic strain rates. Material properties of the placental tissue were evaluated at a strain rate of 7.0 strains/s, 0.70 strains/s, and 0.07 strains/s. The test data have an average failure strain of 0.49, 0.53, and 0.56 respectively. A failure stress of 10.8 kPa, 11.4 kPa, and 18.6 kPa correspond to an increase in strain rate from 0.07 strains/s to 7.0 strains/s. The results indicate rate dependence only when comparing the highest strain rate of 7.0 strains/s to either of the lower rates. There is no significant rate dependence between 0.07 strains/s and 0.70 strains/s. When compared to previous testing of placental tissue, the current study addresses the material response to more strain rates as well as provides a much larger set of available data. In summary, tensile material properties for the placenta have been determined for use in computational modeling of pregnant occupant kinematics in events ranging from low impact activities to severe impacts such as in motor vehicle crashes.

Chapter 6: Dynamic Biaxial Tissue Properties of Pregnant Porcine Uterine Tissue

Introduction

Although there have been several research efforts to determine the loading and failure properties of uterus and pregnant uterus, the data are limited in their ability to accurately represent the fundal uterine tissue response to loading in a motor vehicle crash. For an anisotropic material that is loaded in biaxial tension *in vivo*, a biaxial material test is more suitable than a uniaxial test to determine the material response (Humphrey et al. 1987, Shah et al. 2006). Specifically biaxial tests load multiple fiber directions at one time. This is a better model for the pregnant uterus than uniaxial tension which loads only one fiber direction at a time. Therefore, to measure material properties of the uterine tissue, biaxial tests were chosen. Because pregnant human uterine tissue samples were not large enough for biaxial tissue testing, pregnant porcine uterine tissue was chosen as a surrogate. The purpose of this study is to determine the material properties for pregnant porcine tissue when tested in biaxial dynamic tension.

Methods

Tissue Sample Preparation. Whole porcine uterine tissues were collected from five pregnant sows at the time of death. All tissues were kept fresh in saline, which preserved the integrity of the tissue, and tested within 7 days of extraction. Individual test specimens were cut from the whole uterus. There were approximately 8 samples from each sow for a total of 39 specimens. Only one uterine horn was used from each donor. In a porcine uterus, the uterine wall meets at the mesometrium and forms a tubular shape. The samples for this study were taken on the side of the uterine wall opposite the mesometrium connection (Figure 41).

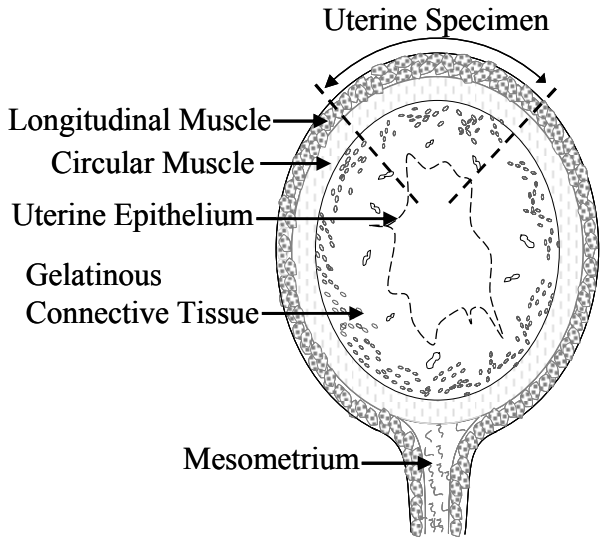

Figure 41: Cross sectional view of a porcine uterus.

For this study, 16 specimens were cruciform shape with the specimen material axes offset 22 degrees (Figure 42). The testing also included 23 specimens with the specimen material axes aligned with the loading axes, an offset of 0 degrees (Figure 42). Each specimen was cut using a steel rule die stamp. When the tissue was aligned to be stamped, the longitudinal fibers of the uterine specimen were rotated using a protractor 22.0 ± 0.5 degrees to the right from the center of the clamp or 0.0 ± 0.5 degrees (Figure 43). These are for the offset and aligned specimens respectively. The longitudinal fibers are identifiable macroscopically and were measured for each specimen. The cruciform specimen is pulled in two dimensions referred to as X and Y in this paper.

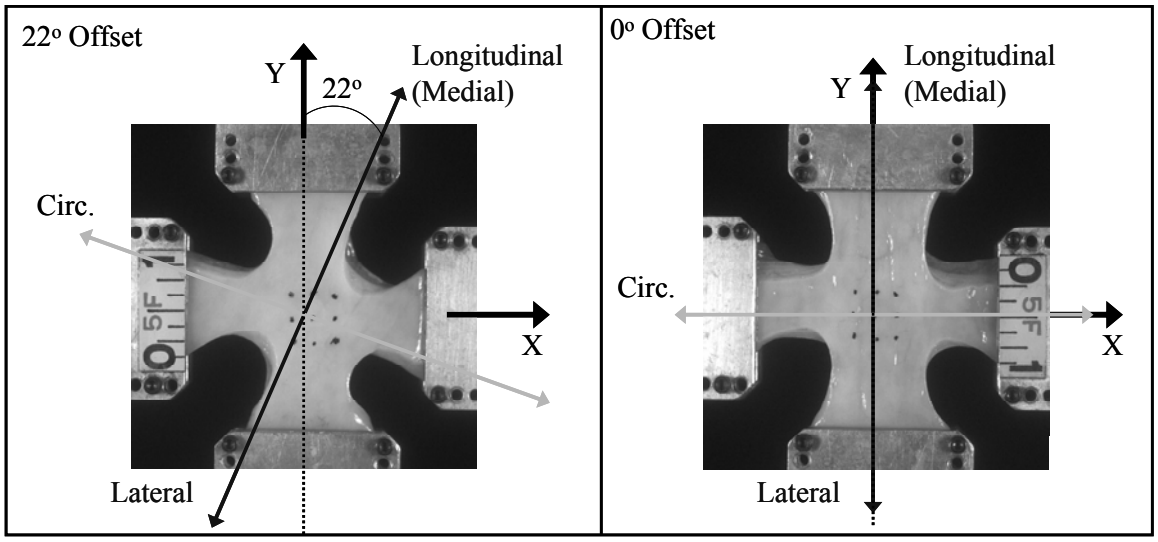

Figure 42: Specimens either have a 22 or 0 degree offset of the material axes from the loading axes.

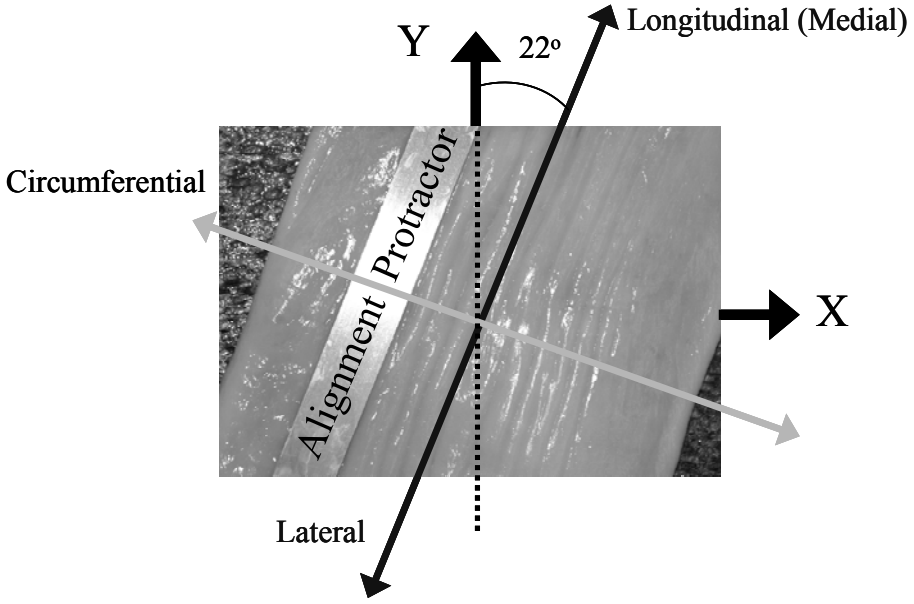

Figure 43: The longitudinal direction is measured macroscopically

Biaxial Test System. Biaxial dynamic tensile tests were performed using a custom designed system of linear motors to pull the cruciform specimen in tension simultaneously with four tissue clamps (Manoogian et al. 2007b) (Figure 44). The system included one multi axis controller (Parker ACR9000, Irwin, PA) that served as a power supply for two motor drivers (Parker ViX, Irwin, PA) which controlled four linear motors with stages (Parker Daedal MX80S, Irwin, PA). The four individual stages were each instrumented with a load cell (OMEGA LC201, 100 lbf,

Stamford, CT), potentiometer (Space Age Control, 160-1705, 540 mm, Palmdale, CA), and accelerometer (Endevco 7264B, 2000 G, San Juan Capistrano, CA). The inertial load of the mass (0.0374 kg) in front of the load cell was multiplied by the acceleration to compensate the measured reaction load.

Specimens were kept moist prior to testing by storing them in saline, and during testing they were sprayed with saline solution. No preconditioning was applied before the failure test. For the tests with no offset and with an offset, each test began with the same initial conditions. To ensure a proper initial geometry, the specimens were mounted in the grips so that the initial shape matched the original stamp shape (Fung 1967, Martin 2000, Duma et al. 2003). This resulted in a slight variation of the grip loads giving a standard deviation in the preload for all tests of ±0.13 N which corresponds to approximately 1% of the average peak load for each test. This technique ensured that each test began with no slack in the specimen and the initial condition for each stress versus strain curve was the resting state of the porcine uterus *ex vivo*.

The thickness for each specimen was acquired before the failure test. A FARO Laser ScanArm (FARO Technologies Inc., Platinum Laser ScanArm, Lake Mary, FL) was used to scan the top and bottom surfaces of the tissue specimen. This data provided two surface geometries that represented the top and bottom of the tissue. From the surface geometries, an average thickness could be obtained for the region of interest for each individual specimen. The average thicknesses, with an accuracy of ±0.1 mm, are used in the stress calculations.

On each of the 4 sides of the test specimen, the direct path from the tissue clamp went through the load cell and was rigidly connected to the linear motor stage (Figure 44). A multi axis controller provided synchronized motion of all four linear stages to move at 0.05 m/s for a displacement of 0.06 m. This distance assured failure occurred and corresponded to a strain rate of approximately 1 strains/s. This rate was approximated from previous research on modeling of a pregnant occupant, restrained properly by a three-point seat belt, in a frontal impact with a 35 kph change in velocity (Moorcroft et al. 2003a, Moorcroft et al. 2003c).

Local deformation was recorded using high-speed video (Phantom V4, Wayne, NJ) at 1000 frames per second with 512 by 512 resolution to track ink markers added to the tissue immediately before testing. Optical marker tracking was performed with TEMA® Advanced

Motion Analysis Software (Linköping, Sweden). Using the configuration for these tests, the error in the motion analysis was 0.065 mm.

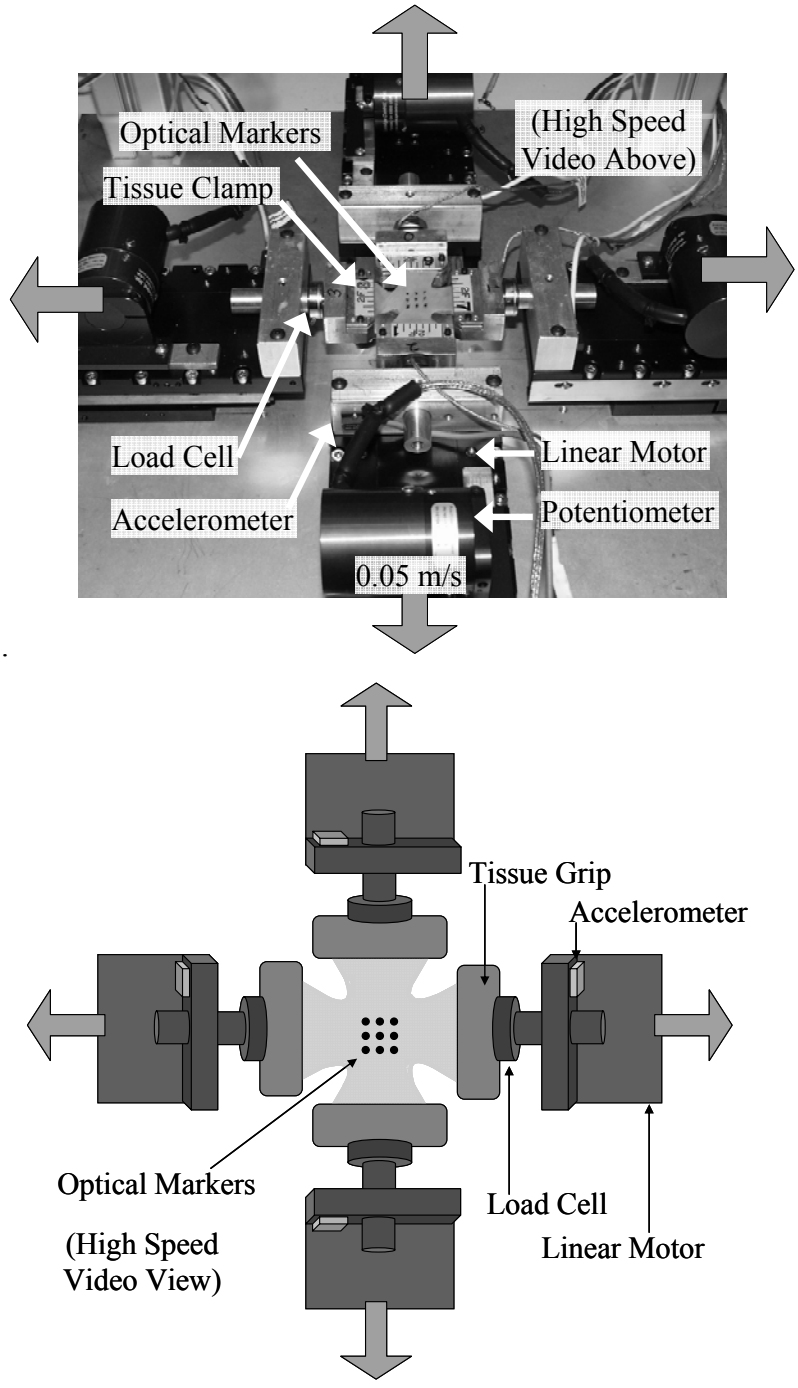

Figure 44: Four individual platforms pull the tissue in biaxial tension and are instrumented with an accelerometer, potentiometer, and load cell (Photograph Top, Illustration Bottom).

Data Processing and Analysis. The test series included 39 failure tests with corresponding X and Y direction stress and strain measurements of the central region of the specimen. Two stresses were calculated for these tests. One was an average in the X or horizontal direction and the other was the average in Y or vertical direction. These calculations were established in previous biaxial testing research (Sacks and Sun 2003, Shah et al. 2006). The process was the same for both directions but the horizontal direction is discussed as an example. For the horizontal direction, this process took the measured loads at grips X_1 and X_2 inertially compensated and scaled them individually. Scaling of the loads was necessary because the load measured was greater than the load transferred through the region where strain was measured. Assuming an equal transfer of load from the grip to the center of the specimen, a length ratio could be used to scale each load (Figure 45, eq. 1). All of the load must be transferred through the smallest width of the cruciform arm, L_1. The load from this region was scaled down to the load that passed through the outer two optical markers. The distance between those markers is L_2 and is measured optically. This scaling process was completed for each side of the specimen. The average of the two scaled loads in the X direction gave an average load at the region of interest for that direction. By assuming incompressibility, the tissue thickness at each time step was calculated. An initial thickness was measured for each specimen as previously discussed. The time history of the region of interest surface area was calculated from the optical markers. Given incompressibility, the thickness at each new time step could be calculated. Although the markers start in a square, they do not remain in that shape. Therefore, in order to determine the cross section for the stress calculation, an average length was found using two opposing sides of the region of interest. The true stress calculation for the horizontal direction used the average force and the average cross sectional area at each time step. The same procedure was completed for the vertical direction. The true stress in the X and Y directions as previously described are reported for each biaxial test with the fibers aligned along the loading axes. The X direction corresponds to the circumferential direction and the Y direction corresponds to the longitudinal direction. For the offset tests, a transformation was used to calculate the values that represent the stresses along the material axes (eq. 2, eq. 3). The true stresses reported for the offset tests are along the material axes, circumferential and longitudinal, rather than the loading axes.

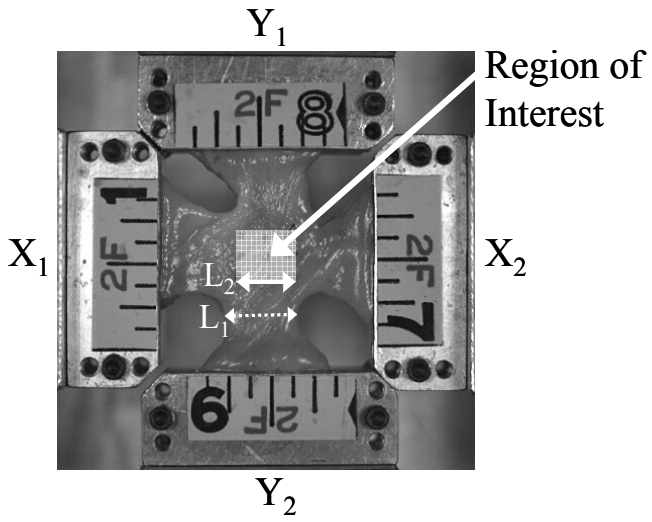

Figure 45: The four corner markers create a region of interest in which the strain and stress were calculated.

$$F_{AreaofInterest} = \frac{(tL)_{AreaofInterest} F_{grip}}{(tL)_{grip}} = \frac{L_2 F_{grip}}{L_1} \quad \text{(eq. 1)}$$

$$\sigma_{x'} = \frac{\sigma_x + \sigma_y}{2} + \frac{\sigma_x - \sigma_y}{2}\cos(2\theta) + \tau_{xy}\sin(2\theta) \quad \text{(eq. 2)}$$

$$\sigma_{y'} = \frac{\sigma_x + \sigma_y}{2} - \frac{\sigma_x - \sigma_y}{2}\cos(2\theta) - \tau_{xy}\sin(2\theta) \quad \text{(eq. 3)}$$

The Green-Lagrange strains were calculated for the X and Y directions using the optical markers on the specimen (Humphrey et al. 1987, Sacks and Sun 2003, Shah et al. 2006). An average was calculated using the four triangles that connect the corners of the area of interest to the center point (Figure 46). The deformation gradient, F, was calculated from the matrix representing the deformed state of the markers times the inverse of the matrix with the undeformed coordinates of the markers (Figure 47, eq. 4). For each triangle, the deformation gradient tensor provided information to compute the Green- Lagrange strain tensor (eq. 5). The principal Green-Lagrange strains, E_{11} and E_{22}, were averaged separately to represent the respective X and Y directions. These are the strains reported for each test. The eigenvalues of the Green-Lagrange strain tensor are the maximum and minimum principal strains (Ivarsson et al. 2000). The shear strain was determined from the change in angle between the two originally orthogonal vectors and the final state (Humphrey et al. 1987) (eq. 6). The strains in the X and Y directions as previously described are reported for each biaxial test with the fibers aligned along the loading axes. The X

direction corresponds to the circumferential direction and the Y direction corresponds to the longitudinal direction. A transformation equation was used to determine the strains along the material axes for the offset tests (eq. 7, eq. 8). The strains reported for the offset tests are along the material axes, circumferential and longitudinal, rather than the loading axes.

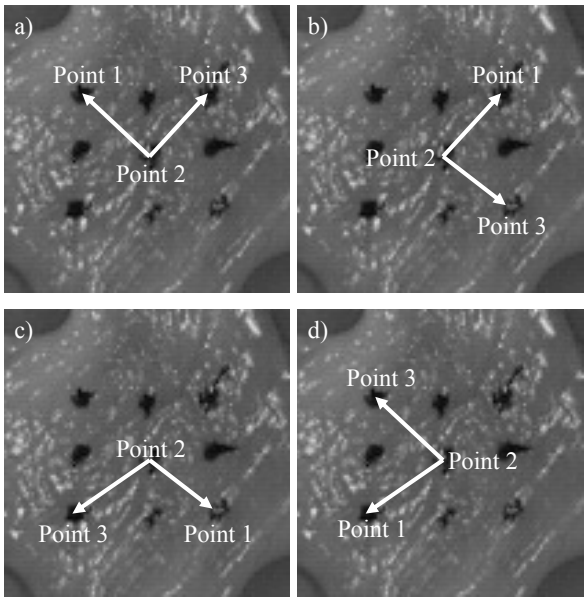

Figure 46: The four groups of vectors (a-d) connecting the center point to two of the corner points are used to calculate X and Y strains that are averaged to establish an X and Y strain value for the specimen.

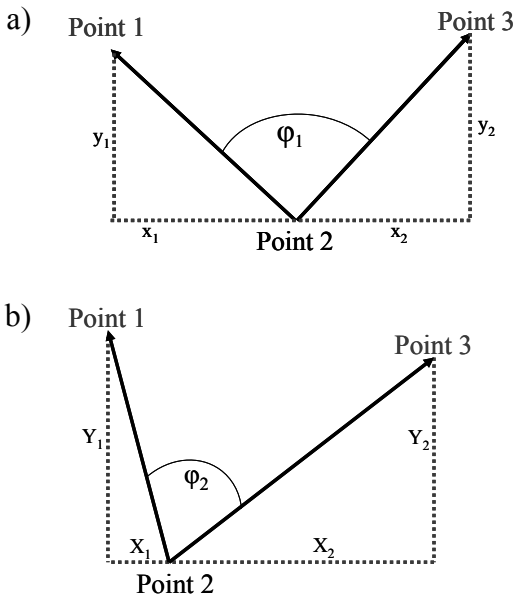

Figure 47: a) The initial state of two corner markers is described by vectors (x_1,y_1) and (x_2,y_2). b) The deformed state of two corner markers is described by vectors (X_1,Y_1) and (X_2,Y_2).

$$\mathbf{F} = \left(\begin{bmatrix} X_1 & X_2 \\ Y_1 & Y_2 \end{bmatrix}_{t=1} \right) \left(\begin{bmatrix} x_1 & x_2 \\ y_1 & y_2 \end{bmatrix}_{t=0} \right)^{-1} \quad \text{(eq. 4)}$$

$$\mathbf{E} = \begin{bmatrix} E_{11} & E_{12} \\ E_{21} & E_{22} \end{bmatrix} = \frac{1}{2}\left(F^T F - I\right) \quad \text{(eq. 5)}$$

$$\gamma = \frac{1}{2}\arcsin\left(\frac{2E_{12}}{\sqrt{1+2E_{11}}\sqrt{1+2E_{22}}} \right) \quad \text{(eq. 6)}$$

$$\varepsilon_{x'} = \frac{\varepsilon_x + \varepsilon_y}{2} + \frac{\varepsilon_x - \varepsilon_y}{2}\cos(2\theta) + \varepsilon_{xy}\sin(2\theta) \quad \text{(eq. 7)}$$

$$\varepsilon_{y'} = \frac{\varepsilon_x + \varepsilon_y}{2} - \frac{\varepsilon_x - \varepsilon_y}{2}\cos(2\theta) - \varepsilon_{xy}\sin(2\theta) \quad \text{(eq. 8)}$$

A standard method of determining the characteristic average was used for both the circumferential and longitudinal sets of stress versus strain data (Lessley et al. 2004). This process began with normalizing each strain curve to its respective maximum. Interpolation routines determined the stress for each test at set increments of strain. These stress values were averaged for the average stress data. The strain data that corresponds to these stress values were obtained by multiplying the normalized strain by the average maximum strain of all tests. The result of this process was average stress-strain curves for both the circumferential and longitudinal directions for all 16 specimens with an offset. Additionally, there are stress-strain curves for all 23 specimens with no offset for both the circumferential and longitudinal direction. The linear elastic modulus is calculated in two regions for the characteristic average curve of each data set. One linear elastic modulus is reported for the toe region of the curve and another value is reported for the failure slope of the stress versus strain curve. These two values provide a maximum and minimum slope of the data set. Matched paired t-tests were used to test for significant differences between the circumferential and longitudinal directions for peak strain, stress, and elastic modulus. A one way ANOVA analysis tested all 5 donors for any significant difference from the others for peak stress and strain in circumferential and longitudinal. A

regression analysis was performed on the peak values to determine any regional significance based on proximity to the ovary or vagina on the uterine horn.

Results

In this section, stress versus strain curves in the circumferential and longitudinal directions are presented for the biaxial tension failure of the porcine uterine specimens. These results are for 23 tests with the material axes inline with the loading axes and 16 tests with the material axes 22 degrees offset from the loading axes. For the strain measurements, the tracking accuracy of the markers is 0.065 mm/pixel which corresponds to approximately 1.6% of the original distance between two corner markers that compose one side of the central region. This error decreases for larger strains. The displacement measurement error of 1.6% also affects the load scaling and cross sectional area part of the stress calculation. For example, for a tissue strain measure of 20%, the error from the video measurement would be ± 0.3% strain.

Aligned Material Axes. Video captures of a test show a typical failure of a uterine specimen with material axes aligned with the loading axes pulled in biaxial tension at 1 strains/s (Figure 48). All of the stress-strain data for the tests without an offset are plotted together with the average and standard deviation for the stress at each strain for the circumferential direction (Figure 49). The average peak stress in the circumferential direction is 500±219 kPa. The corresponding peak Green-Lagrangian strain is 0.43±0.18. All of the stress-strain data are plotted together with the average and standard deviation for the longitudinal direction (Figure 50). The peak stress for the longitudinal direction is 320±176 kPa. The peak Green-Lagrangian strain in the longitudinal direction is 0.42±0.16. Although the peak stresses are significantly different for the two directions ($p<0.001$), the peak strains are not significantly different ($p=0.79$). The characteristic average curves show the average shape of the stress-strain curves in both directions for the 23 tests of pregnant porcine uterine tissue with the material axes aligned with the loading axes (Figure 51).

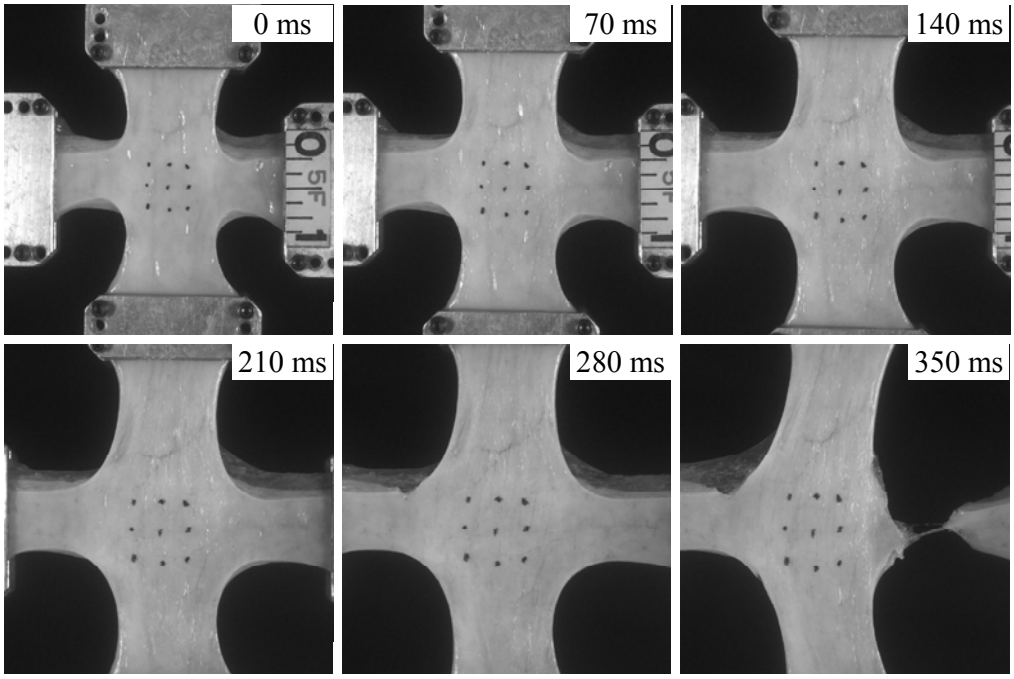

Figure 48: The specimens with the material axes aligned with the loading axes fail in the arm of the cruciform shape.

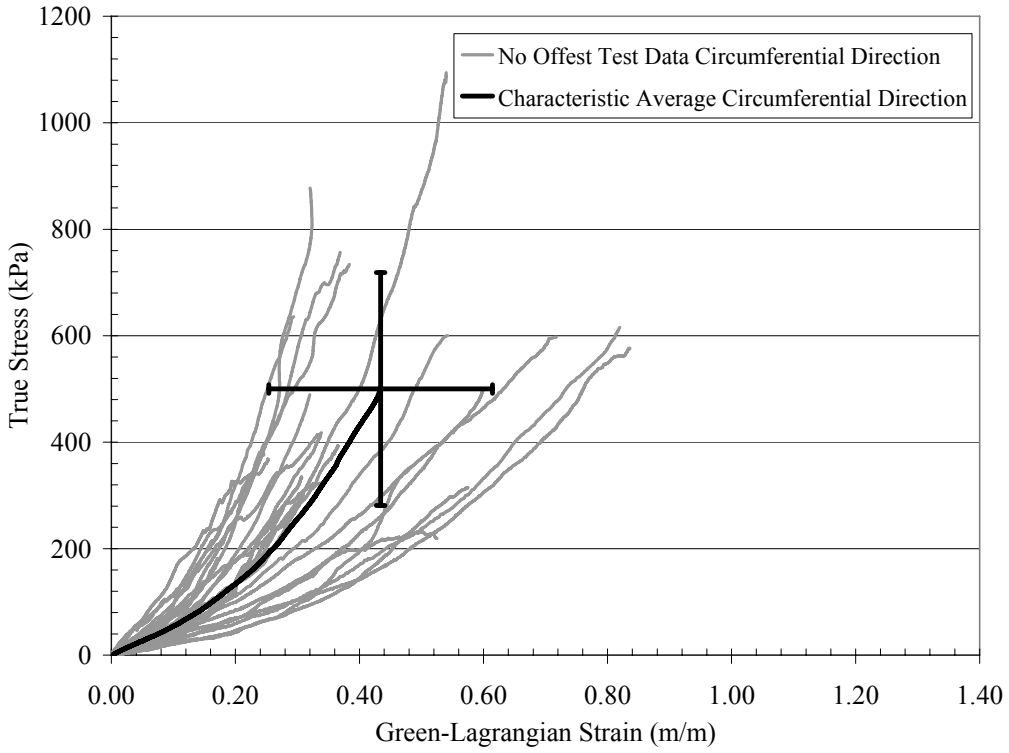

Figure 49: The average stress-strain curve in the circumferential direction has a peak of 500±219 kPa and 0.43±0.18 strain.

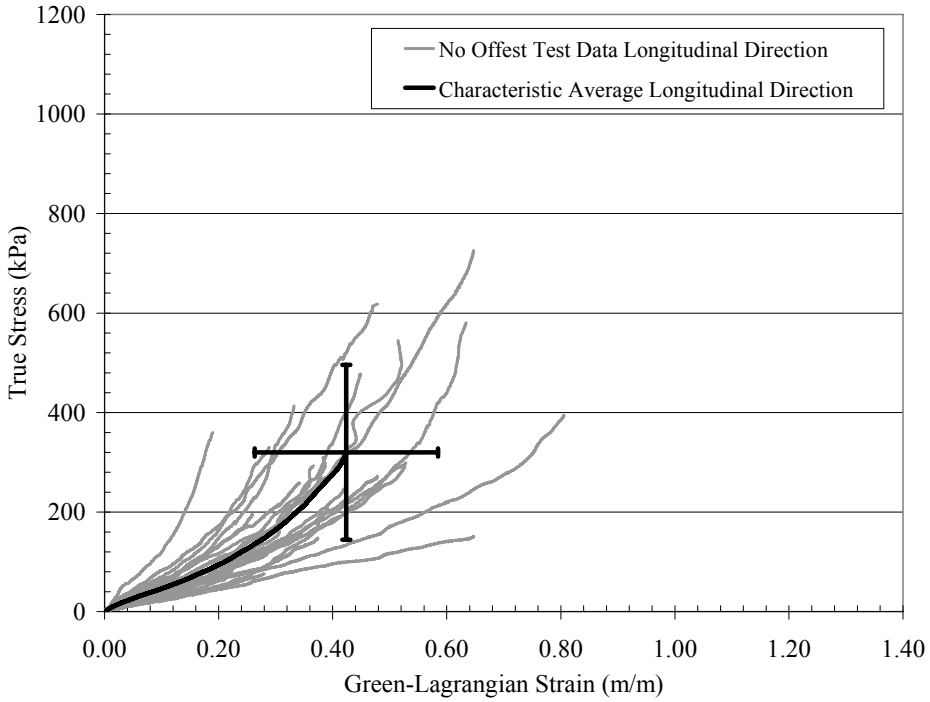

Figure 50: The average stress-strain curve in the longitudinal direction has a peak of 320±176 kPa and 0.42±0.16 strain.

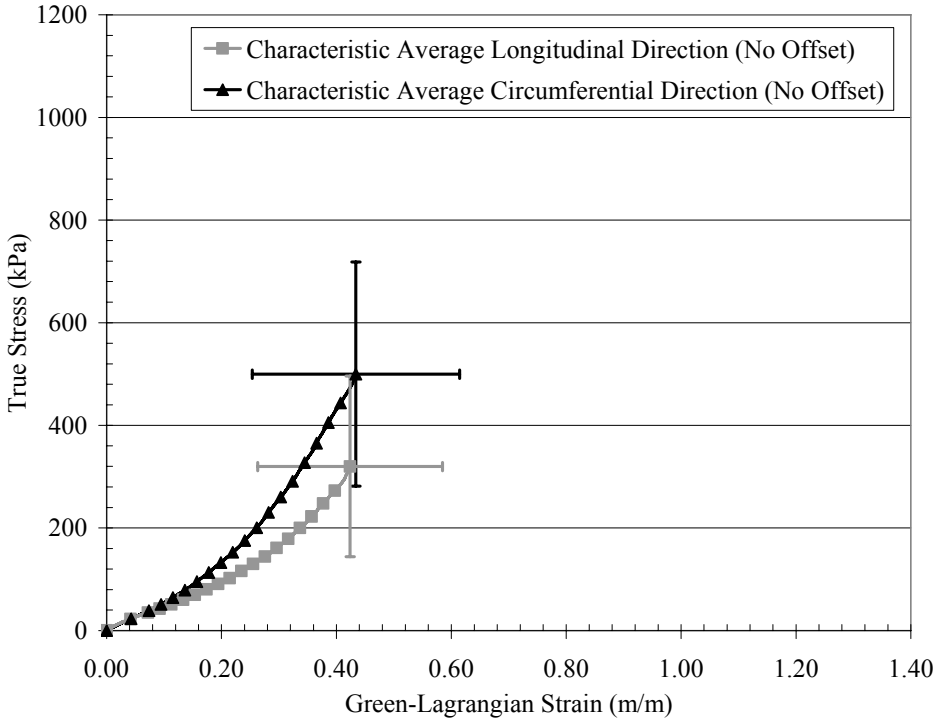

Figure 51: The average curve for the circumferential direction and the average curve for the longitudinal direction.

Offset Material Axes. The specimens with offset material axes have failure initiate at the stress concentration where the cruciform arms meet when pulled in biaxial tension at 1 strains/s (Figure 52). For the 16 tests with the material axes offset from the loading axes, the circumferential direction stress-strain data are plotted together with the average and standard deviation (Figure 53). The circumferential direction for the offset tests has an average peak stress of 456±146 kPa. The average peak Green-Lagrangian strain is 0.74 ± 0.25. Stress versus strain data for the longitudinal direction are plotted together with their corresponding average and standard deviation (Figure 54). In the longitudinal direction, the peak stress for the offset tests is 557 ± 178 kPa. The peak Green-Lagrangian strain in the longitudinal direction is 0.66 ± 0.21. The peak strain for the longitudinal direction is not significantly different from the average peak strain in the circumferential direction ($p=0.09$). However, the peak stresses are significantly different for the two directions ($p=0.03$). The characteristic average curves show the average shape of the stress-strain curves in both directions for the 16 tests of pregnant porcine uterine tissue with the material axes offset from the loading axes (Figure 55). The quadratic polynomials that describe the best fits for these two curves are provided (Table 4). Additionally, the quadratic equation that describes the average of both the circumferential and the longitudinal directions when grouped together is given (Table 4). For the one way ANOVA analysis of the peak values for each donor set, no donors were found to be significantly different ($p>0.25$).

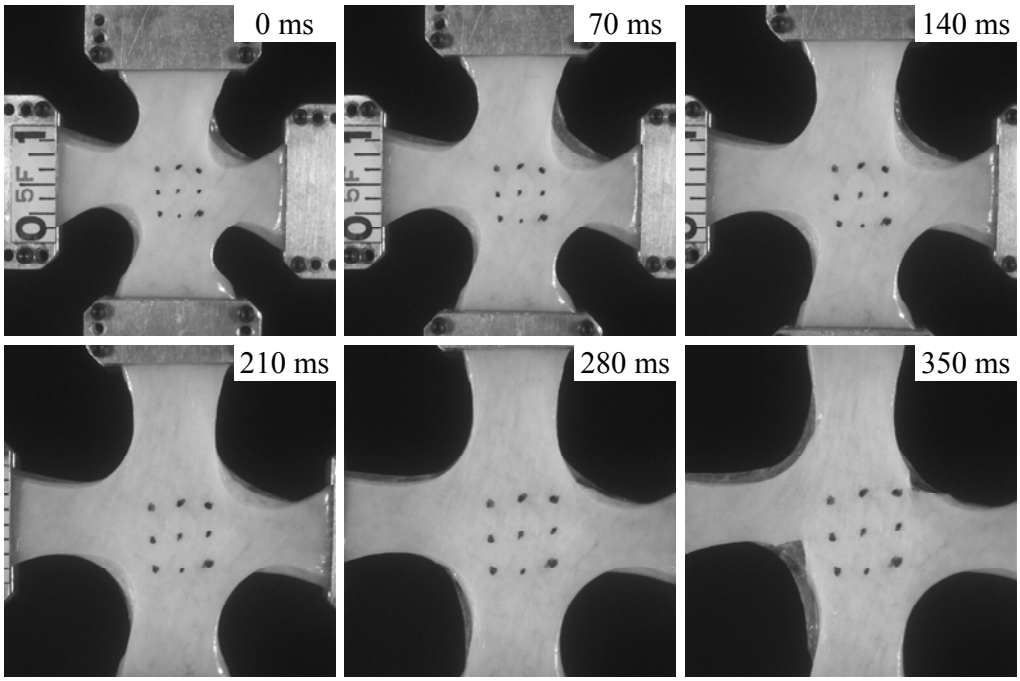

Figure 52: Video captures of a test show a typical failure of a uterine specimen with offset material axes pulled in biaxial tension at 1 strains/s.

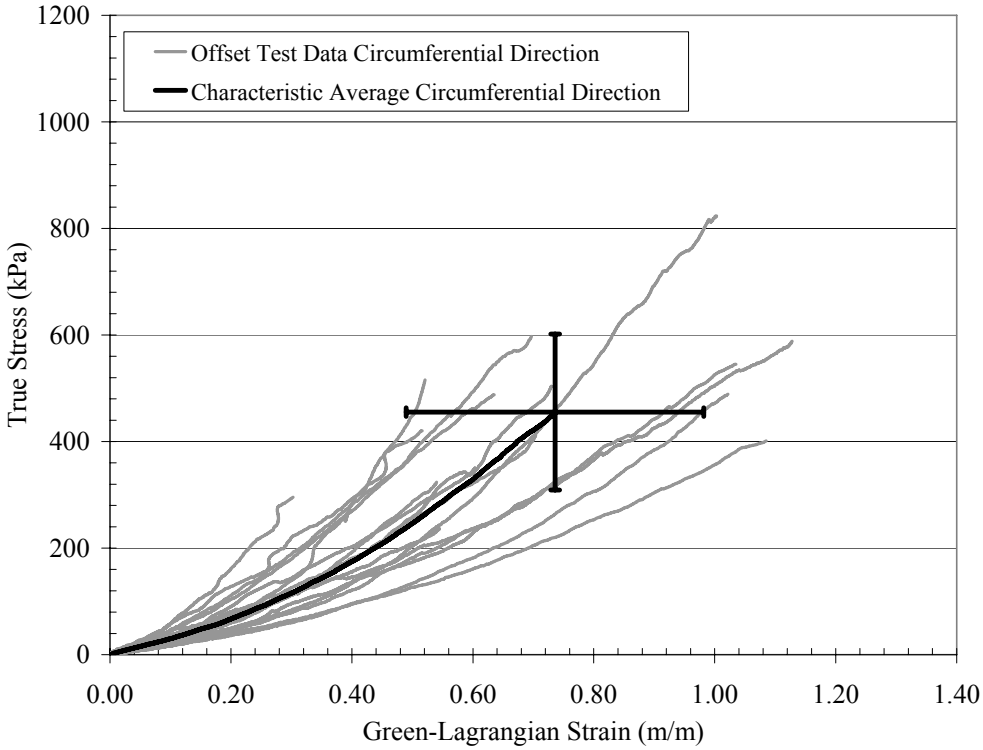

Figure 53: The average stress-strain curve in the circumferential direction has a peak of 456±146 kPa and 0.74 ± 0.25 strain.

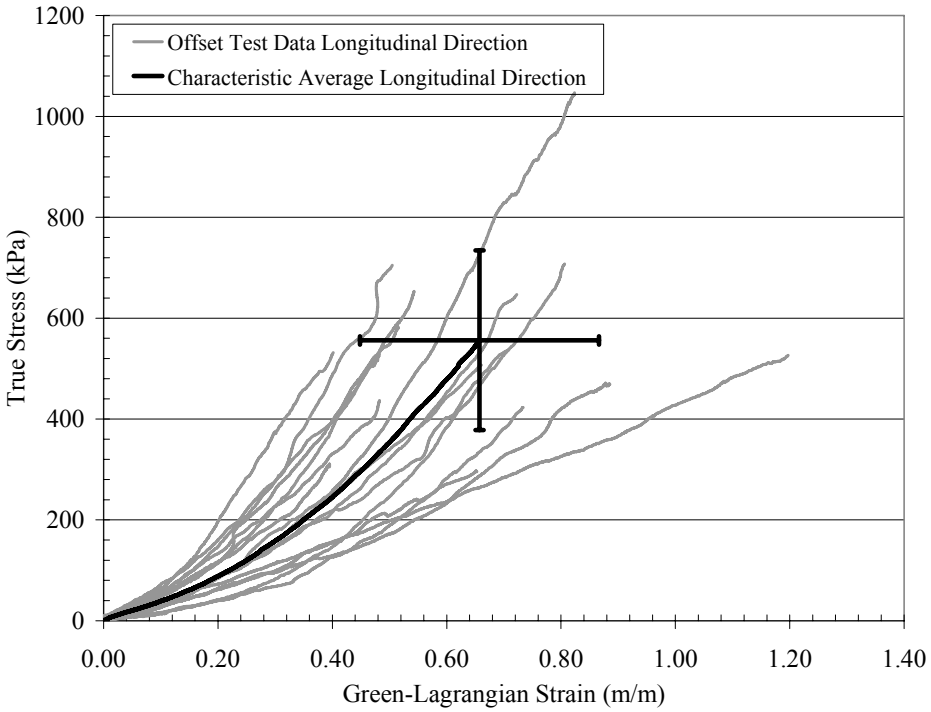

Figure 54: The average stress-strain curve in the longitudinal direction has a peak of 557 ± 178 kPa and 0.66 ± 0.21 strain.

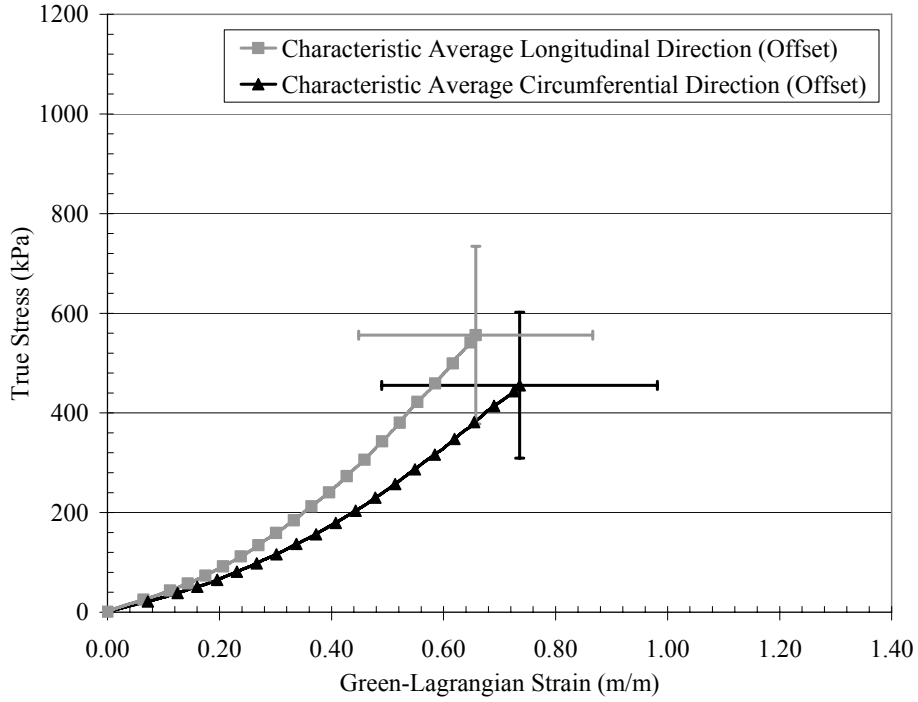

Figure 55: The average curve for the circumferential direction and the average stress-strain curve for the longitudinal direction.

Table 4: Quadratic terms that describe the average stress-strain curves for the offset tests.

	x^2	x	R^2
Circumferential	538.99	224.38	0.9998
Longitudinal	888.87	263.48	0.9998
All Offset Tests	696.48	243.35	0.9998

Discussion

Specimen Offset. The motivation for biaxial tissue testing in this study is to obtain stress versus strain data for the tissue in response to loading both directions of muscle fibers. Although previous researchers established that an offset of the material axes from the loading axes was beneficial, this study confirmed that assumption for the pregnant porcine uterine tissue. The reason for a specific offset of 22 degrees is that this offset was found to minimize shear compared to 0, 45, and 90 degrees (Lanir et al. 1996, Shah et al. 2006).

A previous study by Shah (2006) used biaxial tissue testing to evaluate failure of a cruciform specimen with anisotropy. When the specimen was loaded inline with the fiber axes, the central region of the tissue remained intact and the arm of the cruciform specimen failed in the weakest direction. As a result, the data from the tests were limited because they had peak stresses and strains much lower than similar tests with material axes offset. With the material axes offset, the tissue failure initiated at the corner where the cruciform arms met and propagated at a diagonal into the central region of the specimen (Shah et al. 2006). As a result, a higher strain was recorded for the specimens with material axes offset from the loading axes (Shah et al. 2006).

These same results were verified with the pregnant porcine uterine tissue. When the material axes were aligned with the loading axes, all of the tests had failure initiate in the arm of the specimen outside of the region where strain was calculated. Because necking of the specimen occurs in the cruciform arm, the circumferential direction strain is underreported at the optical markers for the tests with no offset. On the other hand, the tests with the 22 degree offset had the failure initiate at the corner of the central region of the specimen at the stress concentration. By creating an offset between the loading axes and the material axes, the strain was evenly distributed to the region encompassed by the optical strain markers. Ultimately this also allowed for a greater stress and strain to be recorded before failure occurred in the specimen and therefore

allowed for more data to be collected for the biaxial loading of pregnant porcine uterine tissue. The peak longitudinal stress, peak longitudinal strain, and peak circumferential strain were all significantly lower for the tests with no offset of the material axes ($p<0.001$). The peak stress in the circumferential direction was not significantly different between the two test series ($p=0.45$).

There is a discrepancy between the stress versus strain curve for the circumferential direction in the 0 and 22 degree offset test series (Figure 56). This is attributed to the under estimate of circumferential strain at the location of the optical markers in the no offset scenario. The longitudinal direction stress versus strain curve is similar for both of the test series and therefore indicates the 22 degree offset does not have an adverse effect on the material response. For the discussion of dynamic biaxial tissue testing of pregnant porcine uterine tissue, the stress and strain data from the 22 degree offset tests will be used.

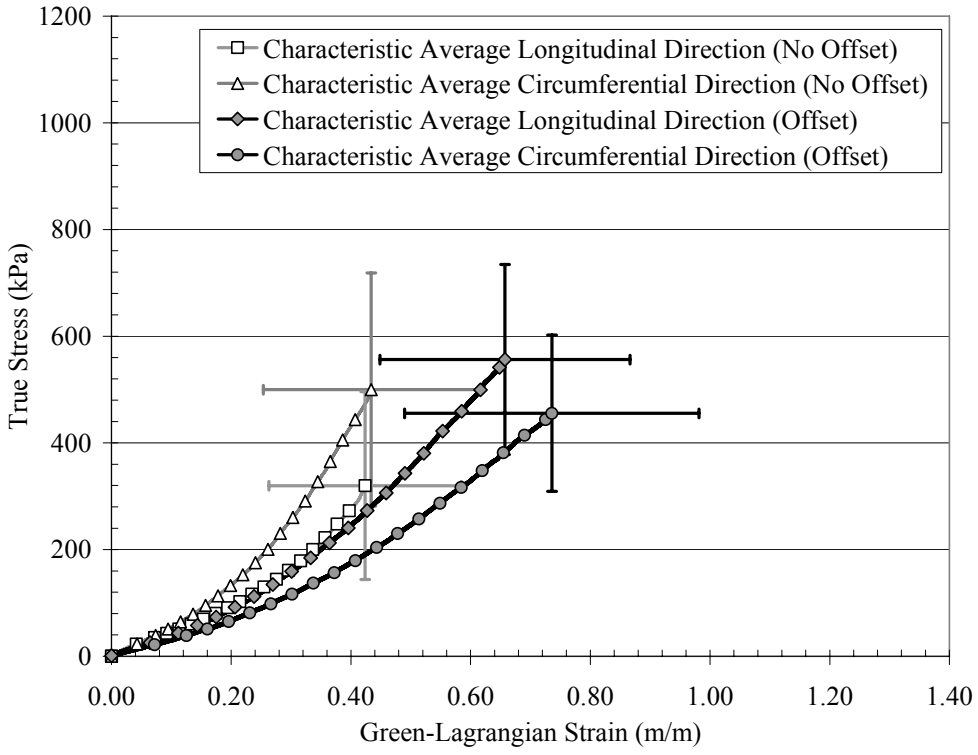

Figure 56: The characteristic curves for the 22 degree offset data are compared to the characteristic curves for the 0 degree offset data.

Donors. The five uteri used for the current study do not have significant differences in peak stress or peak strain values for the circumferential and longitudinal directions ($p>0.25$). Therefore, the data from all uteri were averaged to present loading and peak stress-strain data. Because the information regarding sow age and number of fetuses for each uterus is not known, this study could not address the effects of those variables. Future research could perform more testing to address variability in the stress-strain curve as a function of several gestational variables. Moreover, the regression analysis indicated there were no significant differences in the peak stress and strain of the specimens based on their proximity to the ovary or vagina along the uterine horn ($p>0.10$).

Comparison to Previous Studies.

The stresses, strains, and elastic moduli from the current study are compared to previous research studies (Table 5). Only the data from the tests with material axes 22 degrees offset from the loading axes are used in the comparison. Although the results for this study are presented in Green-Lagrangian strain, true strain values will be used in the comparison of the current study to previous literature. Similarly, the previous published data in engineering strain values were converted to true strain values. Because there has not been a study that tested porcine uterus samples or uterus with a biaxial test setup, there is not a direct source for comparison. The data are compared primarily to the two most extensive previous studies by Pearlman and Pearsall (Pearsall and Roberts 1978, Pearlman 1999). The other studies are limited in their data available for comparison as well as the number of tests completed.

Peak Stress. The peak stress data in the current study are similar to the peak stress reported for unfrozen human pregnant uterine tissue tested in uniaxial tension at quasi-static rates (Wood 1964). The quasi-static peak stress of 483 kPa, measured by Wood (1964), is similar to the circumferential direction average peak stress for dynamic biaxial tests of the uterine tissue measured in this study. The longitudinal direction peak stress in the current study is slightly higher. Due to the viscoelastic behavior of muscle, it is expected a quasi-static loading rate such as Wood et al. tested would provide a lower peak stress than the current study using dynamic loading conditions. Peak strain is not reported for the human tissue tests performed by Wood.

When compared to non-pregnant human uterus material data, the peak stresses from biaxial porcine samples are lower (Pearsall and Roberts 1978). The range of peak stresses for Pearsall's failure tests on human non-pregnant uteri is 550-2069 kPa and the range of peak stresses for the current study is 237-1047 kPa. There are a few reasons for this difference. First, pregnant tissue is more elastic due to the changes in the myometrium and can strain more with a lower peak stress than non-pregnant tissue (Cunningham and Williams 2005). Moreover, the peak stress reported in the biaxial tests is only indicative of the loading until failure occurred. Therefore, this peak is a lower bound on failure stress, which should be greater than or equal to this value due to the stress concentration at the corner of the specimen. Finally, it is possible that this difference could be because the porcine uterus might have a lower peak stress than human uterus; however, there are no studies to show this.

Peak Strain. The peak strain for the porcine uterine tissue, reported as true strain, had a minimum value of 0.24 and a maximum value of 0.61. Previously published research on uniaxial human uterine tissue failure tests reported peak true strain values from 0.30 to 0.95 (Pearsall and Roberts 1978). This includes a higher range of peak strains than the current study using dynamic biaxial testing methods. The loading rate of the tissue could contribute to this difference. The biaxial tests are at a dynamic loading rate which is associated with a lower failure strain for viscoelastic tissue. In addition, the biaxial specimens are being strained equally in two dimensions, which causes the peak strain to be less than a peak uniaxial strain for the same tissue (Bass et al. 2004). Furthermore, for the biaxial tests the peak strain is recorded at the time the tissue fails in the corner of the specimen which is sub-failure strain at the region in the center of the specimen.

Pearlman's lower uterine segment samples had sub-failure strains from uniaxial tension in the range 0.36 to 0.55 when converted to true strain (Pearlman 1999). The only study to use pregnant uterine tissue from the fundal region of the uterus was one test by Aston-Miller in which the peak strain in the uterus was recorded as 0.60 when the UPI failed (Rupp et al. 2001b). Assuming this is reported as engineering strain, the true strain equivalent is 0.47. Both of the lower uterine segment samples as well as the single test from the fundal region have peak strain values that match the current biaxial pregnant porcine uterine tissue data set.

Moveover, when considering the long term goal of this research to provide information necessary in predicting placental abruption, it is noted that the material response of the uterus is very different than the material response previously reported for placental tissue (Figure 57) (Chapter 4). Placental abruption, failure of the uteroplacental interface, was discussed as the injury mechanism due to different material properties of the uterus and placenta (Pearlman 1997). Since it is not possible at this time to complete material tests on the human uteroplacental interface, knowing the material properties and peak strains of the uterus and placenta are important factors in addressing failure of the uteroplacental interface.

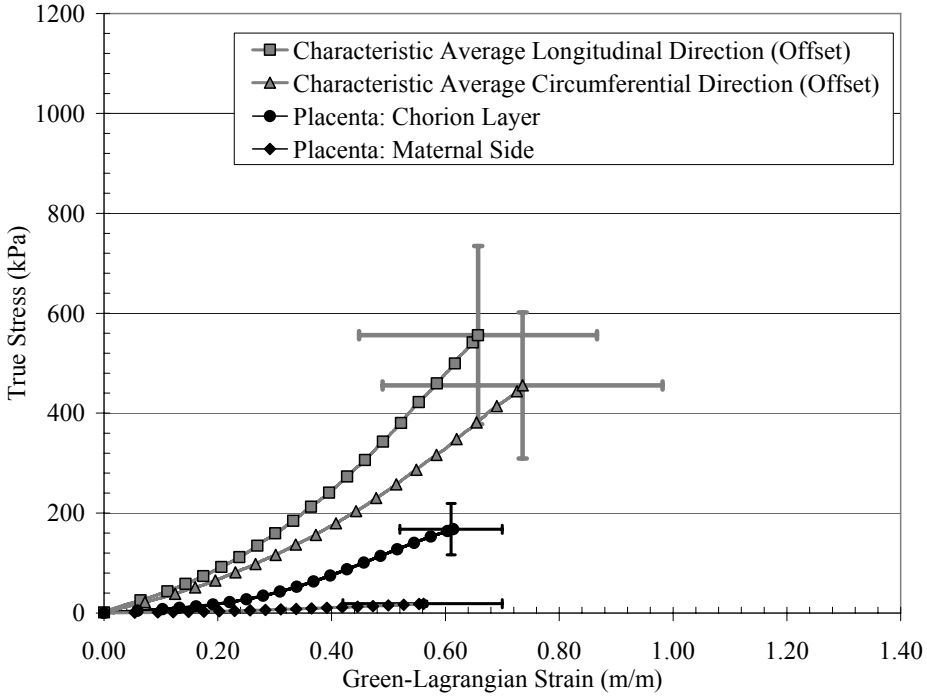

Figure 57: The pregnant porcine uterus characteristic curves are compared to human placental tissue data.

Elastic Modulus. The linear elastic moduli for the biaxial porcine data are reported for the toe and failure regions on the characteristic average curves. The toe region slopes are 393 kPa and 467 kPa. The failure regions have elastic moduli values of 1974 kPa and 2500 kPa for the circumferential and longitudinal directions respectively. Pearsall's human non-pregnant tissue had a linear elastic modulus values from 500 kPa to 1378 kPa when tested in uniaxial tension at a quasi-static rate (Pearsall and Roberts 1978). The moduli for the toe region of the porcine stress-strain curves are at the lower range of moduli reported for Pearsall's tests. When the failure region is used for the modulus calculation, the biaxial porcine tests greatly exceed the range for

non-pregnant quasi-static tissue tests. For a non-linear material response, the region of the curve in which the modulus is calculated can dramatically change the value. Pearsall calculated the tangent to the stress-strain curve at a stress value of 70 kPa for all of the specimens. This is approximately 3%-12% of the failure stress. As a result of taking the modulus in this region, the values reported by Pearsall are generally under representative of the slope of the curve during failure. In addition to the possible inconsistency between studies in calculating a linear elastic modulus, there are other reasons the dynamic biaxial porcine moduli would be different than the non-pregnant quasi-static uniaxial testing moduli. For a viscoelastic tissue, such as the uterus, a dynamic loading condition should produce a higher elastic modulus. However, pregnant tissue is more elastic from the changes in the myometrium and therefore would have a lower elastic modulus (Cunningham and Williams 2005). Because the non-pregnant uterus is tested in uniaxial tension and the pregnant porcine tissue is tested in biaxial tension, the difference in elastic modulus can be a result of the different loading conditions (Bass et al. 2004). The reason for this is that with biaxial testing the tissue is resisting load in two dimensions rather than one. As a result, the higher peak stress at a given strain is associated with biaxial tests compared to uniaxial tests (Bass et al. 2004). This would cause a higher elastic modulus for a biaxial test of the same tissue tested in uniaxial tension.

Table 5: Summary of material properties of uterine tissue.

Source (Year)	Tissue Type	Pregnant	Test	Peak Stress Range (kPa)	Max True Strain	Linear Modulus Range (kPa)	Failure
Ohara (1953)	Rabbit	No	Quasi-static Uniaxial tension	177	0.92*		Yes
Wood (1964)	Human - cesarean section	Yes	Quasi-static Uniaxial tension	483		1207	
Conrad (1966)	Human –cesarean section	Yes	Quasi-static Uniaxial tension			586	
Conrad (1966)	Human - hysterectomy	No	Quasi-static Uniaxial tension			965	
Pearsall (1978)	Human- hysterectomy	No	Quasi-static Uniaxial tension (parallel to long axis)	550-2069	0.30-0.95	500-1378	20+ Failure
Pearlman (1999)	Human - cesarean section then frozen	Yes	Quasi-static Uniaxial tension	9-105	0.36-0.55*	20-279	4 Sub-Failure
Ashton-Miller (2001)	Human –with UPI	Yes	Quasi-static Uniaxial tension		0.47*		Yes
Manoogian (2008)	Porcine Circumferential Direction	Yes	Dynamic Biaxial	456±146 237-824	0.45±0.20 0.24-0.59	393/1974	16 Failure
Manoogian (2008)	Porcine Longitudinal Direction	Yes	Dynamic Biaxial	557±178 297-1047	0.42±0.17 0.29-0.61	467/2500	16 Failure

* These values have been converted to true strain from their published values.

Specimen Properties

Specimen Shape. In previous research, biaxial tensile tests have been conducted primarily on square or cruciform shape specimens. While both geometries have their limitations, the more common geometry is the cruciform shape (Waldman and Lee 2005). In biaxial research for composite, fabric, and planar connective tissues, the cruciform shape has been used extensively (Monch and Galster 1963, Flynn et al. 1998, Langdon et al. 1999, Tandon et al. 2002). Due to Saint-Venant's principle stating that the gripping of the specimen only affects the local stresses, the long sample arms provide the advantage of maximizing the distance from the grip to the regions where the strains are measured. For this study, the modified cruciform shape was chosen. The modified cruciform shape with the arm width at the grip being wider than the width at the innermost region of the arm provides the best loading profile for a dynamic test (Shah et al. 2005, Shah et al. 2006).

Tissue Degradation. All uterine tissues used for testing in this study were extracted from the animal immediately following death. They were stored submerged in saline and refrigerated until just prior to testing when they were allowed to reach room temperature. All tests were completed within 7 days of the hysterectomy. A previous study on muscle tissue analyzed the effects of postmortem time and storage on material properties (Van Ee et al. 2000). It was determined that muscle tissue would not break down over the course of a few days if kept hydrated and refrigerated (Van Ee et al. 2000). The uterine tissue for this study was never frozen. The *in vivo* state of the tissue thickness and hydration are not known. Therefore, the stresses using the thickness at the time of testing are presented in this study. Additional studies could be preformed to track the changes of the uterine thickness from the initial removal from the donor and as time progressed after removal. As a result of storing the tissue in saline, refrigerated, and never frozen, the integrity of the muscle was maintained prior to testing for the current study.

Biaxial Test Considerations

Peak Data. The cruciform shape creates a stress concentration in the corner of the central region when tension is applied. Stresses and strains were measured in the central region of the specimen where the optical markers were located. Because data were only collected until the

tissue failure was observed in the video, the peak stresses and strains from the central region are sub-failure measurements. Failure in the video was used to mark the end of a test because strain data was collected with optical markers which no longer accurately represented strain once failure occurred in the specimen. Moreover, the load was no longer distributed evenly between the four grips. These sub-failure peak stresses and strains are considered a conservative estimate for the failure stresses and strains. Although the musculature structure of the uterus is uniform, the presence of blood vessels creates local material differences. It was not possible to control for vasculature when extracting samples. As a result, this contributes to the variability in peak values from the porcine tissue.

Testing muscle tissue in dynamic loading without preconditioning is more similar to the *in vivo* response of the tissue than it is with preconditioning (Van Ee et al. 2000). Because this tissue was not preconditioned prior to dynamic loading, it is assumed that the dynamic response measured from the specimen and reported in this study is most similar to the *in vivo* state of the porcine uterine tissue.

Tissue Grips. The two methods to grip biaxial specimens are clamps or sutures. While sutures are recommended for reducing the boundary condition effects, in a dynamic test clamps provide a more rigid coupling to the tissue (Sun et al. 2005). Sutures can expand and tear through the material. Additionally, clamps more closely model *in vivo* loading of the tissue by pulling uniformly across the specimen (Sacks and Sun 2003). Research has shown that gripping the tissue specimen with clamps provides a uniform loading of the material fibers versus discrete loads from sutures (Waldman and Michael Lee 2002, Waldman and Lee 2005). To prevent slipping of the tissue, the clamps in this study had a serrated grip.

Assumptions. The assumptions made to calculate the material properties are that the soft tissue is incompressible and has a uniform thickness. The assumption that soft tissue is incompressible has been established by previous researchers for uterine muscle tissue (Deyer et al. 2000). A Poisson's ratio of 0.5 was used for this study. If the actual Poison's ratio were less than this, it would result in an overestimate of the actual tissue thickness. Therefore, the actual stresses would be slightly higher than reported in this paper.

A necessary assumption to calculate stresses at the center of the specimen is that there is an even load transmission from the grip to the center of the specimen. It is not possible to quantify the edge effects from the grips and consider those when scaling the load to the central region where the optical markers are present. Thus, the load at the grip is simply scaled linearly using the length relationship between the central markers to the width where the specimen arm is connected. Previous biaxial tissue research using small angle light scattering mapped collagen fiber orientations in specimens during loading with both clamps and sutures as the gripping mechanism (Waldman et al. 2002). While the specimen shape was square and not crucible, both gripping mechanisms resulted in edge effects that made the stress distribution in the center of the specimen not uniform. Previous research with the crucible shape specimen predict that not compensating for the edge effects causes a small over prediction of stress (Shah et al. 2006).

Future Applications

Studies on uterine tissue properties prior to the current study focused on uniaxial tension response with quasi-static loading conditions. Uterine tissue response at dynamic rates for biaxial loading will advance the design of pregnant occupant models to represent more accurately *in vivo* pregnant uterine tissue response to high rate impacts. Uterine tissue loading information combined with research on placental material properties will augment the current methods of predicting placental abruption. Placental abruption, failure of the uteroplacental interface, occurs much more often than uterine rupture. The peak stress data for the uterine wall will give researchers insight on uteroplacental failure properties since that tissue has been too difficult to acquire for materials testing. Moreover, updating the material properties in the uterine wall for pregnant occupant models will provide a more accurate non-linear response to dynamic impacts. Updated pregnant computational models can also aid in the development of pregnant crash test dummies. Additionally, parametric studies with pregnant computational models can provide a method to define global injury measures that correspond to local tissue failure. These global injury measures such as deflection or pressure can then be used with pregnant crash test surrogates.

Conclusion

Currently pregnant occupant computational models and crash test dummies are designed from limited available uterine tissue material data. The current study presents stress-strain data for pregnant porcine uterine tissue when loaded biaxially in tension at a dynamic rate. A total of 39 tests were completed and analyzed to develop stress-strain curves and peak strain data for pregnant porcine uterine tissue. At a loading rate of 1 strains/s, the circumferential direction peak stress component is 456 ± 146 kPa with a corresponding peak strain 0.45 ± 0.20. The peak stress for the longitudinal direction is 557 ± 178 kPa with a peak strain 0.42 ± 0.17. It has been shown that due to the muscle fiber orientation and gestational changes in the uterine muscle tissue, the circumferential direction has a greater peak strain than the longitudinal direction with similar peak stresses. The results presented in this paper will be useful in modeling pregnant uterine tissue response to dynamic loading and evaluating the risk of placental abruption due to strain in the uterus.

Chapter 7:
Dynamic Material Properties of Pregnant Human Uterus and Pregnant Porcine Uterus

Introduction

Although human uterine tissue has been tested, there are limitations with non-pregnant and hysterectomy uterus samples as material models for the fundal region of a pregnant uterus. Additionally, all of the previous uterine tissue tests are at quasi-static rates but loading in a motor vehicle crash is at a dynamic rate. Soft tissue such as the uterus is viscoelastic; therefore, it should be loaded at the rate in which the material properties are needed (Weiss et al. 1996, Sacks and Sun 2003). In previous studies, the porcine uterus has been used as a model of the pregnant human uterus because of its similarity and availability. The purpose of this study is to obtain material properties for pregnant human uterine tissue as well as pregnant porcine uterine tissue at a dynamic loading rate. This information will advance the ability of pregnant occupant models to predict the uterine tissue response in a motor vehicle crash. Moreover it will determine if the porcine uterus can be used accurately as a surrogate for the pregnant human uterus.

Methods

A strip of pregnant human uterine tissue along the transverse incision was obtained during a typical cesarean section procedure and placed in a saline bath until testing. All tissue samples were tested within 36 hours of surgery. Donor tissue followed the Wake Forest University Baptist Medical Center Institutional Review Board informed consent procedures. Each donor specimen varied in size and shape but was approximately 5 cm long and 1.5 cm wide and included the full thickness of the lower uterine segment. The full specimens were sectioned into smaller individual pieces using a series of long steel razor blades that were spaced 5mm apart (Figure 58). After acquiring the thin tissue slices, a steel bent stamp was used to obtain a dog bone shape coupon from the rectangular slice (Figure 58). A sharpened edge to the steel stamp minimized sheer stress in the tissue during the stamping procedure. The result of the stamping procedure was individual tissue coupons from the same donor with a uniform shape. Each

coupon was kept hydrated throughout the preparation and prior to testing. Human uterine tissue came from 3 donors with 4, 2, and 3 individual specimens resulting from each donor piece respectively.

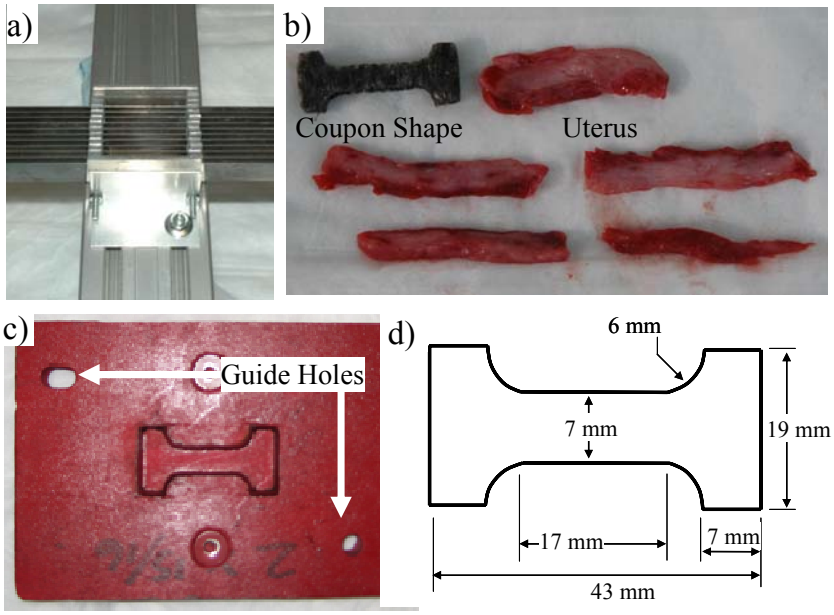

Figure 58: a) A series of blades 5 mm apart cuts the tissue into sections. b) Four or less usable pieces are obtained from each donor. c) A steel bent stamp is used to cut the tissue into a dogbone shape. d) The stamp provides uniform tissue samples.

Porcine uterine tissue was tested within 36 hours following death. One horn from the whole porcine uterus was used to obtain samples oriented in both the longitudinal and circumferential directions (Figure 59). In a porcine uterus, the uterine wall meets at the mesometrium and forms a tubular shape. The samples for this study were taken on the side of the uterine wall opposite the mesometrium connection (Figure 60). Because the circumferential and longitudinal fibers cross perpendicularly, the specimens with a circumferential orientation had the circumferential fibers aligned with the loading axis. The longitudinal specimens had the longitudinal fibers aligned with the loading axis. Along the length of the uterine horn, specimens were taken in order with each piece alternating orientation. In the same manner as for the human uterine tissue, each specimen was stamped into a dog bone coupon shape. From each of the three porcine uteri a total of 6, 9, and 15 specimens were tested. A total of 15 specimens had the longitudinal orientation and 15 had the circumferential orientation.

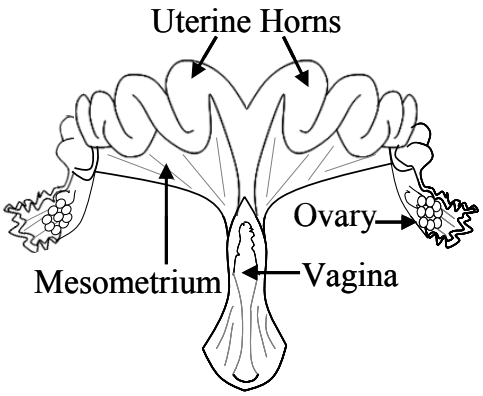

Figure 59: Diagram of a bicornuate porcine uterus.

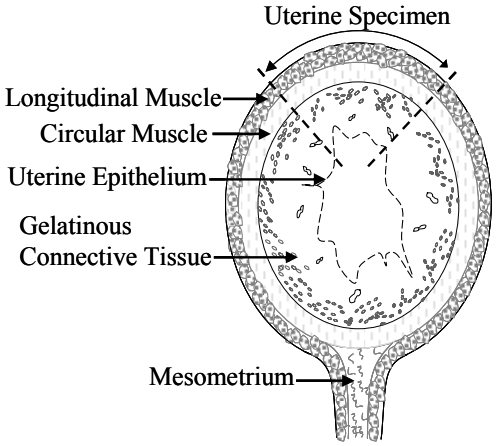

Figure 60: Cross sectional view of a porcine uterus.

A custom designed system of linear motors was used for uniaxial dynamic tensile tests of uterine tissue coupons (Figure 61). The system included one multi axis controller (Parker ACR9000, Irwin, PA) that served as a power supply for a motor driver (Parker ViX, Irwin, PA) which controlled the two linear motors with stages (Parker Daedal MX80S, Irwin, PA). The two individual stages were each instrumented with a load cell (OMEGA LCFL, 10 lbf, Stamford, CT), potentiometer (Space Age Control, 160-1705, 540 mm, Palmdale, CA), and accelerometer (Endevco 7264B, 2000 G, San Juan Capistrano, CA. On each side of the test specimen, the direct path from the tissue clamp went through the load cell and was rigidly connected to the linear motor stage. The inertial load of the mass (0.0374 kg) in front of the load cell was multiplied by the acceleration to compensate the measured reaction load. Synchronous motion of the motors allowed both of the stages to pull the tissue in tension at the same time for an overall velocity which corresponded to the desired strain rate. The strain rate chosen for this study was approximately 1.5 strains/s. This rate represents loading expected in a motor vehicle crash as determined from previous computational modeling (Moorcroft et al. 2003a).

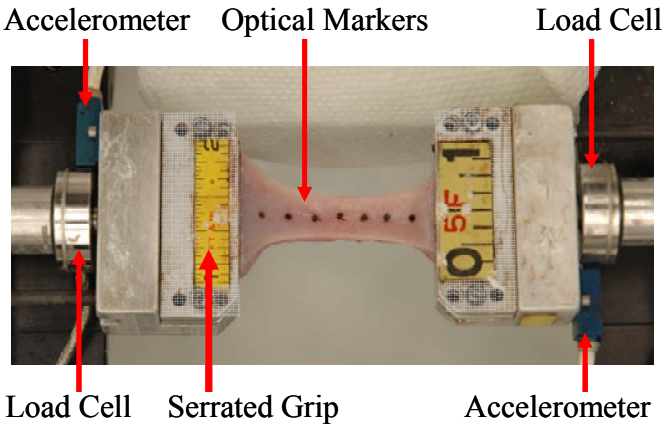

Figure 61: The specimen is mounted between two serrated grips which are instrumented with both a load cell and an accelerometer while high speed video records the test event.

Each specimen was mounted in the testing setup with the same initial conditions. The specimen was aligned in the grip along the centerline of the loading axis. Each test began with a small amount of slack in the specimen. By supporting only its own weight, the tissue had a minimal preload condition. Optical markers were applied to the tissue after the specimen was mounted.

Local stress and strain were calculated for each specimen. Local deformation was recorded using high-speed video (Phantom V4, Wayne, NJ) at 500 frames per second with 512 by 512 resolution. Optical marker tracking was performed with TEMA® Advanced Motion Analysis Software (Linköping, Sweden). Using the configuration for these tests, the error in the motion analysis is 0.02 mm. The optical markers on either side of the location where the specimen tore were used to calculate the local strain. The measured displacement data are fit with a 5^{th} order polynomial. The average R^2 value for the displacement curve fit is 0.995 ± 0.007. In the same manner, the measured force data were fit with a 5^{th} order polynomial with an average R^2 value of 0.999 ± 0.001. Local stress was acquired by determining the location on the specimen where failure occurred and then taking the width and thickness of the specimen in that location from the pretest pictures as the initial cross sectional area. The approximate error in the width and thickness measurements from the pretest pictures is ±0.12 mm. From the initial area measurement, the cross sectional area at the time of failure was calculated using the local strain and a Poisson's ratio value of 0.5. The assumption that uterine muscle tissue is incompressible has been established by previous researchers (Deyer et al. 2000).

The initial point for each stress versus strain curve was determined from previous studies measuring intrauterine pressure during labor for humans. Caldeyro-Barcia *et al.* determined that the baseline pressure in the uterus during the first stage of labor is 10 mm Hg (Cunningham and Williams 2005). Using the average crown to rump length of 360 mm as the diameter and an average thickness at the lower uterine segment equal to 0.5 cm, a spherical pressure vessel assumption estimates the baseline pressure in the uterine wall is 23.9 kPa (Cunningham and Williams 2005, Stitzel et al. 2007). The engineering stress for each test was calculated from the time the stages began to move. When the engineering stress value was equal to 23.9 kPa, the stress and strain were set to zero and the data reported are in reference to that pre-stress condition. This allowed all of the data reported to have physiological start point and be consistent with one another. True stress and Green-Lagrangian strain are reported for each test until failure occurs in the tissue.

Statistical tests were completed for the peak stress and peak strain data. A standard two sample t-test procedure assuming unequal variances was used to determine statistically significant differences between the peak values among the human uterus, circumferential porcine uterus, and longitudinal porcine uterus test series for both peak strain and peak stress. To determine any significant differences between human uterine tissue donors, a one-way ANOVA analysis was completed with the peak stress data and with the peak strain data. A standard method of determining the characteristic average was used to determine the average response for each of the three test series (Lessley et al. 2004). Three curves represent the pregnant human uterine tissue tests, circumferential porcine uterine tissue tests, and longitudinal porcine uterine tissue tests respectively. Standard deviations of the peak stress and strain values were also calculated for each group of tests.

Results

Data for dynamic tensile tests are reported in Green Lagrangian strain and true stress values. Frames from the high-speed video of a test show the tissue specimen fails in the gage length of the dog bone shape coupon (Figure 62).

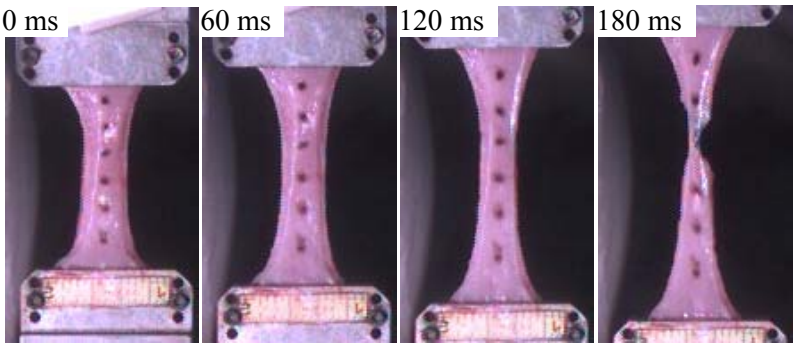

Figure 62: A typical specimen fails in the gage length of the coupon.

All of the human uterine tissue stress versus strain data are plotted together with the average and peak standard deviations (Figure 63). The stress versus strain data for pregnant human uterine tissue have an average peak strain of 0.61 ± 0.11 and a corresponding peak stress of 934.4 ± 645.6 kPa. The ANOVA analysis indicated no significant differences between the peak stress data ($p>0.05$) or peak strain data ($p>0.05$) for the three donor groups.

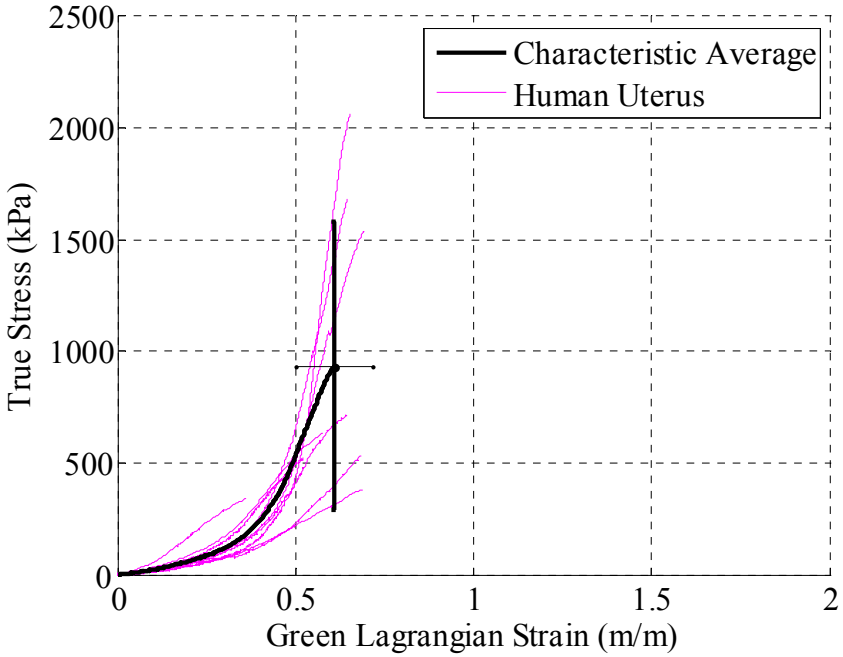

Figure 63: The average pregnant human uterine tissue response has a peak stress of 934.4 ± 645.6 kPa with a peak strain equal to 0.61 ± 0.11.

For the porcine tissue tests, the results are reported separately for the circumferentially oriented tissue specimens and the longitudinally oriented tissue specimens. The circumferentially oriented porcine uterine tissue tests have an average peak strain of 0.38 ± 0.12 and a

corresponding peak stress of 670.1 ± 315.0 kPa (Figure 64). However, the longitudinal porcine uterine tissue tests have an average peak of 517.4 ± 287.5 kPa and 1.06 ± 0.37 strain (Figure 65).

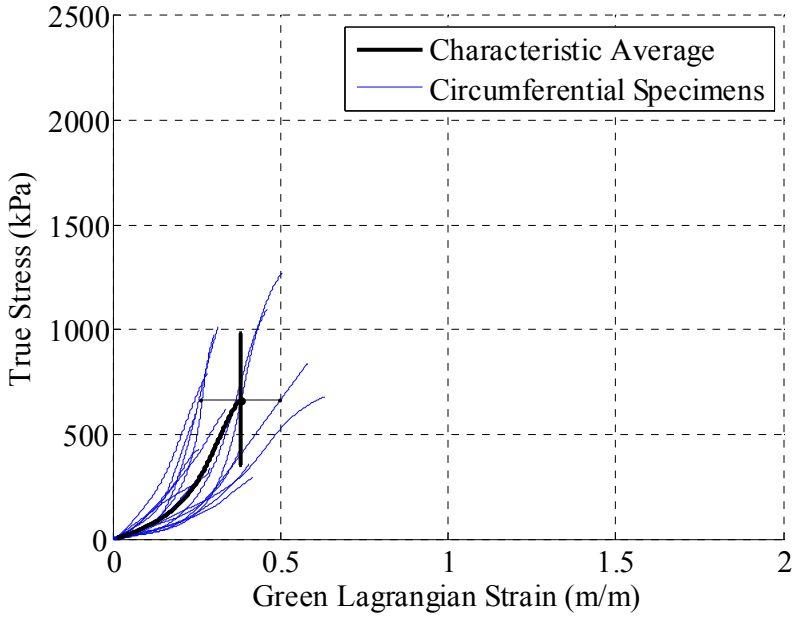

Figure 64: The average response of the porcine tissue in the circumferential direction has a peak stress of 670.1 ± 315.0 kPa with a corresponding peak strain 0.38 ± 0.12.

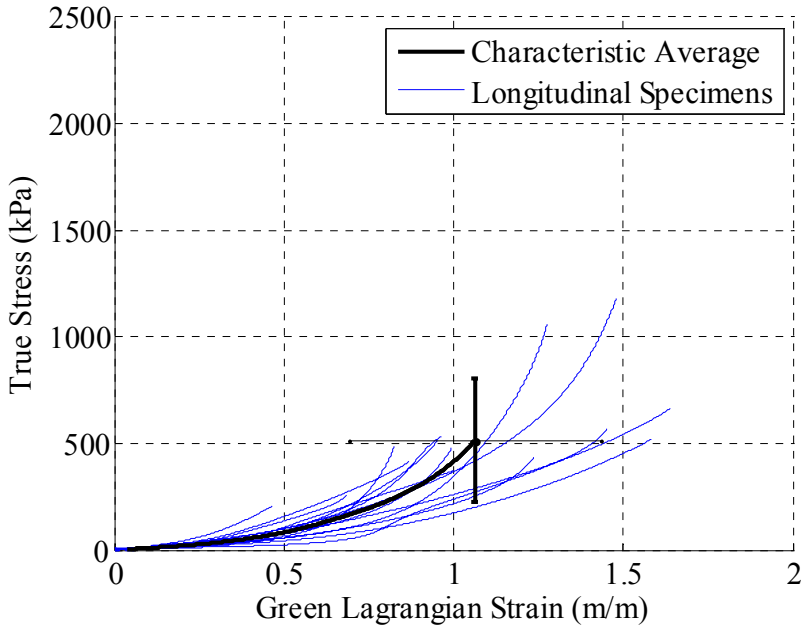

Figure 65: The average response of the porcine tissue in the longitudinal direction has a peak stress of 517.4 ± 287.5 kPa with a corresponding peak strain 1.06 ± 0.37.

The standard two sample t-test procedure was used to evaluate the failure stresses among the three test series. No statistically significant differences were found between the circumferential porcine, longitudinal porcine, and human pregnant uterine test series peak stresses ($p>0.1$). The same statistical test was also used to evaluate the peak strain among the three test series. All three combinations of test data had statistically significant differences in the failure strain measurement ($p<0.0005$) (Figure 66).

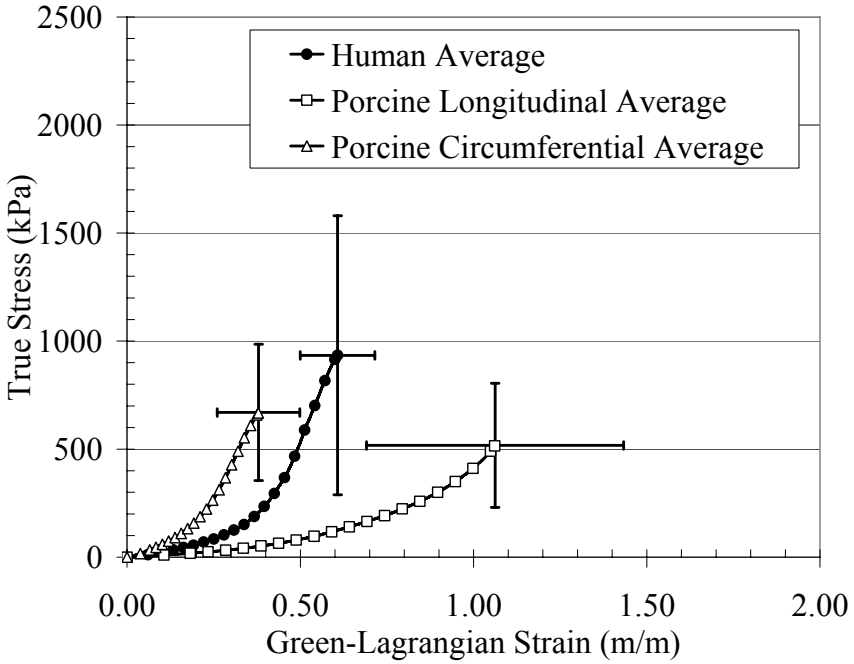

Figure 66: The average response of the porcine tissue in two orientations is compared to the human tissue response.

Discussion

The results from this study give stress versus strain curve loading and failure information for the pregnant human uterine tissue and pregnant porcine uterine tissue. When comparing the three test series, the human tissue has a similar failure stress value as both of the porcine test series. However, the orientation of the porcine tissue determines whether it has a higher or lower failure strain than the human tissue. Although there is variability in the data, the standard deviations in the failure values are assumed to be dependent on specimen variability since the testing procedure was the same for each specimen.

There are limitations with this study in that several gestational variables in the human could not be addressed. Only uterine specimens from women in their late stages of gestation were obtained. Additionally, there were not enough donors to characterize the specimens based on parity, age, or other parameters. The gestational information was unknown for the porcine tissue and therefore was not reported as a variable in the study. For the human tissue, the tissue was collected from the location of the cesarean incision. Typically this is at the lower uterine segment which can be a more elastic tissue than the fundus of the uterus where the placenta typically attaches (Cunningham and Williams 2005). By testing the lower uterine segment, the study is accounting for changes in the uterine tissue during gestation. However, it is suggested in the literature the tissue properties for the upper uterus would be less elastic and therefore have a higher stress and lower strain at failure. Because it is not possible to readily collect pregnant uterine tissue pieces at the fundus, the lower uterine segment is a suitable substitute. For the porcine uterus, there is no regional variation along the uterine horn and all specimens were extracted from the same location opposite the mesometrium in the circumferential direction (Chapter 6).

The current study has a similar range of human tissue failure stress values, 339.9 kPa to 2063.4 kPa, as the previous study by Pearsall and Roberts of human uterine specimens (Pearsall and Roberts 1978). Additionally, the range of peak strains, 0.36-0.69, is also similar between the two studies using human uterine tissue. The specimens used by Pearsall (1978) were non-pregnant and loaded at a quasi-static rate. Non-pregnant uterine tissue is expected to have a less elastic stress-strain response than pregnant uterine tissue. However, loading the same viscoelastic tissue at a quasi-static rate compared to a dynamic rate would produce a more elastic stress-strain response (Fung 1993). Due to the rate of loading, it is expected the current study should have a higher failure stress and strain than Pearsall (1978) but the pregnant tissue would have a lower failure stress and strain than the non-pregnant tissue in the previous study. Because of these two compounding factors, the tissue response is actually similar to that reported by Pearsall (1978).

The test series by Pearlman in 1999 is a more suitable comparison of pregnant human uterine tissue (Pearlman 1999). However these tests are limited in number and report sub-failure measurements only. At an equivalent strain value, the quasi-static tests by Pearlman (1999) had a much lower stress value than the current study measured. This is expected from a viscoelastic

tissue at a quasi-static loading rate. More tissue tests at a quasi-static rate would be necessary to have a statistical significance.

The previous research using pregnant porcine uterine tissue included dynamic biaxial tissue loading until failure (Chapter 6). For those tests, the reported circumferential peak stress was 456 ± 146 kPa with a corresponding peak true strain 0.45 ± 0.20 and the longitudinal peak stress was 557 ± 178 kPa with a corresponding peak true strain 0.42 ± 0.17. The peak strains for the biaxial porcine tests are closer to the human response than the uniaxial porcine tests. Although, the peak stresses are different, the stress versus strain curves match closely up to 200 kPa (Figure 67).

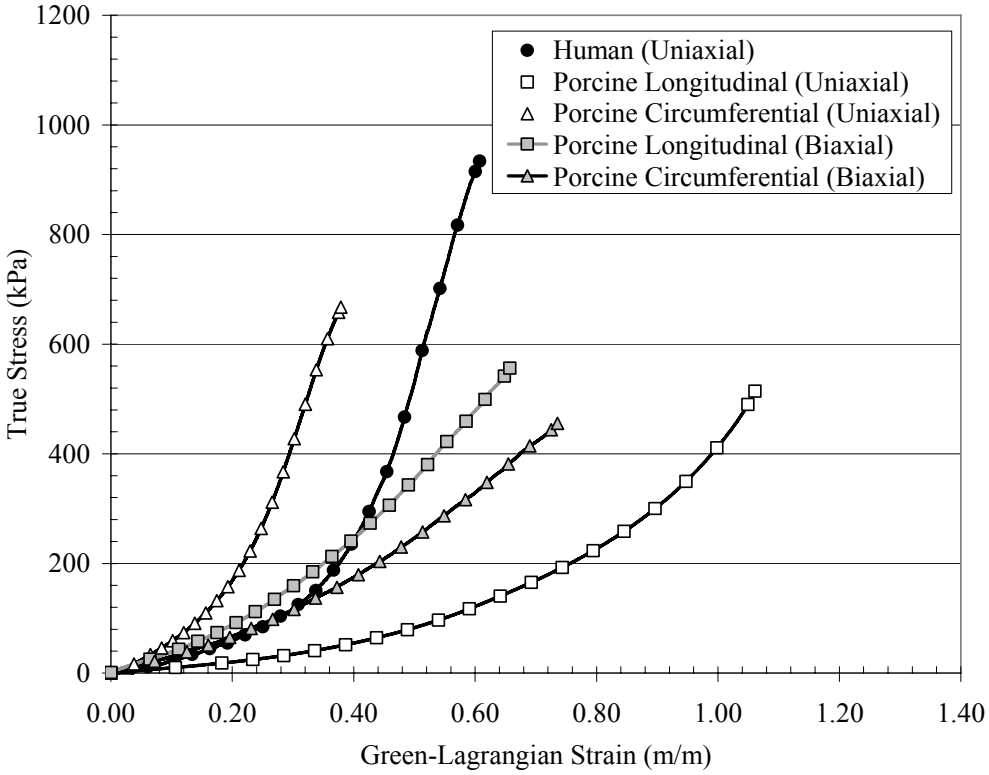

Figure 67: The uniaxial and biaxial dynamic tensile tests of pregnant porcine uterus are compared to the uniaxial dynamic tensile tests of pregnant human uterus.

In general, the pregnant human uterine tissue tests are similar to the limited available previous human uterus data. The matched uniaxial tests with the pregnant porcine uterine tissue have a comparable peak stress value, but do not model the stress-strain response of the human uterus accurately. The longitudinal direction over predicts the strain and the circumferential direction

under predicts the strain at the same stress value. However, the previous research using pregnant porcine tissue in biaxial tension is a better approximation of the human uterine tissue response. Although more testing with pregnant human uterine tissue is needed, this study provides useful information on the response to a dynamic tensile load. Moreover, because the porcine biaxial data is in agreement with the human data, it is reasonable to use the pregnant porcine uterus as a surrogate for more advanced research when the human tissue is limited in size and availability.

Conclusion

This study presents 9 uniaxial tensile tests for pregnant human uterine tissue and 30 uniaxial tensile tests for pregnant porcine uterine tissue. Material properties of the both uterine tissues were evaluated at 1.5 strains/s. In addition to providing failure stress and strain data, the study compares the responses of the two tissues. The porcine tissue has a similar failure stress to the human. However, the direction of loading dictates whether the porcine failure strain over or under estimates the human tissue behavior. Based on comparing the results from this study to previous research, the porcine uterus is an appropriate model for the human uterus when loading in biaxial tension as it would be during gestation. When compared to previous testing of uterine tissue, the current study compares favorably to the available human uterine tissue data. This study provides additional data for the non-linear elastic response in a dynamic loading condition using fresh pregnant uterine tissue samples. In summary, tensile material properties for the human pregnant uterus have been determined at a dynamic rate for use in the advancement of pregnant occupant computational modeling.

Chapter 8: Summary of Research and Major Contributions to the Field of Biomechanics

Research Summary

As stated in the introduction, this dissertation provides new and significant research to the field of injury biomechanics. Specifically, the research objectives focus on providing data for modeling of pregnant tissue. First, current research tools were used to evaluate the risk to a pregnant occupant in a severe frontal motor vehicle crash as well as during everyday activities. Next, uniaxial tensile tests were used to characterize the various layers of placental tissue from quasi-static to dynamic loading rates. Additionally, pregnant porcine uterine tissue was evaluated in dynamic biaxial tension while pregnant human uterine tissue material properties were determined in uniaxial dynamic tensile tests. As a whole, these objectives provide data that can advance pregnant occupant modeling and ultimately advance pregnant occupant protection in motor vehicle crashes. In order to achieve the ultimate goal of characterizing the uterine and placental tissues for pregnant occupant modeling, there are multiple research objectives that were addressed.

As a result of these studies, multiple research objectives have been addressed:

1. The risk to a pregnant occupant from inertial loading only in a standard NCAP frontal barrier impact was determined.
2. The risk to a pregnant female from inertial loading only in everyday activities and exercises was determined.
3. The effect of the chorion layer on the stress versus strain curve, the ultimate stress, and ultimate strain for human placental tissue when tested in dynamic tension was determined.
4. The stress versus strain curve, the ultimate stress, and ultimate strain for the villous section of the placenta at quasi-static and dynamic strain rates were determined.

5. The stress versus strain curve, the peak stress, and peak strain for pregnant porcine uterine tissue when tested in biaxial dynamic tension were determined.
6. The stress versus strain curve, the peak stress, and peak strain for pregnant human uterine tissue and pregnant porcine uterine tissue when tested in uniaxial dynamic tension were determined.

Determining the risk of adverse fetal outcome using the currently available pregnant occupant model addresses the effectiveness of current vehicle standards in protecting pregnant occupants. Although this model has been validated and provides useful data, advancements in the known properties for the uterus and the placenta will enhance the information available from the simulations. In the current pregnant occupant model, the placenta and uterus are defined as having a linear elastic stress versus strain curves due to limited available information in the literature. Dynamic human placenta testing will improve this and other models by providing the nonlinear stress versus strain loading data with failure stress and strain values. Moreover, the separate material properties for the fetal and maternal sides are determined. Nonlinear stress versus strain data with failure values are provided for pregnant human uterine tissue in uniaxial tension. Because pregnant human uterine tissue is not available for advanced materials testing, dynamic biaxial tests of pregnant porcine uterine tissue were also completed. The biaxial tests model the *in vivo* loading conditions of the uterus while providing stress versus strain data for tissue very similar in structure to pregnant human uterine tissue. The new material characterizations of the placenta and pregnant uterine tissue when loaded dynamically in tension will allow researchers and engineers an unprecedented capability to evaluate pregnant occupant response to dynamic impacts to determine the risk of adverse fetal outcome.

Publications

In summary, this research answers scientific questions previously not addressed in the literature. Each research hypothesis along with the methodology and results that answer that hypothesis will be published in a scientific journal. The research may also be presented at relevant scientific conferences. Currently, it is expected that the research outlined in chapters two through seven will be published as shown (Table 6).

Table 6: Publications plan for research hypotheses outlined in this proposal.

Dissertation Chapter	**Topic**	**Anticipated Journal Submission** *(Auxiliary Conference Presentations)*
Chapter 2	Pregnant Occupant Risk in a Standard Frontal NCAP Motor Vehicle Crash	*(Enhanced Safety of Vehicles)* *(Biomedical Sciences Instrumentation)*
Chapter 3	Evaluation of Pregnant Female Injury Risk During Everyday Activities	*(Biomedical Sciences Instrumentation)*
Chapter 4	Effect of Chorion on Dynamic Tensile Material Properties of Human Placenta	Journal of Biomechanics *(NHTSA Human Subjects Workshop)* *(Biomedical Sciences Instrumentation)*
Chapter 5	Effect of Strain Rate on Material Properties of Human Placenta in Tension	Journal of Biomechanical Engineering
Chapter 6	Dynamic Biaxial Tissue Properties of Pregnant Porcine Uterine Tissue	Stapp Car Crash Journal *(Biomedical Sciences Instrumentation)*
Chapter 7	Dynamic Material Properties of Pregnant Human Uterus and Pregnant Porcine Uterus	Journal of Biomechanics

References

(1999) ACOG educational bulletin. Obstetric aspects of trauma management. Number 251, September 1998 (replaces Number 151, January 1991, and Number 161, November 1991). American College of Obstetricians and Gynecologists. International Journal of Gynaecology and Obstetrics 64(1): 87-94.

(2003) Exercise during pregnancy and the postpartum period. Clinical Obstetrics and Gynecology 46(2): 496-9.

Artal, R., O'Toole, M. (2003) Guidelines of the American College of Obstetricians and Gynecologists for exercise during pregnancy and the postpartum period. Br J Sports Med 37(1): 6-12; discussion 12.

Attico, N.B., Smith, R.J., FitzPatrick, M.B., and Keneally, M. (1986) Automobile safety restraints for pregnant women and children. The Journal of Reproductive Medicine 31(3): 187-92.

Bass, E.C., Ashford, F.A., Segal, M.R., and Lotz, J.C. (2004) Biaxial testing of human annulus fibrosus and its implications for a constitutive formulation. Annals of Biomedical Engineering 32(9): 1231-42.

Conrad, J.T., Kuhn, W. (1967) The active length-tension relationship in human uterine muscle. American Journal of Obstetrics and Gynecology 97(2): 154-60.

Csapo, A., Goodall, M. (1954) Excitability, length tension relation and kinetics of uterine muscle contraction in relation to hormonal status. The Journal of Physiology 126(2): 384-95.

Cunningham, F.G., Williams, J.W. (2005) Williams obstetrics. McGraw-Hill Professional, New York.

Deyer, T.W., Ashton-Miller, J.A., Van Baren, P.M., and Pearlman, M.D. (2000) Myometrial contractile strain at uteroplacental separation during parturition. American Journal of Obstetrics and Gynecology 183(1): 156-9.

Duma, S.M., Cormier, J.M., Hurst, W.J., Stitzel, J.D., and Herring, I.P. (2003) The effects of Seam Design on Airbag Induced Skin Abrasions from High-Rate Shear Loading. The Proceedings of the IRCOBI Conference: 95-107.

Duma, S.M., Moorcroft, D.M., Gabler, H.C., Manoogian, S.M., Stitzel, J.D., and Duma, G.G. (2006a) Analysis of pregnant occupant crash exposure and the potential effectiveness of four-point seatbelts in far side crashes. The Proceedings of the 50th Association for the Advancement of Automotive Medicine Conference 50: 177-88.

Duma, S.M., Moorcroft, D.M., Gabler, H.C., Manoogian, S.M., Stitzel, J.D., and Duma, G.G. (2006b) Analysis of pregnant occupant crash exposure and the potential effectiveness of four-point seatbelts in far side crashes. Annu Proc Assoc Adv Automot Med 50: 177-88.

Fatality Analysis Reporting System. (2005) National Highway Traffic Safety Administration.

Finn, C.A., Porter, D.G. (1975) The uterus. Elek, London.

Flynn, D.M., Peura, G.D., Grigg, P., and Hoffman, A.H. (1998) A finite element based method to determine the properties of planar soft tissue. Journal of Biomechanical Engineering 120(2): 202-10.

Fung, Y.C. (1967) Elasticity of soft tissues in simple elongation. American Journal of Physiology 213(6): 1532-44.

Fung, Y.C. (1993) Biomechanics : mechanical properties of living tissues. Springer-Verlag, New York.

Funk, J.R., Hall, G.W., Crandall, J.R., and Pilkey, W.D. (2000) Linear and quasi-linear viscoelastic characterization of ankle ligaments. Journal of Biomechanical Engineering 122(1): 15-22.

Hardy, W.N., Schneider, L.W., and Rouhana, S.W. (2001) Abdominal impact response to rigid-bar, seatbelt, and airbag loading. Stapp Car Crash Journal 45: 1-32.

Hasberry, S., Pearcy, M.J. (1986) Temperature dependence of the tensile properties of interspinous ligaments of sheep. J Biomed Eng 8(1): 62-6.

Humphrey, J.D., Vawter, D.L., and Vito, R.P. (1987) Quantification of strains in biaxially tested soft tissues. Journal of Biomechanics 20(1): 59-65.

Ivarsson, J., Viano, D.C., Lovsund, P., and Aldman, B. (2000) Strain relief from the cerebral ventricles during head impact: experimental studies on natural protection of the brain. Journal of Biomechanics 33(2): 181-9.

Jernigan, M.V. (2002) Statistical analysis and computational modeling of injuries in automobile crashes.

Jin, X., Lee, J.B., Leung, L.Y., Zhang, L., Yang, K.H., and King, A.I. (2006) Biomechanical response of the bovine pia-arachnoid complex to tensile loading at varying strain-rates. Stapp Car Crash J 50: 637-49.

King, A.I., Eppinger, R.H., Crosby, W.M., and Stout, L.C. (1971) Effects of Lap Belt and Three-Point Restraints on Pregnant Baboons Subjected to Deceleration. Stapp Car Crash Journal 15: 68-83.

Klinich, K.D., Schneider, L.W., Eby, B., Rupp, J.D., and Pearlman, M.D. (1999a) Seated Anthropometry During Pregnancy. University of Michigan Transportation Research Institute, UMTRI-99-16.

Klinich, K.D., Schneider, L.W., Moore, J.L., and Pearlman, M.D. (1999b) Investigations of Crashes Involving Pregnant Occupants. University of Michigan Transportation Research Institute, UMTRI-99-29.

Klinich, K.D., Schneider, L.W., Moore, J.L., and Pearlman, M.D. (2000) Investigations of crashes involving pregnant occupants. The Proceedings of the 44th Association for the Advancement of Automotive Medicine Conference, Chicago, Illinois.

Lam, T.C., Thomas, C.G., Shrive, N.G., Frank, C.B., and Sabiston, C.P. (1990) The effects of temperature on the viscoelastic properties of the rabbit medial collateral ligament. J Biomech Eng 112(2): 147-52.

Langdon, S.E., Chernecky, R., Pereira, C.A., Abdulla, D., and Lee, J.M. (1999) Biaxial mechanical/structural effects of equibiaxial strain during crosslinking of bovine pericardial xenograft materials. Biomaterials 20(2): 137-53.

Lanir, Y., Lichtenstein, O., and Imanuel, O. (1996) Optimal design of biaxial tests for structural material characterization of flat tissues. Journal of Biomechanical Engineering 118(1): 41-7.

Lessley, D., Crandall, J., Shaw, G., Kent, R., and Funk, J. (2004) A Normalization Technique for Developing Corridors from Individual Subject Responses. SAE Technical Paper Series 2004-01-0288: 1-11.

Manoogian, S.J., Duma, S.M., and Moorcroft, D.M. (2007a) Pregnant Occupant Injury Risk Using Computer Simulations with NCAP Vehicle Crash Test Data. The 20th International Technical Conference on the Enhanced Safety of Vehicles Conference, Lyon, France.

Manoogian, S.J., McNally, C., Calloway, B.R., and Duma, S.M. (2007b) Methodology for dynamic biaxial tension testing of pregnant uterine tissue. Biomedical Sciences Instrumentation 43: 230-5.
Manoogian, S.J., McNally, C., Calloway, B.R., Duma, S.M., and Mertz, H.L. (2007c) Utilizing cryogenic grips for dynamic tension testing of human placenta tissue. Biomedical Sciences Instrumentation 43: 354-9.
Marrable, A.W. (1971) The embryonic pig: a chronological account. Pitman Medical, London,.
Martin, P.G. (2000) Properties of Human Skin. PhD Dissertation, University of Virginia, Charlottesville.
Mizrahi, J., Karni, Z. (1975) A Mechanical Model for Uterine Muscle Activity during Labor and Delivery. Israel Journal of Technology 13: 185-191.
Mizrahi, J., Karni, Z., and Polishuk, W.Z. (1980) Isotropy and anisotropy of uterine muscle during labor contraction. Journal of Biomechanics 13(3): 211-8.
Monch, E., Galster, D. (1963) A method for producing a defined uniform biaxial tensile stress field. British Journal of Applied Physics 14: 810-812.
Moorcroft, D.M., Duma, S.M., Stitzel, J.D., and Duma, G.G. (2003a) Computational model of the pregnant occupant: predicting the risk of injury in automobile crashes. American Journal of Obstetrics and Gynecology 189(2): 540-4.
Moorcroft, D.M., Duma, S.M., Stitzel, J.D., and Duma, G.G. (2003b) The Effects of Uterine Ligaments on the Fetal Injury Risk in Frontal Automobile Crashes. Journal of Automobile Engineering Part D 217: 1049-1055.
Moorcroft, D.M., Duma, S.M., Stitzel, J.D., and Duma, G.G. (2003c) A finite element and multi-body model of the pregnant occupant for the analysis of restraint effectiveness. SAE Technical Paper Series 2003-01-0157: 1-11.
Moorcroft, D.M., Duma, S.M., Stitzel, J.D., and Duma, G.G. (2004) The effect of pregnant occupant position and belt placement on the risk of fetal injury. SAE Technical Paper Series 2004-01-0324: 1-8.
Ng, T.P., Bussone, W.R., Duma, S.M., and Kress, T.A. (2006) Thoracic and lumbar spine accelerations in everyday activities. Biomed Sci Instrum 42: 410-5.
Ohara, T. (1953) On the comparison of strengths of the various organ-tissues. Journal of Kyoto Preferred Medical University 53: 577-597.
Pearlman, M.D. (1997) Motor vehicle crashes, pregnancy loss and preterm labor. International Journal of Gynaecology and Obstetrics 57(2): 127-32.
Pearlman, M.D. (1999) Data Acquisition for Development of a Uteroplacental Interface for the Second-Generation Pregnant Abdomen. University of Michigan Health Systems, D.8. Final Report.
Pearlman, M.D., Phillips, M.E. (1996) Safety belt use during pregnancy. Obstetrics and Gynecology 88(6): 1026-9.
Pearlman, M.D., Tintinalli, J.E. (1991) Evaluation and treatment of the gravida and fetus following trauma during pregnancy. Obstetrics and gynecology clinics of North America 18(2): 371-81.
Pearlman, M.D., Tintinalli, J.E., and Lorenz, R.P. (1990a) Blunt trauma during pregnancy. The New England Journal of Medicine 323(23): 1609-13.
Pearlman, M.D., Tintinallli, J.E., and Lorenz, R.P. (1990b) A prospective controlled study of outcome after trauma during pregnancy. American Journal of Obstetrics and Gynecology 162(6): 1502-10.

Pearsall, G.W., Roberts, V.L. (1978) Passive mechanical properties of uterine muscle (myometrium) tested in vitro. Journal of Biomechanics 11(4): 167-76.

Ramsey, E.M. (1975) The placenta of laboratory animals and man. Holt, Rinehart and Winston, New York.

Rupp, J.D., Klinich, K.D., Moss, S., Zhou, J., Pearlman, M.D., and Schneider, L.W. (2001a) Development and testing of a prototype pregnant abdomen for the small-female hybrid III ATD. Stapp Car Crash Journal 45: 61-78.

Rupp, J.D., Schneider, L.W., Klinich, K.D., Moss, S., Zhou, J., and Pearlman, M.D. (2001b) Design, Development, and Testing of a New Pregnant Abdomen for the Hybrid III Small Female Crash Test Dummy. University of Michigan Transportation Research Institute, UMTRI-2001-07.

Sacks, M.S., Sun, W. (2003) Multiaxial mechanical behavior of biological materials. Annual Review of Biomedical Engineering 5: 251-84.

Shah, C.S., Hardy, W.N., Mason, M.J., Yang, K.H., Van Ee, C.A., Morgan, R., and Digges, K. (2006) Dynamic biaxial tissue properties of the human cadaver aorta. Stapp Car Crash Journal 50: 217-46.

Shah, C.S., Mason, M.J., Yang, K.H., Hardy, W.N., Van Ee, C.A., Morgan, R., and Digges, K. (2005) High-Speed Biaxial Tissue Properties of the Human Cadaver Aorta. ASME International Mechanical Engineering Congress 2005-82085: 1-9.

Stitzel, J.D., Halsey, M., Loftis, K., Yu, M., and Anthony, L. (2007) Seated Anthropometry During Pregnancy. Wake Forest University, WFU-10-04-07.

Sun, W., Sacks, M.S., and Scott, M.J. (2005) Effects of boundary conditions on the estimation of the planar biaxial mechanical properties of soft tissues. Journal of Biomechanical Engineering 127(4): 709-15.

Tandon, G.P., Kim, R.Y., and Bechel, V.T. (2002) Fiber-matrix interfacial failure characterization using a cruciform-shaped specimen. Journal of Computational Materials Science 36: 2667-2691.

van Dommelen, J.A.W., Ivarsson, J., Jolandan, M.M., Millington, S.A., Raut, M., Kerrigan, J.R., Crandall, J.R., and Diduch, D.R. (2005) Characterization of the Rate- Dependent Mechanical Properties and Failure of Human Knee Ligaments. SAE Technical Paper Series 2005-01-0293: 1-11.

Van Ee, C.A., Chasse, A.L., and Myers, B.S. (2000) Quantifying skeletal muscle properties in cadaveric test specimens: effects of mechanical loading, postmortem time, and freezer storage. Journal of Biomechanical Engineering 122(1): 9-14.

Waldman, S.D., Lee, J.M. (2005) Effect of sample geometry on the apparent biaxial mechanical behaviour of planar connective tissues. Biomaterials 26(35): 7504-13.

Waldman, S.D., Michael Lee, J. (2002) Boundary conditions during biaxial testing of planar connective tissues. Part 1: dynamic behavior. Journal of Materials Science: Materials in Medicine 13(10): 933-8.

Waldman, S.D., Sacks, M.S., and Michael Lee, J. (2002) Boundary conditions during biaxial testing of planar connective tissues. Part 2: Fiber orientation. Journal of Materials Science Letters 21: 1215-1221.

Weiss, H.B. (1999) The Epidemiology of Perinatal Traumatic Fetal Injury Mortality. PhD Dissertation, University of Pittsburgh, Pittsburgh.

Weiss, H.B. (2001) The epidemiology of traumatic injury-related fetal mortality in Pennsylvania, 1995-1997: the role of motor vehicle crashes. Accident Analysis and Prevention 33(4): 449-54.
Weiss, H.B., Strotmeyer, S. (2002) Characteristics of pregnant women in motor vehicle crashes. Injury Prevention 8(3): 207-211.
Weiss, J.A., Maker, B.N., and Govindjee, S. (1996) Finite element implementation of incompressible, transversely isotropic hyperelasticity. Computer Methods in Applied Mechanics and Engineering 135: 107-128.
Weiss, S., Jaermann, T., Schmid, P., Staempfli, P., Boesiger, P., Niederer, P., Caduff, R., and Bajka, M. (2006) Three-dimensional fiber architecture of the nonpregnant human uterus determined ex vivo using magnetic resonance diffusion tensor imaging. The Anatomical Record Part A 288(1): 84-90.
Woo, S.L., Gomez, M.A., and Akeson, W.H. (1981) The time and history-dependent viscoelastic properties of the canine medical collateral ligament. J Biomech Eng 103(4): 293-8.
Wood, C. (1964) Physiology of Uterine Contractions. Journal of Obstetrics and Gynaecology of the British Commonwealth 71: 360-373.
Yamada, H. (1970) Strength of Biological Materials. F. G. Evans. Williams and Wilkins, Baltimore.
Young, R.C., Hession, R.O. (1999) Three-dimensional structure of the smooth muscle in the term-pregnant human uterus. Obstetrics and Gynecology 93(1): 94-9.